Mechanistic and structural characterization of human L-asparaginases

Dissertation

for the award of the degree
"Doctor rerum naturalium"
of the Georg-August-University Göttingen

within the doctoral program
"Biomolecules: Structure-Function-Dynamics"
of the Georg-August-University School of Science (GAUSS)

submitted by
Nora Katharina Eulig
from Hannover, Germany

Göttingen, 2022

Members of the Thesis Advisory Committee

Prof. Dr. Kai Tittmann (Reviewer)	Department of Molecular Enzymology
	Georg-August University Göttingen
Prof. Dr. Dirk Görlich (Reviewer)	Department of Cellular Logistics
	Max Planck Institute for Multidisciplinary Sciences
Prof. Dr. Holger Stark	Department of Structural Dynamics
	Max Planck Institute for Multidisciplinary Sciences

Further members of the Examination Board

Prof. Dr. Ricardo Mata	Research Group Computational Chemistry and Biochemistry
	Georg-August University Göttingen
Dr. Sonja Lorenz	Research Group Ubiquitin Signaling Specifity
	Max Planck Institute for Multidisciplinary Sciences
Dr. Alexander Stein	Research Group Membrane Protein Biochemistry
	Max Planck Institute for Multidisciplinary Sciences

Date of submission: 17.02.2022
Date of oral examination: 05.04.2022

Hereby I declare that I prepared the doctoral thesis at hand titled “Mechanistic and structural characterization of human L-asparaginases” independently and with no sources and aids other than quoted. This thesis has not been submitted elsewhere.

Göttingen, 17.02.2022

Nora Eulig

Abstract

L-asparaginases are therapeutic proteins against acute lymphoblastic leukaemia (ALL), especially in children. As lymphoblastic cells depend on L-asparagine in the blood serum, its depletion by L-asparaginases leads to starvation and ultimately the death of leukemic cells. However, currently available drugs derive from bacterial L-asparaginases causing severe side effects and immune response against the foreign enzymes. Though treatment with a human enzyme could remedy these issues, the human L-asparaginase has a significantly lower affinity for the substrate L-asparagine than bacterial homologs and therefore cannot be used in the therapy of ALL.

In this thesis the human asparaginase 1 was biochemically and structurally analysed. This work presents a novel crystal structure for the previously not structurally characterized human protein. Based on this, structural variants were engineered that possess significantly improved kinetic properties compared to the wild type enzyme. Thereby, they constitute a new foundation for the development of a therapeutically active human L-asparaginase enzyme for the treatment of ALL.

Contents

List of Figures

List of Tables

Abbreviations

ACN	Acyl intermediate of asparagine
ADAs	Anti-drug antibodies
AEI	Acyl-enzyme intermediate
Ala (A)	Alanine
ALL	Acute lymphoblastic leukemia
APS	Ammonium persulfate
Arg (R)	Arginine
Asn (N)	Asparagine
ASNase	Asparaginase
ASNS	Asparagine synthase
Asp (D)	Aspartic acid
ATP	Adenosine triphosphate
bdSENP1	SUMO-protease from *Brachypodium distachyon*
CC	Correlation coefficient
CV	Column volume
Cys (C)	Cysteine
ddH_2O	double-distilled water
DESY	Deutsches Elektronen-Synchrotron
DMSO	Dimethyl sulfoxide
DNA	Deoxyribonucleic acid
DNase	Deoxyribonuclease
dNTP	Deoxyribonucleoside triphosphate
*Dpn*I	Methylation-sensitive restriction enzyme
DTT	Dithiothreitol
EC	Enzyme Commission number
E. coli (*Ec*)	*Escherichia coli*
*Ec*ASNase1	Asparaginase of type 1 from *Escherichia coli*
*Ec*ASNase2	Asparaginase of type 2 from *Escherichia coli*
EDTA	Ethylenediaminetetraacetic acid
ϵ_{280nm}	extinction coefficient at 280 nm
Eq.	Equation
EwASNase	Asparaginase from *Erwinia chrysanthemi*
f.c.	final concentration
fl	full-length
FT	Flow through

GDH	Glutamate dehydrogenase
Gln (Q)	Glutamine
Glu (E)	Glutamic acid
Gly (G)	Glycine
gpASNase1	Asparaginase of type 1 from guinea pig
GOL	Glycerol
hASNase1	Asparaginase of type 1 from human
hASNase3	Asparaginase of type 3 from human
HEPES	2-[4-(2-Hydroxyethyl)piperazin-1-yl]ethane-1-sulfonic acid
hgpASNase-tr	Chimeric asparaginase including sequence from human and guinea pig
His (H)	Histidine
His_6-tag	Hexa-histidine tag
HPLC	High performance liquid chromatography
Ile (I)	Isoleucine
IMAC	Immobilized metal affinity chromatography
IPTG	Isopropylβ-D-thiogalactopyranoside
k_{cat}	turnover rate
K_M	Michaelis constant
kDa	Kilodalton
KLD reaction	Kinase-Ligase-DpnI reaction
LB	Lysogeny broth
Leu (L)	Leucine
Lys (K)	Lysine
MEG	Monoetylene glycol
MES	2-(*N*-morpholino)ethanesulfonic acid
Met (M)	Methionine
MW	Molecular weight
MWCO	Molecular weight cut-off
N.A.	not applicable
NAD^+	Nicotinamide adenine dinucleotide (oxidized form)
NADH	Nicotinamide adenine dinucleotide (reduced form)
Ni-Sepharose	Nickel Sepharose
OD_{600nm}	Optical density at 600 nm
PAGE	Polyacrylamide gel electrophoresis
PCR	Polymerase chain reaction
PDB	Protein data bank
PEG	Polyethylene glycol

PIPES	1,4-Piperazinediethanesulfonic acid
Phe (F)	Phenylalanine
PMSF	Phenylmethanesulfonylfluoride
Pro (P)	Proline
psi	Pound-force per square inch
REU	Rosetta energy units
rmsd	Root-mean-square deviation
RNA	Ribonucleic acid
rpm	Revolutions per minute
RT	Room temperature
SDS	Sodium dodecyl sulfate
SEC	Size exclusion chromatography
Ser (S)	Serine
SOC	Super optimal broth with catabolite repression
SUMO protease	Small Ubiquitin-like Modifier protease
TAE	Tris-Acetate-EDTA
TB	Terrific broth
TEMED	N,N,N',N'-Tetramethylethylenediamine
TEV	Tobacco etch virus
Thr (T)	Threonine
tNCS	translational noncrystallographic symmetry
tr	truncated
Tris	Tris-(hydroxymethyl)-aminomethan
Trp (W)	Tryptophan
Tyr (Y)	Tyrosine
UV-Vis	Ultraviolet and visible fraction of electromagnetic radiation
v/v	Volume/volume
Val (V)	Valine
w/v	Weight/volume
wt	Wild type
XDS	X-ray Detector Software

Acknowledgments

First and foremost, I would like to thank PROF. DR. KAI TITTMANN for giving me the opportunity to continue the work on this exciting project during my PhD thesis. Without his supervision and constant encouragement this thesis would not have been possible.

Furthermore, I want to thank my co-supervisor PROF. DR. DIRK GÖRLICH for accepting responsibility of being the second reviewer and being member of my thesis advisory committee. I am thankful to him for greatly supporting part of the molecular biology work of my thesis.

My special thanks also go to PROF. DR. HOLGER STARK for co-supervision of the thesis and for being member of my thesis advisory committee. Additionally, I want to acknowledge his support in attempting to solve the protein structure with help of Cryo-EM.

I am grateful to PROF. DR. RICARDO MATA, DR. SONJA LORENZ and DR. ALEXANDER STEIN for agreeing to be part of the extended examination board.

I would like to thank ELHAM PAKNIA for supporting me in the crystallization screening and my thanks are also extended to the MAX PLANCK INSTITUTE OF MULTIDISCIPLINARY SCIENCES for the generous access to the crystallization facilities.

I am thankful to PROF. DR. RALF FICNER for access to the laboratories and instrumentation and the other members of the DEPARTMENT OF MOLECULAR STRUCTURAL BIOLOGY for practical and scientific support at all times.

Further, I want to thank DR. PIOTR NEUMANN and DR. GLEB BOURENKOV. They provided essential input on X-ray crystallography ranging from sample preparation to data processing. Additionally, I would like to thank the staff of the P14 beamline of the DEUTSCHES ELEKTRONENSYNCHROTRON.

I am thankful to RENATE REES for greatly supporting part of the molecular biology work on a new asparaginase construct.

In addition, I especially want to acknowledge the great work of the GGNB office team and for always being helpful and understanding concerning all administrative questions.

Thanks also go to my Bachelor and lab rotation students Eva Brencher, Janna Scherf, Lena Fütterer and Michelle Mahler, who contributed to this thesis by their hard work.

I am extremely grateful to all my colleagues from the Department of Molecular Enzymology. I greatly enjoyed the pleasant and uncomplicated working atmosphere. Special thanks go to my former colleague Dr. Viktor Sautner for valuable advice and scientific discussions during the initial phases of the project and my PhD thesis. My special thanks also go to Marie Wensien and Laura Kirck for joining me as fellow PhD students. I am especially thankful to Dr. Fabian Rabe von Pappenheim for his valuable input in the final phases of my work in the lab and on X-ray crystallography as well as for proof-reading this thesis. Further, I would like to deeply thank Lisa-Marie Funk, who supported me not only on technical and scientific issues at all times but far beyond.

Finally, I want to express my deepest gratitude to my family for supporting me morally and financially during all the years of study. Thanks a lot, Patrick, for your endless encouragement and for always being there for me!

1 Introduction

1.1 L-asparaginases in general

1.1.1 Introduction and history

Enzymes are large biochemical molecules that catalyze chemical reactions. Thereby, they accelerate and are often even essential for the formation or breakdown of bonds. In 1902 [Gonnermann, 1902] a new group of enzymes belonging to the class of hydrolases, that catalyzes the breakdown of amide-bonds, was discovered. One of the enzymes from this group is L-asparaginase (ASNase) (EC 3.5.1.1). It catalyzes the hydrolysis of the amino acid L-asparagine (L-Asn) to L-aspartic acid (L-Asp) and ammonia (Figure 1, A). Additionally, most asparaginases are at least to some extent also able to convert the closely related amino acid L-glutamine (L-Gln) to L-glutamic acid (L-Glu) (Figure 1, B).

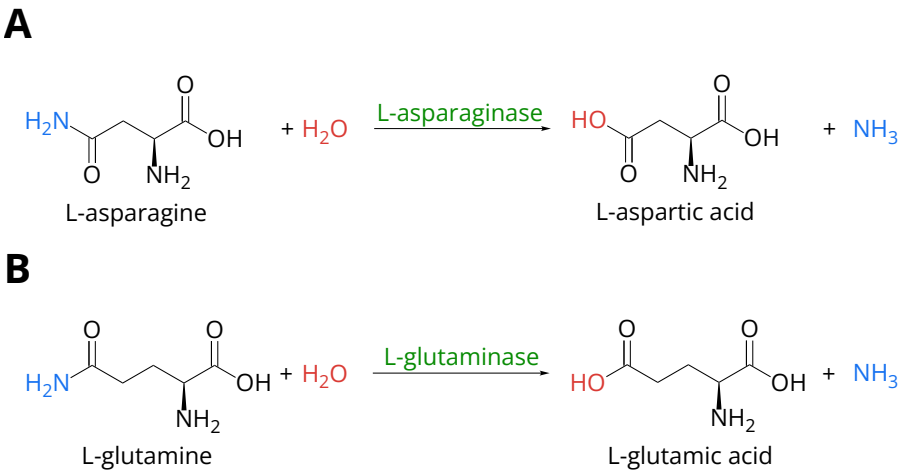

▲ **Figure 1: Reactions catalyzed by L-asparaginases.** L-asparaginases predominately catalyze the hydrolysis of asparagine to aspartic acid and ammonia (**A**). Some asparaginases possess an additional glutaminase activity converting glutamine into glutamic acid and ammonia (**B**).

The existence of enzymes which hydrolyze L-asparagine was first detected in suspensions of beef liver [Lang and Uber, 1904], horse and pig tissues [Fürth and Friedmann, 1910], and some years later also in guinea pig serum [Clementi, 1922]. A distinctive feature of guinea pig serum is its anti leukemic effect [Kidd, 1953]. It was not until 1961 that Broome drew the conclusion that this effect can be attributed to the enzymatic activity of L-asparaginases [Broome, 1961]. However, the guinea pig serum L-asparaginase could not be identified until much later. Additionally, extensive use of guinea pig serum itself in the treatment of leukemia or the production of L-asparaginase from guinea pig serum was not possible. Therefore, other sources of L-asparaginases with possible anti tumor activity had to be searched for and a promising candidate was found in *Escherichia coli* (*E. coli*) [Mashburn and Wriston, 1964]. Nonetheless, further studies showed that *E. coli* does not only encode an L-asparaginase with anti-

leukemic properties but also a second L-asparaginase enzyme which is pharmacologically inactive [Campbell et al., 1967].

1.1.2 Classification of different L-asparaginases

Based on the first identified L-asparaginases from bacteria and plants later enzymes were differentiated between the families of bacterial-type and plant-type asparaginases according to their structural similarities. Bacterial-type asparaginases can be further distinguished between either cytoplasmic (type 1) and periplasmic enzymes (type 2) [Michalska and Jaskolski, 2006], named according to the cellular localization of the two *E. coli* asparaginases mentioned before. This classification is historically established even though the two families also include enzymes from the respective other family as well as asparaginases from archaea, fungi and animals. A third family of L-asparaginases was introduced in 2001 with the identification of an asparaginase from the bacterium *Rhizobium etli* [Borek and Jaskólski, 2001]. Even tough this classification may be misleading and seems outdated, the terminology will be used in the present work considering the widespread use of the historical numerical names for the bacterial L-asparaginases focused on in this thesis.

Of particular interest for the subject of this thesis are the bacterial-type asparaginases listed in Table 1. Among them are the only therapeutically used enzymes *Escherichia coli* asparaginase 2 (*Ec*ASNase2) and the homologous asparaginase from *Erwinia chrysanthemi* (EwASNase). The bacterium *Erwinia chrysanthemi* has been reassigned to *Dickeya dadantii* in 2005 [Samson et al., 2005] but due to the established use of its old name in the context of asparaginase research, it will be used in this thesis. Both enzymes share the high substrate affinity for asparagine with K_{M} values in a micromolar range [Nguyen et al., 2016, Schalk et al., 2014] which distinguishes bacterial-type 2 ASNases from the other subgroup of the same family. Examples for mammalian bacterial-type asparaginases are human 60-kDa lysophospholipase [Karamitros and Konrad, 2014], called human asparaginase 1 (hASNase1) due to its N-terminal L-asparaginase domain, and the guinea pig asparaginase 1 (gpASNase1) [Schalk et al., 2014]. Even though both proteins are homologous to the cytosolic *Escherichia coli* asparaginase of type 1 (*Ec*ASNase1), they significantly differ in their affinity for L-asparagine. Whereas both *Ec*ASNase1 and hASNase1 have low affinities for L-asparagine [Karamitros and Konrad, 2014], the K_{M} value of gpASNase1 is in a micromolar range [Schalk et al., 2014] which is comparable to that of therapeutic enzymes, which are categorized as bacterial periplasmic asparaginases.

Another factor which significantly influences the catalytic performance of enzymes is allosteric regulation. For both *Ec*ASNase1 and hASNase1 enzymatic assays have displayed sigmoidal kinetics, indicating positive cooperativity with the substrate L-Asn as allosteric activator [Karamitros and Konrad, 2014, Yun et al., 2007]. However, positive cooperative effects lead to low reaction velocities at low substrate concentrations. As the concentration of asparagine

in the human blood amounts to only 50 µM [Cooney et al., 1970], allosterically regulated enzymes are not qualified for therapeutic use.
Apart from the differences in affinity for the substrate L-asparagine, the discussed asparaginases also differ in their substrate specificity. In addition to the hydrolysis of L-Asn, those enzymes with actual bacterial origin also catalyze the enzymatic conversion of L-glutamine to L-glutamic acid (Table 1) [Narta et al., 2007]. On the other hand, the mammalian asparaginases show no glutaminase activity [Schalk et al., 2014, Karamitros and Konrad, 2014]. The relevance of this will be further elaborated on in Chapter 1.2.2.

▼ **Table 1: L-asparaginases of particular interest for this thesis.** The L-asparaginases listed here are of particular interest for the subject of this thesis either because of their therapeutic activity or due to their homology to the human enzyme of bacterial-type 1 asparaginases. Their major catalytic properties are categorized as either high/applicable (+) or low/not applicable (-).

Name	Abbreviation	Uniprot Entry	Substrate affinity	Allosteric effect	Glutaminase activity
Escherichia coli asparaginase 1	*Ec*ASNase1	P0A962	-	+	+
Escherichia coli asparaginase 2	*Ec*ASNase2	P00805	+	-	+
Erwinia chrysanthemi asparaginase	EwASNase	P06608	+	-	+
Guinea pig asparaginases 1	gpASNase1	H0W0T5	+	-	-
Human asparaginase 1	hASNase1	Q86U10	-	+	-

1.1.3 Structure

All bacterial-type asparaginases share a highly conserved tertiary structure. Each protomer is build up by a larger N-terminal and a smaller C-terminal domain. They are connected by a linker which can possess highly variable sequences [Loch and Jaskolski, 2021]. In contrast to the L-asparaginases from *E. coli* and *Erwinia chrysanthemi*, the mammalian homologs from guinea pig and human have an additional C-terminal domain containing several ankyrin repeats. The specific function of ankyrin repeats in ASNases is still unknown and could not be structurally analyzed. Even though several structures of the guinea pig enzyme were determined [Schalk et al., 2014] the ankyrin domain is not visible in those structures. Furthermore, in the human enzyme the C-terminal ankyrin domain was not needed for formation of a stable and functional L-asparaginase enzyme [Karamitros and Konrad, 2014]. In several other proteins those motifs act as mediators of protein-protein interactions and thereby may be involved in signaling events [Li et al., 2006, Voronin and Kiseleva, 2008].

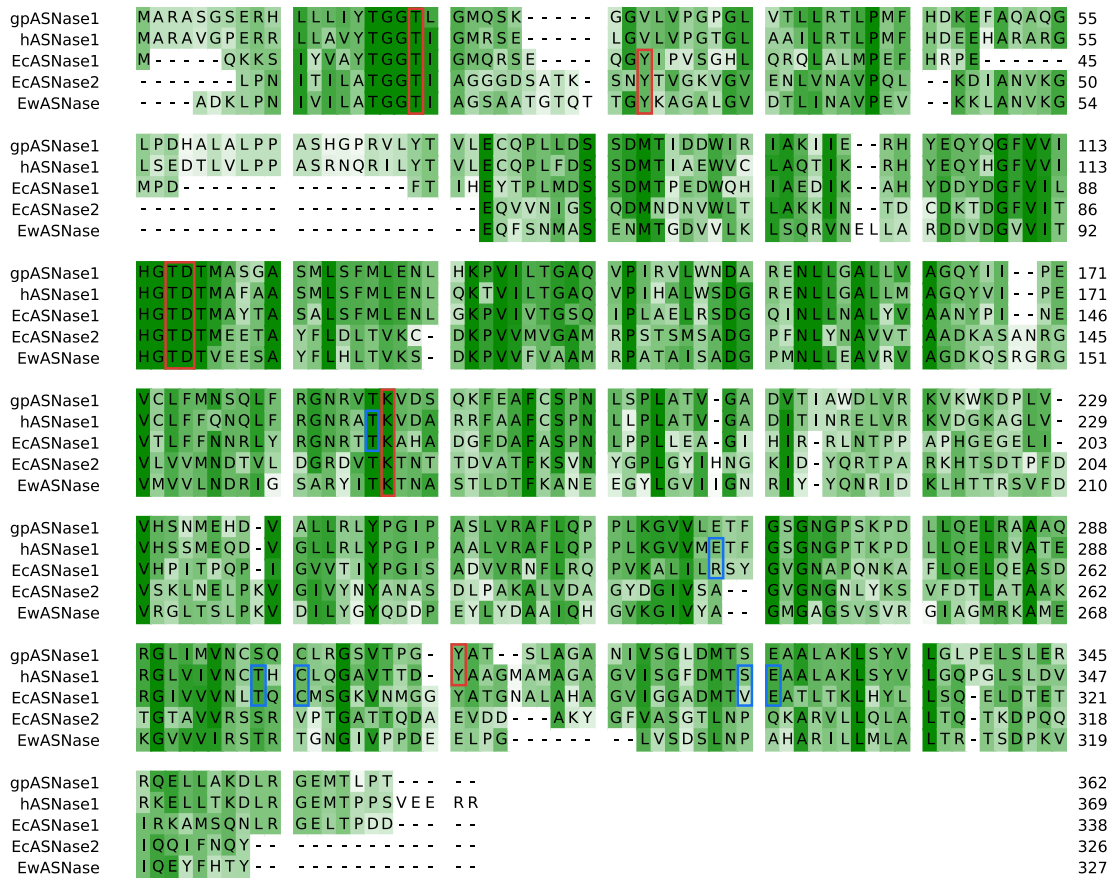

▲ Figure 2: Multiple sequence alignment of gpASNase1 and hASNase1 with bacterial type 1 and 2 L-asparaginases. The multiple sequence alignment was performed for the mammalian asparaginases from guinea pig (gpASNase1, UniProt H0W0T5) and from human (hASNase1, UniProt Q86U10), as well as the type 1 asparaginase from *E. coli* (EcASNase1, Uniprot P0A962) and the therapeutically used enzymes of type 2 from *E. coli* (EcASNase2, Uniprot P00805) and *Erwinia chrysanthemi* (EwASNase, Uniprot P06608). Green shading indicates the level of conservation. Darker color represents highly conserved amino acid residues. Highlighted in red are active site residues, and in blue the allosteric site residues of *Ec*ASNase 1 as well as the corresponding residues in hASNase1. The alignment was carried out using MAFFT [Katoh et al., 2019] with BLOSUM62 [Henikoff and Henikoff, 1992] as substitution matrix and visualized with Biotite [Kunzmann and Hamacher, 2018]. Not depicted are the ankyrin domains of the mammalian enzymes gpASNAse1 and hASNase1, as well as the signal peptides of the periplasmic (type 2) enzymes *Ec*ASNase2 and EwASNase.

The quaternary structure of L-asparaginases is also highly conserved. The enzymes form symmetric homotetramers which can be described as dimer of two dimers [Swain et al., 1993, Yun et al., 2007, Lubkowski et al., 2003, Schalk et al., 2014]. It remains a question until today why these assemble in a tetramer as each close dimer makes up two complete active sites.

The active sites are built up by five main residues vital for catalysis and located in the N-terminal domain: two threonine residues, tyrosine, aspartic acid and lysine (Figure 2, red). The active site is complemented by several other residues, some of which are contributed by the C-terminal domain of the intimate dimer partner. They are of importance for the binding

of the substrate, stabilization of intermediates and specificity [Lubkowski et al., 2020]. A common structural motif of the compared bacterial L-asparaginases is an N-terminal flexible loop referred to as active site flexible loop [Lubkowski and Wlodawer, 2021]. It comprises one of the threonines involved in catalysis as well as the active site tyrosine and is usually disordered when no ligand is bound. This flexibility is retained for the corresponding loop in gpASNase1 even though the catalytic tyrosine is contributed to the active site by another loop in the C-terminal domain of the adjacent monomer [Schalk et al., 2014].
Of particular interest is also an auxiliary substrate binding site found in the crystal structure of *Ec*ASNase1 [Yun et al., 2007]. The involved residues are marked in blue in Figure 2. It is located in the C-terminal domain near the dimer interface and in close proximity to the active site.

1.1.4 General mechanism

Due to the highly conserved composition of amino acids in the active site the three amino acids Asp90-Lys162-Thr89 were proposed to be involved in the hydrolysis of asparagine early on [Swain et al., 1993]. This so called catalytic triad is reminiscent of another triad found in serine proteases. There it consists of the amino acids Asp-His-Ser where the name-giving serine provides hydroxyl side chain residues that serve as nucleophiles for the attack of the carbonyl-carbon of the substrate [Carter and Wells, 1988, Seemüller et al., 1996]. However, none of the proposed amino acids in asparaginases are typical amino acids contributing as nucleophile to the acylation step required for hydrolysis of asparagine. It was suggested that the threonine residue takes over this role. This suggestion led to another point of debate as it was not possible to determine whether the proposed Thr89 or the second conserved active site threonine Thr12 acts as the primary nucleophile. Furthermore, a second main question remained with the possibility of two different general mechanisms for nucleophilic substitution reactions.
The first mechanism involves the nucleophilic attack of one of the threonine residues onto the substrate by forming a covalent intermediate and subsequent release of the first product NH_3. This is followed by hydrolysis of the covalent intermediate by a water molecule and formation of the second product L-aspartic acid. This mechanism is called double-displacement or ping-pong-mechanism as the substrates appear to bounce on and off the enzyme comparable to a ping-pong ball on the table (Figure 3, A). In contrast to this, the alternative direct-displacement mechanism proceeds via a single nucleophilic substitution by the water molecule. Thereby, the products NH_3 and L-aspartic acid are released simultaneously and the substrate is only non-covalently bound to the enzyme (Figure 3, B).
Over the years of study in the field of L-asparaginases, researchers have argumented for and against both mechanisms. While the first crystal structure of an L-asparaginase in complex with aspartic acid bound as a covalent acyl-enzyme intermediate supported the proposal of a

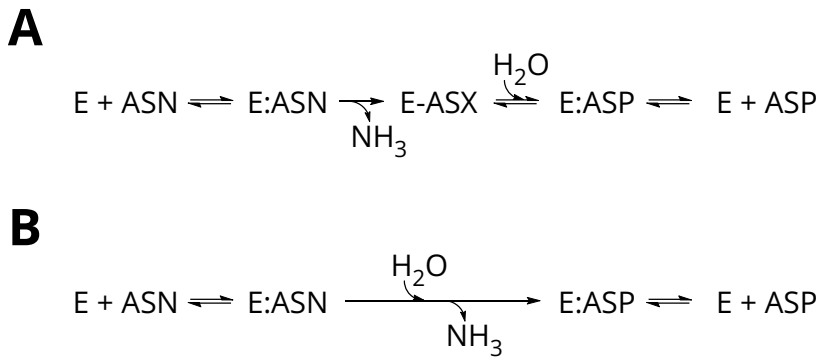

▲ **Figure 3: Schematic representation of the two proposed mechanisms for L-asparaginases.** **A** Representation of double-displacement mechanism and consecutive formation of a covalent intermediate (symbolized by "-"). **B** Representation of the alternative direct-displacement mechanism with non-covalent intermediate (symbolized by ":").

double-displacement mechanism [Palm et al., 1996], subsequent reports challenged this opinion based on theoretical [Gesto et al., 2013] and experimental [Schalk et al., 2016] studies.

1.1.5 Double-displacement reaction

In the following, the double-displacement mechanism will be described in more detail as recent studies support the formation of a covalent substrate-intermediate rather than a single-displacement mechanism at least for bacterial asparaginases of type 2. The authors also suggest, that the mechanism may be further extended to all bacterial-type asparaginases due to the high conservation of catalytic residues [Lubkowski et al., 2020]. As the residues which appear to be crucial for the catalysis are conserved, the residue numbering from the extensively studied *E. coli* L-asparaginase 2 will be maintained for the following description of the mechanism. However, the multiple sequence alignment in Figure 2 gives an overview over the corresponding residue numbering in other asparaginases. It is important to note that in bacterial-type asparaginases from group 1 the active-site tyrosine is contributed by the respective complementary protomer within the intimate dimer.

As shortly described earlier, the first nucleophilic attack on the substrate is carried out by an unusual threonine residue. Structural data of *Ec*ASNase2 with a covalent intermediate bound to Thr12 strongly supported the double-displacement mechanism and strengthened the role of Thr12 as the primary nucleophile [Palm et al., 1996, Lubkowski et al., 2020]. The nucleophilic attack is facilitated by the activation of Thr12 through abstraction of a proton. The proton is transferred to Asp90 over the hydroxyl group of Tyr25 and three linking water molecules (Figure 4, A). With the protonation of the negatively charged Asp90 and the formation of the covalent bond between Thr12 and the C-atom of the amide group the first tetrahedral intermediate is formed. It is stabilized by a second unique motif in hydrolases, an oxyanion hole

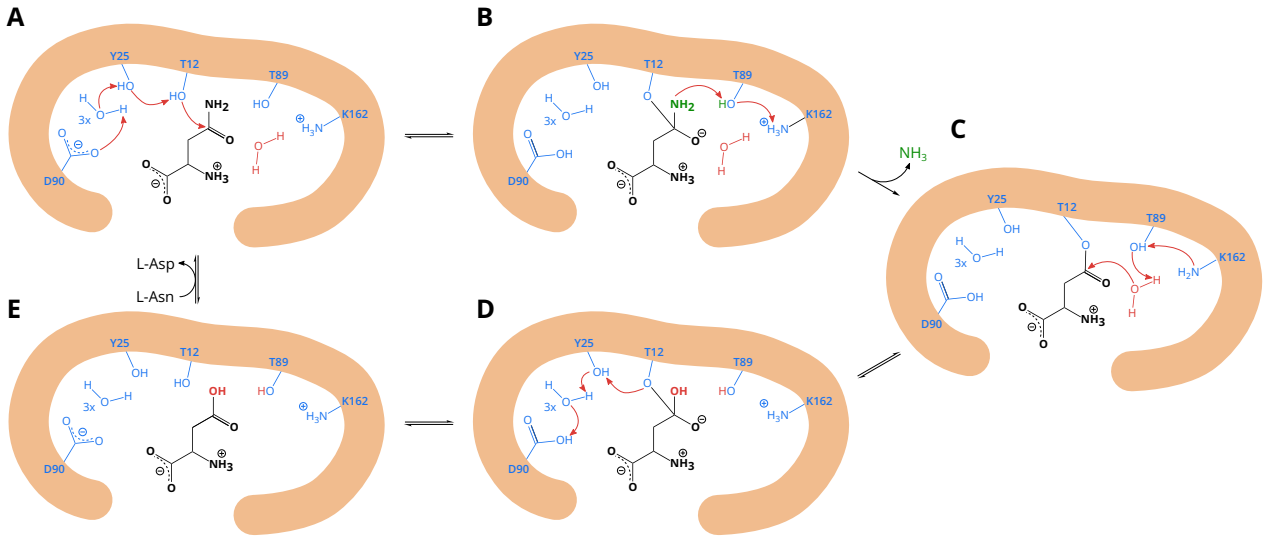

▲ **Figure 4: Double-displacement mechanism of *E. coli* L-asparaginases 2 in detail.** The illustrated steps are based on the reaction mechanism proposed by [Lubkowski et al., 2020]. The positioning of the amino acids does not represent the actual orientation towards each other as seen in crystal structures but is rather meant to support the understanding of the mechanism. Depicted are only the active site residues and water molecules involved in actual catalysis (blue). The conserved water molecule, responsible for the second nucleophilic attack, is highlighted in red and the product NH_3 is colored in green. The substrate asparagine (L-Asn), intermediates and the reaction product aspartic acid (L-Asp) are shown in black. Red arrows represent proton transfers. Additional residues aiding in e.g. stabilization are not shown.

including an alanine residue and a conserved water molecule. NH_3 is released from the enzyme after the leaving group of the substrate accepts a proton from Lys162 via the second active-site threonine Thr89 (Figure 4, B). The second nucleophilic attack is initiated by another conserved water molecule. The nucleophilicity of the water molecule is increased as Lys162 which became uncharged in the previous step recovers a proton from the water molecule again via Thr89 resulting in the strong base OH^- (Figure 4, C). Another tetrahedral oxyanion transition state similar to the first one is formed (Figure 4, D). The carbonyl double bond is regenerated by the final proton transfer from Asp90 to Thr12 through the water molecule chain and Tyr25 and the second product L-aspartic acid is released (Figure 4, E).

Further elucidation of the exact reaction mechanism is important to understand the biochemical properties of asparaginases.

1.2 L-asparaginases as therapeutic

1.2.1 Mode of action

The interest in the research of asparaginases first increased when Kidd reported that guinea pig serum could kill certain cancer cells in mice [Kidd, 1953]. Until today, cancer is one of the major causes of death in industrial countries and the development of specific treatments and especially cures is still very difficult [Cantor et al., 2012]. In general, cancer is a disease effecting the growth and replication of abnormal cells. Abnormal cells develop when mutations occur. This leads to the uncontrolled reproduction of non-functional cells which has numerous disadvantageous consequences for the metabolism in healthy tissues. Cancer cells of all kind proliferate fast. For cell division they require large amounts of biochemical building blocks such as nucleotides and amino acids to synthesize lipids, nucleic acids and proteins [Pavlova and Thompson, 2016, National Cancer Institute, 2021]. However, some cancers are vulnerable due to the fact that modifications to their metabolism cause a reliance on a supply of additional nutrients such as amino acids from an extracellular source. Their growth can be hindered if either the *de novo* synthesis in the cancer cells or the supply from surrounding healthy tissue is restricted. This has shown to be an interesting target mechanism for cancer therapeutics. As the restriction of certain amino acids through specific diets is usually neither specific nor effective enough, the administration of enzymes which mediate the degradation of certain amino acids has gained therapeutic purpose [Endicott et al., 2021].

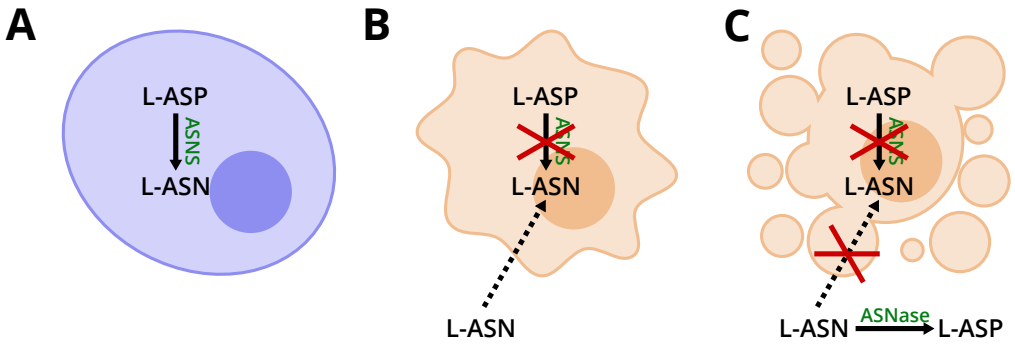

▲ **Figure 5: Mode of action of L-asparaginases against cancer cells.** The schematic illustrates the mode of action of asparaginases against cancer cells. Healthy cells are able to produce asparagine intracellularly with help of the enzyme asparagine synthase (ASNS) (**A**) while tumor cells depend on an exogenous supply of asparagine (**B**). If asparaginase (ASNase) is administered intravenously, the serum asparagine is depleted and the tumor cells die (**C**).

The anti-tumor effect of L-asparaginases is due to the fact that certain cancer cells, such as acute lymphoblastic leukemia (ALL) cells, are unable to synthesize enough of the amino acid asparagine while healthy cells can synthesize asparagine intracellularly from aspartic acid. The reaction is catalyzed by the enzyme asparagine synthase (ASNS) (Figure 5, A). The tumor cells however have a low expression level of ASNS [Stams et al., 2005]. Therefore, they depend on

an exogenous supply of asparagine from the blood serum (Figure 5, B). If patients with a tumor are treated with asparaginase as drug enzyme, the serum asparagine is depleted (Figure 5, C). This leads to starvation and eventually death of the tumor cells [Ho et al., 1970], as asparagine is needed for DNA, RNA and protein synthesis.
Even though the central role of asparagine lies in protein synthesis, recent studies have shown that it has additional importance as metabolite and regulator [Jiang et al., 2021]. In consequence, asparagine acts in supporting growth or survival of cancer cells at various stages from tumor formation over progression to metastasis. Therefore, the interest in L-asparaginases even increased in recent years when it became clear that not only ALL cancer cells are susceptible to asparagine depletion.

1.2.2 Application in cancer treatment

The main cancer target of L-asparaginase therapeutics is acute lymphoblastic leukemia which is the most common form of cancer in children [Howlader et al., 2021]. ALL is a quickly developing type of blood cancer. It begins in the bone marrow affecting white blood cells called lymphocytes. These cells do not reach complete maturity and are non-functional. Additionally, they grow and divide at a faster pace than normal cells, overcrowding the bone marrow and spreading into the blood [Cancer Research UK, 2021b]. The high level of abnormal white blood cells hinders the development of healthy blood cells including white and red blood cells and platelets as well as causes built-up of cancerous cells in organs such as the liver and the central nervous system. Thereby, symptoms of ALL include for example feeling tired and breathless, stomach pains, bruising and bleeding easily, and being more likely to pick up infections [Cancer Research UK, 2021a].
L-asparaginases have already been used to treat other types of hematological malignancies like the closely related myeloid leukemia [Perel et al., 2002]. Furthermore, recent studies suggest that the target of L-asparaginases, the substrate L-asparagine, might influence growth and proliferation of solid tumors and thereby play a critical role in tumor progression and metastasis. Examples are prostate cancer [Linares et al., 2017, Sircar et al., 2012], epithelial breast cancer [Pavlova et al., 2018], and breast cancer metastasis [Knott et al., 2018].
As briefly mentioned before, until today only the type 2 asparaginases from *Escherichia coli* (*Ec*ASNase2) and *Erwinia chrysanthemi* (EwASNase) have been used in chemotherapeutic applications. Several therapeutics derived from these enzymes have been developed. Table 2 gives an overview over some of the current treatments which were either approved and are clinically available or which are still in clinical development. The design of new asparaginase drugs so far has mainly focused on improvements which decrease the required amount of administered therapeutic by reducing dose-frequency and pharmacokinetics of the two bacterial L-asparaginases [Covini et al., 2012]. PEGylation of therapeutic enzymes for example is a common procedure

to increases the molecular weight and hydrophilicity of the drug which in turn can improve solubility, stability and can hinder proteolytic degradation leading to a longer half-life of the L-asparaginase drug in the blood [Dinndorf et al., 2007, Radadiya et al., 2020].

▼ **Table 2: Overview of L-asparaginase based drugs.** Some of these preparations are no longer available in the respective country but may be offered by additional companies under individual trade names.

Generic name	**Trade name**	**Biological origin**	**Modification**	**Pharmaceutical company**	**Status**
Asparaginase	Elspar	*E. coli*	Native enzyme	Merck & Co, Inc., West Point, PA, USA	FDA approved (1978), withdrawn (2012)
Asparaginase	Spectrila	*E. coli*	Recombinant enzyme	medac GmbH, Wedel, Germany	EU approved (2016)
Crisantaspase	Erwinaze	*Erwinia chrysanthemi*	Native enzyme	Jazz Pharmaceuticals plc, Dublin, Ireland	UK approved (1985), FDA approved (2011)
Crisantaspase	Rylaze	*Erwinia chrysanthemi*	Recombinant enzyme	Jazz Pharmaceuticals plc, Dublin, Ireland	FDA approved (2021)
Pegaspargase	Oncaspar	*E. coli*	PEGylated (SS-linker) enzyme	Laboratoires Servier, Suresnes, France	FDA approved (1994)
Calaspargase	Asparlas	*E. coli*	PEGylated (SC-linker) enzyme	Laboratoires Servier, Suresnes, France	FDA approved (2018)
Pegcrisantaspase	Asparec	*Erwinia chrysanthemi*	PEGylated recombinant enzyme	Jazz Pharmaceuticals plc, Dublin, Ireland	Clinical trials (Phase II/III)
Eryaspase	GRASPA	*E. coli*	Enzyme encapsulated within erythrocytes	Erytech Pharma S.A., Lyon, France	Application withdrawn (2018)

Even though various of the developed L-asparaginase therapeutics successfully act against ALL, various side effects appear as a result of the current treatments. These include coagulation disorder, hyperglycaemia, impaired liver function and alterations of the gastrointestinal system and central nervous system. The effects range from from less severe reactions such as fever, nausea and agitation to critical conditions including coma and acute pancreatitis [Covini et al., 2012]. In this context it is important to remark again that some L-asparaginases do not only catalyze the hydrolysis of asparagine to aspartate. Both *Ec*ASNase2 and EwASNase possess a secondary L-glutaminase activity. Many of the side effects are believed to be caused by the disruption of protein synthesis induced by the L-glutaminase activity of L-asparaginase drugs. However, the role of glutaminolytic activity of asparaginases is still debated as it is unclear whether it might be necessary to a certain level for effective elimination of leukemia cells or it only impairs therapeutic effects [Avramis, 2014, Beckett and Gervais, 2019, Chan et al., 2014, Chan et al., 2019]. An even more serious threat to successful administration of the developed L-asparaginase drugs is that patients can also develop hypersensitivity and even resistance to the treatment as a result of the immune response to an enzyme from a foreign organism and the subsequent production of anti-drug antibodies (ADAs) against bacterial L-asparaginases. The concern of immunogenic-

ity is in part also addressed by PEGylation of enzymes. Due to the attached PEG polymers the surface area of the proteins and in particular immunogenic epitopes are masked from the human immune system, thereby reducing both the immune response and inactivation of the drug. Additionally, it is possible to switch to an asparaginase drug with a different origin after a certain time of administrating the first choice treatment. This is done to either circumvent the emergence of an immune response to the first treatment all along or to react to it with an alternative asparaginase which does not cross-react immunologically with the antibodies developed against the first asparaginase drug [Fonseca et al., 2021].
The immune response to foreign enzymes is much stronger than to enzymes of human origin. In addition to that, the discovered human L-asparaginases in contrast to the current bacterial therapeutics show no L-glutaminase activity. Therefore, the drawbacks of bacterial L-asparaginases, side-effects associated with L-glutaminase activity and immunogenicity, could be overcome by developing an enzymatic therapeutic based on L-asparaginases of human origin.

1.3 Objective

Since the discovery of the anti leukemic effect of guinea pig serum [Kidd, 1953] and the conclusion that it is based on the degradation of L-asparagine by the enzyme L-asparaginase [Broome, 1961], intense research on ASNases from different families and various organisms has been conducted.

However, the current state of research is far from understanding all aspects of L-asparaginases in general and especially lacks fundamental insights into the nature of human ASNases. Therefore, this PhD thesis is focused on the enzymatic and structural characterization of human asparaginases.

One of the major tasks of the present work was to solve the protein structure of the human asparaginase 1 (hASNAse1) which has been unknown to date. Structural information could both help to understand the mechanism as well as substrate recognition. Additionally, it could serve to identify relevant residues for the activity in order to engineer a variant of the human enzyme hASNase1 with favorable kinetic properties for the treatment of acute lymphoblastic leukemia.

Studies on L-asparaginases with human origin are of high interest to researchers because of the potential therapeutic relevance of the enzymes. However, a major drawback is the low affinity of the known human ASNases for the substrate L-asparagine. Therefore, as wildtype enzymes they are ineffective in the needed depletion of blood serum L-asparagine which is critical for successful treatment of ALL. Their K_{M} is drastically higher than the concentration of L-Asn in the human blood and considerably poorer than that of the therapeutic bacterial ASNases.

Previous reports have already shown, that variants of hASNases which have an increased catalytic efficiency compared to the wildtype enzymes can be obtained by both directed evolution (hASNase1) [Rigouin et al., 2017] or focused mutagenesis of active site residues (hASNase3) [Karamitros and Konrad, 2016].

The primary goal of this PhD thesis is to design variants of the human enzyme hASNase1 and to analyze them both structurally and biochemically and to find out whether they could become suitable for replacing bacterial enzymes in the treatment of ALL.

2 Material

2.1 Material

2.1.1 Chemicals

Product	Supplier
Acetic acid	AppliChem GmbH (Darmstadt, Germany)
Acrylamide (Rotiphorese Gel 30 (37.5:1))	Carl Roth GmbH & Co. KG (Karlsruhe, Germany)
Agar Bacteriology grade	AppliChem GmbH (Darmstadt, Germany)
Agarose	AppliChem GmbH (Darmstadt, Germany)
Ammonium chloride (NH_4Cl)	AppliChem GmbH (Darmstadt, Germany)
Ammonium persulfate (APS)	Carl Roth GmbH & Co. KG (Karlsruhe, Germany)
L-asparagine	Sigma-Aldrich (St. Louis, MO, USA)
L-aspartate	Sigma-Aldrich (St. Louis, MO, USA)
Bromophenol blue	AppliChem GmbH (Darmstadt, Germany)
Calcium chloride ($CaCl_2$)	Carl Roth GmbH & Co. KG (Karlsruhe, Germany)
Coomassie Brilliant Blue G250	AppliChem GmbH (Darmstadt, Germany)
Dimethyl sulfoxide (DMSO)	Sigma-Aldrich (St. Louis, MO, USA)
Dipotassium phosphate (K_2HPO_4)	AppliChem GmbH (Darmstadt, Germany)
Disodium phosphate (Na_2HPO_4)	AppliChem GmbH (Darmstadt, Germany)
Dithiothreitol (DTT)	AppliChem GmbH (Darmstadt, Germany)
Ethanol (denatured)	Apotheke Frau Magerkuth (Göttingen, Germany)
Ethidium bromide	Carl Roth GmbH & Co. KG (Karlsruhe, Germany)
Ethylenediaminetetraacetic acid (EDTA)	AppliChem GmbH (Darmstadt, Germany)
D-Glucose	AppliChem GmbH (Darmstadt, Germany)
Glycerol	AppliChem GmbH (Darmstadt, Germany)
Glycine	Carl Roth GmbH & Co. KG (Karlsruhe, Germany)
HEPES	AppliChem GmbH (Darmstadt, Germany)
2,5-Hexanediol	Sigma-Aldrich (St. Louis, MO, USA)
Hydrochloric acid (HCl) (37 %)	Carl Roth GmbH & Co. KG (Karlsruhe, Germany)
Imidazole	AppliChem GmbH (Darmstadt, Germany)
Isopropyl β-D-1-thiogalactopyranoside (IPTG)	AppliChem GmbH (Darmstadt, Germany)
Kanamycine sulfate	AppliChem GmbH (Darmstadt, Germany)

α-ketoglutaric acid	Sigma-Aldrich (St. Louis, MO, USA)
D-Lactose	AppliChem GmbH (Darmstadt, Germany)
Magnesium chloride ($MgCl_2$)	Carl Roth GmbH & Co. KG (Karlsruhe, Germany)
Magnesium sulfate ($MgSO_4$)	Carl Roth GmbH & Co. KG (Karlsruhe, Germany)
Manganese(II) chloride ($MnCl_2$)	AppliChem GmbH (Darmstadt, Germany)
β-Mercaptoethanol	Carl Roth GmbH & Co. KG (Karlsruhe, Germany)
Methanol	Carl Roth GmbH & Co. KG (Karlsruhe, Germany)
Monoethylene glycol (MEG)	AppliChem GmbH (Darmstadt, Germany)
Nicotinamide adenine dinucleotide (NADH)	AppliChem GmbH (Darmstadt, Germany)
Phenylmethylsulfonyl fluoride (PMSF)	AppliChem GmbH (Darmstadt, Germany)
Piperazine-N,N'-bis(2-ethane-sulfonic acid) (PIPES)	AppliChem GmbH (Darmstadt, Germany)
Potassium chloride (KCl)	Carl Roth GmbH & Co. KG (Karlsruhe, Germany)
Potassium phosphate (KH_2PO_4)	AppliChem GmbH (Darmstadt, Germany)
Potassium hydroxide (KOH)	AppliChem GmbH (Darmstadt, Germany)
Sodium chloride (NaCl)	Carl Roth GmbH & Co. KG (Karlsruhe, Germany)
Sodium dodecyl sulfate (SDS)	AppliChem GmbH (Darmstadt, Germany)
Sodium hydroxide (NaOH)	AppliChem GmbH (Darmstadt, Germany)
Sodium phosphate (NaH_2PO_4)	AppliChem GmbH (Darmstadt, Germany)
Sodium sulfate (Na_2SO_4)	AppliChem GmbH (Darmstadt, Germany)
D-Sucrose	AppliChem GmbH (Darmstadt, Germany)
Tetramethylethylenediamine (TEMED)	AppliChem GmbH (Darmstadt, Germany)
Tris ultrapure	AppliChem GmbH (Darmstadt, Germany)
Tryptone	Carl Roth GmbH & Co. KG (Karlsruhe, Germany)
Yeast extract	Carl Roth GmbH & Co. KG (Karlsruhe, Germany)

2.1.2 Enzymes

Product	Supplier
DNaseI	AppliChem GmbH (Darmstadt, Germany)
*Dpn*I	Thermo Fisher Scientific (Waltham, MA, USA)
Glutamate dehydrogenase	Sigma-Aldrich (St. Louis, MO, USA)
Lysozyme	AppliChem GmbH (Darmstadt, Germany)
Phusion F-530S (2 U/µL)	Thermo Fisher Scientific (Waltham, MA, USA)
T4-DNA Ligase	Thermo Fisher Scientific (Waltham, MA, USA)
T4-polynucleotide kinase	Thermo Fisher Scientific (Waltham, MA, USA)
TEV protease	Department stock

2.1.3 Bacteria

Product	Supplier
E. coli BL21 Star™ (DE3)	Thermo Fisher Scientific (Waltham, MA, USA)
E. coli DH5α	Thermo Fisher Scientific (Waltham, MA, USA)
E. coli NEBExpress	New England Biolabs (Frankfurt a. M., Germany)

2.1.4 Standards and Kits

Product	Supplier
HF-Buffer (5×)	Thermo Fisher Scientific (Waltham, MA, USA)
GC-Buffer (5×)	Thermo Fisher Scientific (Waltham, MA, USA)
dNTP mix	Thermo Fisher Scientific (Waltham, MA, USA)
T4 ligase buffer	Thermo Fisher Scientific (Waltham, MA, USA)
NucleoSpin Plasmid	Machery-Nagel (Düren, Germay)
NucleoSpin Gel and PCR Clean-up	Machery-Nagel (Düren, Germay)
Pierce™ Unstained Protein MW Marker	Thermo Fisher Scientific (Waltham, MA, USA)
GeneRuler DNA Ladder Mix	Thermo Fisher Scientific (Waltham, MA, USA)
6× DNA loading dye	New England Biolabs (Frankfurt a. M., Germany)

2.1.5 Crystallization screens

Product	Supplier
NeXtal $AmSO_4$ Suite	QIAGEN (Hilden, Germany)
NeXtal Anions Suite	QIAGEN (Hilden, Germany)
NeXtal Cations Suite	QIAGEN (Hilden, Germany)
NeXtal Classics II Suite	QIAGEN (Hilden, Germany)
NeXtal Classics Lite Suite	QIAGEN (Hilden, Germany)
NeXtal ComPAS Suite	QIAGEN (Hilden, Germany)
NeXtal Cryos Suite	QIAGEN (Hilden, Germany)
NeXtal JCSG+ Suite	QIAGEN (Hilden, Germany)
NeXtal MbClass Suite	QIAGEN (Hilden, Germany)
NeXtal MbClass II Suite	QIAGEN (Hilden, Germany)
NeXtal MPD Suite	QIAGEN (Hilden, Germany)
NeXtal PACT Suite	QIAGEN (Hilden, Germany)
NeXtal PEGs Suite	QIAGEN (Hilden, Germany)
NeXtal PEGs II Suite	QIAGEN (Hilden, Germany)
NeXtal Protein Complex Suite	QIAGEN (Hilden, Germany)

2.1.6 Consumables

Product	Supplier
Cellulose Acetate filters, 0.2 µm	Sartorius Stedium (Göttingen, Germany)
Minisart® Syringe filters, 0.2 µm	Sartorius Stedium (Göttingen, Germany)
Spin-X® UF concentrator UF 20, 50K MWCO	Corning® (Kaiserslautern, Germany)
Cryschem M Plate	Hampton Research (Aliso Viejo, CA, USA)
18 mm Circular Cover Slides siliconized	Jena Bioscience (Jena, Germany)
VDXm™ Plate with sealant	Hampton Research (Aliso Viejo, CA, USA)
Crystal Clear Sealing Tape	Hampton Research (Aliso Viejo, CA, USA)

2.2 Devices

2.2.1 Centrifuges

Product	Supplier
Avanti™ JXN-26	Beckman Coulter GmbH (Krefeld, Germany)
Rotor JA-25.50 Ti	Beckman Coulter GmbH (Krefeld, Germany)
Rotor JLA-8.1000	Beckman Coulter GmbH (Krefeld, Germany)
Centrifuge tubes 50 mL	Beckman Coulter GmbH (Krefeld, Germany)
Centrifuge tubes 1000 mL	Beckman Coulter GmbH (Krefeld, Germany)
Eppendorf 5810R	Eppendorf AG (Hamburg, Germany)
Rotor A-4-81	Eppendorf AG (Hamburg, Germany)
Heraeus Multifuge 15-R	Thermo Fisher Scientific (Waltham, MA, USA)
Heraeus Pico 17	Thermo Fisher Scientific (Waltham, MA, USA)
MIKRO 200	Andreas Hettich GmbH & Co.KG (Tuttlingen, Germany)
Rotor 2424-B	Andreas Hettich GmbH & Co.KG (Tuttlingen, Germany)
UNIVERSAL 320R	Andreas Hettich GmbH & Co.KG (Tuttlingen, Germany)
Rotor 1620R	Andreas Hettich GmbH & Co.KG (Tuttlingen, Germany)
Rotor 1420A	Andreas Hettich GmbH & Co.KG (Tuttlingen, Germany)

2.2.2 Spectroscopy

Product	Supplier
NanoDrop One	Thermo Fisher Scientific (Waltham, MA, USA)
UV-vis Spectrometer, V-650	Jasco GmbH (Pfungstadt, Germany)
UV-vis Spectrometer, V-750	Jasco GmbH (Pfungstadt, Germany)
Visible Spectrometer, Libra S11	Biochrom Ltd. (Cambridge, UK)

2.2.3 Liquid chromatography

Product	Supplier
ÄKTA prime plus	GE Healthcare (Little Chalfont, UK)
ÄKTA pure	GE Healthcare (Little Chalfont, UK)
ÄKTA purifier	GE Healthcare (Little Chalfont, UK)
HisTrap™ FF 5 mL	GE Healthcare (Little Chalfont, UK)
HiLoad™ 16/600 Superdex™ 200 pg	GE Healthcare (Little Chalfont, UK)
Superdex® 200 10/300 GL	GE Healthcare (Little Chalfont, UK)
HiPrep™ 26/10 Desalting	GE Healthcare (Little Chalfont, UK)
Superloop 50 mL	GE Healthcare (Little Chalfont, UK)
Superloop 150 mL	GE Healthcare (Little Chalfont, UK)

2.2.4 X-ray

Product	Supplier
X-ray MicroMax™-007 rotating anode X-ray generator	Rigaku Corporation (Tokyo, Japan)
X-stream™ 2000 Cryogenic Crystal Cooler	Rigaku Corporation (Tokyo, Japan)
Mar 345dtb image plate	marXperts GmbH (Norderstedt, Germany)

2.2.5 Other devices

Category	Product	Supplier
Incubators	CERTOMAT® IS	Sartorius Stedium (Göttingen, Germany)
	Multitron Standard	Infors HT (Bottingen, Switzerland)
	Thermomixer comfort	Eppendorf AG (Hamburg, Germany)
Microfluidizer	Microfluidizer™ LM10	Microfluidics (Newton, MA, USA)
pH electrode	Minitrode Hamilton	Mettler Toledo (Giessen, Germany)
PCR cycler	Thermocycler TProfessional	Biometra (Göttingen, Germany)
PCR cycler	MyCycler™ Thermal Cycler System	Bio-Rad Laboratories (Hercules, California, USA)
Microscope	Leica S8 APO	Leica Camera AG (Wetzlar, Germany)

2.3 Plasmids

Product	Supplier
pET-M13b	Manfred Konrad
pET-28a	Thermo Fisher Scientific (Waltham, MA, USA)
pSF1389 (H14-TEV-bdSENP1)	Dirk Görlich, Addgene plasmid #104962
G031 (H14-bdSUMO)	Dirk Görlich

Plasmid maps are depicted in Figure A.3.

2.4 Primers

Target protein	Primer	Primer sequence (5' → 3')
hASNase1-fl	Forward	ATGCTTCATCAGACTGGTGGCAGCGGGGGGGCGAGAGCAGTTGGTCCGGAACGTCGTC
	Reverse	CTTCGTGTCGAGCCTACGAGTTAAACACCAGGCAGCACTTCC
hASNase1-tr	Forward	Phos-TAACTCGTAGGCTCGACACG
	Reverse	Phos-ACGGCGTTCTTCAACG
hASNase1-fl	Forward	GGAAGTTTGTCTGTTTGCGTATAATCAGCTGTTTCG
F175A/Q176Y	Reverse	CGAAACAGCTGATTATACGCAAACAGACAAACTTCC
hASNase1-fl	Forward	GGTGTTATTAGCGGTGGCGATATGACCTC
F322G	Reverse	GAGGTCATATCGCCACCGCTAATAACACC
hASNase1-fl	Forward	CAGGGTGCAGTTACCTATGATTATGC
T305Y	Reverse	GCATAATCATAGGTAACTGCACCCTG
hASNase1-fl	Forward	GTTCTGGGTCCTGGCACCG
V29G	Reverse	CGGTGCCAGGACCCAGAAC
hASNase1-fl	Forward	GCGTAGCGGCCTGGGTGTTC
V29G/E24G	Reverse	GAACACCCAGGCCGCTACGC
hASNase1-tr	Forward	CCTGGCTGGTGCCGGTGTTATT
gp310-312	Reverse	CTGGTTGCATAATCGGTGGTAACTG
hASNase1-tr	Forward	TGTTAATTGTAGCCAGTGTCTGCAGG
gp297-298	Reverse	ATAACCAGACCACGTTCG
hASNase1-tr	Forward	GGTTATGCGACCAGCCTGGCAGGCGCAAATGTTATTAGCGGTTTTGATATG
gp297-316	Reverse	CGGTGTAACGCTACCACGCAGACACTGGCTACAATTAACAATAACCAGAC

2.5 Regular media and buffers

LB medium

10 g/L	Tryptone
5 g/L	Yeast extract
5 g/L	NaCl

LB agar

10 g/L	Tryptone
5 g/L	Yeast extract
5 g/L	NaCl
2 % (w/v)	Agar

TB medium

12 g/L	Tryptone
24 g/L	Yeast extract
4 g/L (w/v)	Glycerol

10× TB salts

0.17 M	KH_2PO_4
0.72 M	K_2HPO_4

Transformation buffer

10 mM	PIPES pH 6.7
15 mM	$CaCl_2$
250 mM	KCl
55 mM	$MnCl_2$

SOC medium

20 g/L	Tryptone
5 g/L	Yeast extract
10 mM	NaCl
2.5 mM	KCl
10 mM	$MgCl_2$
20 mM	Glucose

Glycerol stock solution

25 mM	Tris-HCl pH 8.0
65 % (w/v)	Glycerol
0.1 mM	$MgSO_4$

Autoinduction medium

10 g/L	Tryptone
5 g/L	Yeast extract

25× salt solution (for autoinduction)

625 mM	Na_2HPO_4
625 mM	KH_2PO_4
1250 mM	NH_4Cl
125 mM	Na_2SO_4

50× carbon source solution (for autoinduction)

25.0 % (w/v)	Glycerol
2.5 % (w/v)	Glucose
10.0 % (w/v)	α-Lactose

Separating gel (12.5 %)

1800 µL	Acrylamide
900 µL	1.5 M Tris pH 8.8
45 µL	SDS (10 %)
1740 µL	ddH_2O
5 µL	TEMED
15 µL	APS (10 %)

Stacking gel (5 %)

388 µL	Acrylamide
250 µL	0.625 M Tris pH 6.8
25 µL	SDS (10 %)
1630 µL	ddH_2O
5 µL	TEMED
8.5 µL	APS (10 %)

SDS running buffer

25 mM	Tris
20 mM	Glycine
0.1 % (w/v)	SDS

SDS sample buffer

25 mM	Tris-HCl pH 6.6
25 % (v/v)	Glycerol
0.1 % (w/v)	SDS
0.02 % (w/v)	Bromophenol blue
2.5 % (v/v)	β-mercaptoethanol

Staining solution

0.25 % (w/v)	Coomassie Brilliant Blue
30 % (v/v)	Ethanol
8 % (v/v)	Acetic acid

Destaining solution

10 % (v/v)	Ethanol (100 %)
5 % (v/v)	Acetic acid

2.6 Purification buffers for hgpASNase-tr variants

Lysis buffer

400 mM	KCl
25 mM	Tris-HCl pH 7.5
10 mM	$MgCl_2$
20 % (w/v)	Glycerol

Wash buffer

200 mM	KCl
25 mM	Tris-HCl pH 7.5
10 mM	$MgCl_2$
20 % (w/v)	Glycerol
20 mM	Imidazole

Elution buffer

200 mM	KCl
25 mM	Tris-HCl pH 7.5
10 mM	$MgCl_2$
20 % (w/v)	Glycerol
300 mM	Imidazole

Gel filtration buffer

150 mM	NaCl
20 mM	Tris-HCl pH 7.5
2 mM	DTT

2.7 Purification buffers for bdSENP1

Lysis buffer

290 mM	NaCl
45 mM	Tris-HCl pH 7.5
4.5 mM	$MgCl_2$
10 mM	DTT
15 mM	Imidazole

Elution buffer

290 mM	NaCl
45 mM	Tris-HCl pH 7.5
4.5 mM	$MgCl_2$
10 mM	DTT
400 mM	Imidazole

Gel filtration buffer

290 mM	NaCl
45 mM	Tris-HCl pH 7.5
4.5 mM	$MgCl_2$
5 mM	DTT

2.8 Purification buffers for hASNase proteins

Lysis buffer

300 mM	NaCl
50 mM	Tris-HCl pH 7.5
20 mM	Imidazole
5 mM	DTT

ATP Wash buffer

300 mM	NaCl
50 mM	Tris-HCl pH 7.5
5 mM	$MgCl_2$
5 mM	DTT
1 mM	ATP

Elution buffer

300 mM	NaCl
50 mM	Tris-HCl pH 7.5
400 mM	Imidazole
5 mM	DTT

Gel filtration buffer

300 mM	NaCl
50 mM	Tris-HCl pH 7.5
5 mM	DTT

3 Methods

3.1 Molecular Biology

3.1.1 Polymerase chain reaction

To amplify specific DNA sequences as well as to introduce mutations and generate human asparaginase variants, the polymerase chain reaction (PCR) was applied. The preparation of DNA mixture and the PCR program were adapted according to the manufacturer's manual for the Phusion High–Fidelity DNA Polymerase (Thermo Fisher Scientific, Waltham, MA, USA) following a 3–step protocol. Thus, the annealing temperature was adapted to primer melting temperatures and the extension time chosen according to construct length. To find suitable PCR conditions, a temperature gradient was applied for annealing and both buffers as well as different concentrations of DMSO and template were tested for each amplification individually. Designed DNA oligonucleotide primers were ordered from Sigma-Aldrich (St. Louis, MO, USA) (Chapter 2.4) in desalted quality grade.
After the run, the samples were either stored at -20 °C or analysed via agarose gel electrophoresis.

3.1.2 Generation of new hASNase1 contructs

An initial plasmid was ordered from *GeneArt Gene Synthesis* (Thermo Fisher Scientific, Waltham, MA, USA) in a pET28a vector and the insert sequence (Uniprot entry Q86U10) was codon optimized for expression using the integrated *GeneOptimizer*.
The new construct of hASNase1-fl in the vector G031 (hereafter "H14-bdSUMO") was obtained by Gibson assembly. The vector H14-bdSUMO contains an N-terminal discontinuous polyhistidine tag with 14 histidines in total as well as a following sequence for the cleavage tag of the highly specific SUMO-protease from the bacterium *Brachypodium distachyon* (bdSENP1) [Frey and Görlich, 2014]. The reaction was carried out by Renate Rees in the department Cellular Logistics of Dirk Görlich from the Max Planck Institute of Multidisciplinary Sciences using the primers listed on Page 19 and the vector plasmid as well as components for the reaction from the prepared stocks of the department of Cellular Logistics. The obtained plasmid called pDG03128 will hereafter be referred to as H14-bdSUMO-hASNase1-fl.
The construct for the truncated variant hASNase1-tr lacking the C-terminal ankyrin domain of mammalian asparaginases was obtained by applying site-directed mutagenesis by inverse PCR [Ho et al., 1989]. The used primers (Page 19) are designed to hybridize to the regions on either side of the area to be deleted oriented in the reverse direction. This results in the amplification of the entire circular plasmid except for the desired sequence region. After analysis of PCR

products via agarose gel electrophoresis, the samples with the desired PCR product had to be digested with the restriction enzyme DpnI to remove methylated template DNA. The additional 5'-phosphorylation of the used primers allows ligation and thereby recircularization of the linearized amplification product after PCR. Digestion and subsequent ligation were done according to the respective manufacturer's protocol (Thermo Fisher Scientific, Waltham, MA, USA).
After inactivation of the ligase enzyme, the reaction product was directly used and introduced into chemically competent *E. coli* cells (Chapter 3.2.2) and plated on LB-agar plates with the respective antibiotic for selection. Grown colonies were cultivated in liquid cultures, plasmids purified (Chapter 3.1.5), and the sequence validated by Sanger-sequencing (Chapter 3.1.6).

3.1.3 Generation of Rosetta variants

To obtain variants of the human enzymes with amino acid substitutions, also called mutations, changes were introduced into the DNA sequence by site-directed mutagenesis following the QuikChange Site-Directed Mutagenesis protocol. To this end, the template H14-bdSUMO-hASNase1-fl was used. The primers (Page 19) were designed such that both contain the desired mutation and anneal to the same sequence on opposite strands of the plasmid. Thereby, they are complementary to each other and anneal at the target site of the mutation. Incorporation of the primers into the template plasmid DNA generates an amplification product containing the desired mutation.
After DpnI digestion (Chapter 3.1.2) the PCR product was introduced into chemically competent *E. coli* cells (Chapter 3.2.2) and plated on LB-agar plates with the respective antibiotic for selection. Grown colonies were cultivated in liquid cultures, plasmids purified (Chapter 3.1.5) and the sequence validated by Sanger-sequencing (Chapter 3.1.6).

3.1.4 Generation of structure based variants

Contrary to the generation of the Rosetta variants (Chapter 3.1.3) the plasmid H14-bdSUMO-hASNase1-tr containing the sequence for the truncated human enzyme was used for the generation of the structure based variants. Additionally, the non-overlapping primers (Page 19) were designed with help of the *NEBaseChanger* tool. They are designed in a way so that the forward primer contains the desired mutation in the center and the 5´ ends of the two primers anneal back-to-back.
The PCR products were analyzed with help of agarose gel electrophoresis (Chapter 3.3.1), the desired products were extracted from the stained agarose gel and directly subjected to a Kinase-Ligase-DpnI (KLD) reaction. The reaction mixture of 10 µL contained 50-200 ng PCR-product, 1 µL T4-ligase buffer (10x), 0.5 µL T4-ligase (5 U/mL), 0.5 µL T4-polynucleotide kinase (10 U/mL) and 0.5 µL DpnI (10 U/mL). It was incubated for 2 hours at 37 °C and the reaction

was terminated by incubation at 80 °C for 20 min.
Subsequently, the reaction product was used to transform chemically competent *E. coli* cells (Chapter 3.2.2) and the cells were plated on LB-agar plates with the respective antibiotic for selection. Grown colonies were cultivated in liquid cultures, plasmids purified (Chapter 3.1.5), and the sequence validated by Sanger-sequencing (Chapter 3.1.6).

3.1.5 Plasmid purification

Plasmids were isolated using the kit NucleoSpin™ Plasmid (Machery-Nagel, Düren, Germany). The purification steps were carried out according to the manufacturer's manual.

3.1.6 Sequencing

DNA samples were sent in for sequencing to GATC Biotech (Konstanz, Germany). Samples were prepared by adding 0.2 µL of the respective sequencing primer (100 mM) to 400-500 ng of DNA.

3.2 Microbiology

3.2.1 Preparation of chemically competent cells

Chemically competent *E. coli* cells were prepared by first distributing a frozen culture from the supplier (Page 15) on an LB agar plate without antibiotics and growth overnight at 37 °C. A single colony was used to inoculate 50 mL of LB medium. The cell culture was again incubated overnight at 37 °C and 200 rpm. Cells from the grown preculture were used to inoculate 200 mL of LB medium to an OD_{600nm} of approximately 0.1. The main culture was incubated at 37 °C and 200 rpm until an OD_{600nm} of approximately 0.6 was reached. After cooling the cells on ice for 10 min, they were centrifuged for 10 min at 5000 rpm and 4 °C and the pellet was resuspended in 15 mL of transformation buffer. The incubation ice and centrifugation were repeated before resuspension of the cell pellet in 4 mL of fresh transformation bufffer. Finally, 0.3 mL of DMSO were added and the cells were incubated in ice for 10 min. For storage, the cells were frozen in liquid nitrogen in aliquots of 50 µL and stored at -80 °C.

3.2.2 Transformation of chemical competent cells

Purified plasmid DNA was introduced into chemical competent *E. coli* cells (DH5α, BL21Star™ or NEBExpress) via heat-shock transformation [Inoue et al., 1990]. 50 µL of frozen aliquots were thawed on ice for 5 min. 5-10 ng of plasmid DNA were added, carefully mixed with the cells and incubated for 20-30 min on ice. The mixture was heat-shocked at 42 °C for 45 sec and placed on ice for 5 min. Afterwards, 1 mL of pre-warmed SOC medium were added and the

transformation reaction was incubated for 60-90 min at 37 °C and 500 rpm.
The transformed cells were plated onto LB-agar plates containing the required antibiotics and incubated overnight (at least 16 h) at 37 °C.

3.2.3 Protein expression of hgpASNase-tr variants

For the overexpression of asparaginase hgpASNase-tr variants, *E. coli* BL21 Star™ cells were transformed with the pET-M13b vector containing the sequence for hgpASNase-tr (plasmid provided by Manfred Konrad) or the sequence of one of the three variants (prepared during the preceding Master thesis [Eulig, 2018]). An auto-induction protocol [Studier, 2005] was applied. Precultures of 200 mL LB medium were prepared in 1 L cell culture flasks with chicanes by adding the respective antibiotic (Kanamycine) for selection and four colonies of the transformed cells. The precultures were incubated overnight at 37 °C and 200 rpm. The OD_{600nm} was determined and main cultures of 1 L were prepared in 2 L non-baffled cell culture flasks according to the scheme given in Table 3.

▼ **Table 3: Scheme for preparation of main cultures.**

Component	final concentration	for 1 L
Autoinduction medium		938.8 mL
1 M $MgSO_4$	1 mM	1 mL
25× salt solution	1×	40 mL
50× carbon source solution	1×	20 mL
1000× antibiotic stock	1×	1 mL
Cells from preculture	OD_{600nm} = 0.1	

The main cultures were incubated for 1 h at 37 °C and 200 rpm and then incubated for three days (72 h) at 16 °C and 200 rpm.

3.2.4 Protein expression of bdSENP1

Expression of the highly specific SUMO-protease from the bacterium *Brachypodium distachyon* (bdSENP1) was carried out according to the corresponding publication [Frey and Görlich, 2014]. The expression plasmid pSF1389 encoding His14-TEV-bdSENP1 was a gift from Dirk Görlich (Addgene plasmid #104962 ; `http://n2t.net/addgene:104962`; RRID:Addgene_104962). It was obtained in *E. coli* DH5α as agar stab. Cells from the agar stab were streaked out on LB-agar plates containing the required antibiotic (Kanamycine), plasmids isolated (Chapter 3.1.5) and NEBExpress cells transformed with the plasmid.
A preculture with LB-medium was prepared with grown colonies and antibiotic and incubated overnight at 37 °C. The following day, the OD_{600nm} was determined and the preculture transferred into TB medium supplemented with TB salts (final concentration 1×) so that an OD_{600nm}

of 0.1 was reached. The cells were grown at 37 °C in TB-medium. Overexpression was induced at an OD_{600nm} of 2.0 by adding 0.2 mM isopropylβ-D-1-thiogalactopyranoside (IPTG). The cultures were incubated overnight at 18 °C. Before harvest by centrifugation (Chapter 3.2.7), they were treated with 5 mM ethylenediaminetetraacetic acid (EDTA).

3.2.5 Protein expression of human asparaginases and variants

Overexpression of the human asparaginases hASNase1-fl and hASNase1-tr, and their variants was also attained by auto-induction [Studier, 2005]. In preparation for this the relevant plasmid (H14-bdSUMO vector) was transformed into NEBExpress cells. The auto-induction was then carried out analogously to the expression of hgpASNase-tr variants (Chapter 3.2.3).

3.2.6 Preparation of glycerol stocks

Protein expression was preferably initiated with freshly transformed cells. Alternatively, cells from previously stored glycerol stocks could be distributed on an LB agar plate with the respective antibiotics.
For preparation of the glycerol stocks cells were grown in LB medium to an OD_{600nm} of 0.6-0.8. 500 µL of the precultures were mixed with 500 µL of glycerol stock solution, frozen in liquid nitrogen, and stored at -80 °C.

3.2.7 Cell harvest

After expression of the target protein, the cells were harvested by centrifugation in 1 L beakers for 20 min at 4800 rpm and 4 °C. The cell pellet was washed in the respective lysis buffer, centrifuged in a 50 mL tube for 15 min at 9000 rpm and 4 °C, and the supernatant was discarded. The final cell pellets were weighed, frozen in liquid nitrogen, and stored at -20 °C.

3.2.8 Cell disruption

In the beginning of the purification of each target protein the cell lysis was initiated by resuspending the cell pellet in 2-4 mL of Lysis buffer per 1 g of cells and adding 1 mM phenylmethylsulfonylfluoride (PMSF), a tip of a spatula lysozyme, 5 µg/mL DNaseI and 2 mM $MgCl_2$. To completely resuspend the cell, the mixture was incubated and stirred at 6 °C for 45-60 min.
Cell disruption was performed using a microfluidizer under a pressure of 80 psi in five cycles. The cell lysate was clarified to separate the soluble protein by centrifugation for 60 min at 10 °C (hgpASNase-tr: 30000 xg; hASNase1: 75000 xg).

3.3 Analytical methods

3.3.1 Agarose gel electrophoresis

In order to separate DNA-fragments according to their size and conformation, e.g. after PCR (Chapter 3.1.1), agarose gel electrophoresis was applied. Agarose gels with 1 % agarose in 1× TAE buffer were prepared in a gel chamber. 5 µL of the DNA sample were mixed with 1 µL 6× DNA Loading Dye and 5 µL of the mix were loaded onto the gel. For subsequent size determination, a standard (1 kb Gene Ruler DNA ladder) was run alongside the samples. Electrophoresis was done in 1× TAE buffer at a constant voltage of 100 V for approximately 30 min. Afterwards, the gel was stained in ethidium bromide (2 µg) for 5 min to visualize the DNA-fragments, washed in ddH_2O, and an image was taken under UV-light.
If necessary, the desired DNA-fragments were extracted from the stained agarose gel and purified using a gel extraction kit or the PCR-products were purified using a PCR-product clean-up kit.

3.3.2 Determination of DNA concentrations

DNA concentrations of e.g. plasmids and ligation products were determined at 260 nm using a NanoDrop One UV-Vis spectrophotometer (Thermo Fisher Scientific, Waltham, MA, USA). The instrument assumes an average extinction coefficient and calculates the corresponding nucleic acid concentration in ng/µL.

3.3.3 Sodium dodecyl sulfate polyacrylamide gel electrophoresis

To analyse protein samples from expression and purification Sodium dodecyl sulfate polyacrylamide gel electrophoresis (SDS-PAGE) was used. The discontinuous gels consisting of a separation and a stacking phase were poured between a glass plate and a ceramic plate in a gel caster. SDS sample buffer was added to the protein samples. Before loading them into the sample wells generating by an inserted comb in the stacking phase of the gel, they were heated at 94 °C for 5 min. Gels ran at maximal voltage and 35 mA electric current per gel for 45 min in 1×-SDS running buffer. A protein marker was used as standard. After the run, the gels were stained with coomassie stainer by heating and incubating for approximately 15 min and subsequently destained in destaining solution by heating and incubating overnight. Afterwards, they were kept in water or directly imaged by scanning.

3.3.4 Concentrating protein solutions

In between purification steps and after purification, centrifugal concentrators were either used to decrease the volume or to increase the concentration of protein solutions. The molecular

weight cut off (MWCO) was chosen with a pore size not exceeding half the size of the expected tetrameric enzyme. Centrifugation steps were carried out at 4000 rpm and 4 °C in a swing out centrifuge. After reaching the desired volume or concentration the protein solutions were spinned down at 15000 rpm and 4 °C for 30 min to remove potential aggregates and the supernatant was transferred into a fresh Eppendorf tube.

3.3.5 Determination of protein concentrations

The concentration of purified protein samples was determined using a NanoDrop One UV-Vis spectrophotometer (Thermo Fisher Scientific, Waltham, MA, USA). The instrument calculates the concentration from the measured absorption at 280 nm using the extinction coefficient ($\varepsilon_{280\ \mathrm{nm}}$) and the molecular weight (MW) of the proteins supplied before the measurement. These were obtained from the amino acid sequence using the web tool *ProtParam* [Gasteiger et al., 2005].

▼ **Table 4: Molecular weights and molar extinction coefficients of purified proteins.** The molecular weight (MW) and the extinction coefficient at 280 nm ($\varepsilon_{280\ \mathrm{nm}}$) were determined from the amino acid sequence with help of *ProtParam* [Gasteiger et al., 2005]. For $\varepsilon_{280\ \mathrm{nm}}$ it was assumed that all Cys residues are reduced due to the used buffers containing DTT.

Protein	**MW (g/mol)**	$\varepsilon_{\mathbf{280\ nm}}$ **($\mathbf{M^{-1}cm^{-1}}$)**
hgpASNase-tr	41151.72	22920
hgpASNase-tr Mutant A	41094.63	22920
hgpASNase-tr Mutant B	41086.53	22920
hgpASNase-tr Mutant C	41029.51	22920
hASNase1-fl	60751.76	42400
hASNase1-fl E24G/V29G	60568.51	45380
hASNase1-fl F175/Q176Y	60710.71	43890
hASNase1-fl F321G/T306Y	60682.66	45380
hASNase1-tr	39942.41	22920
hASNase1-tr gp297-298	39919.37	22920
hASNase1-tr gp310-312	39782.16	22920
hASNase1-tr gp297-316	39798.20	22920

If the obtained protein solution was large enough in total volume, the protein concentration (c) could alternatively be determined in a quartz cuvette ($d = 1$ cm) with a photometer. For the blank, buffer was used. The concentration was calculated according to Lambert-Beer law from the extinction (E) at 280 nm:

$$E = \varepsilon \cdot c \cdot d \quad \Longrightarrow \quad c = \frac{E}{\varepsilon \cdot d} \quad . \tag{1}$$

3.4 Chromatographical methods

All proteins were purified using High Performance Liquid Chromatography (HPLC) methods. The purification steps were carried out at 6 °C using the respective buffers listed on Page 22 and following.
Samples of each purification step were analyzed using SDS-PAGE (Chapter 3.3.3). After analysis of the peak fractions from the final purification step the protein of interest was pooled and concentrated with centrifugal concentrators (Chapter 3.3.4) and stored on on ice at 6°C.

3.4.1 Purification of humanized variants of hgpASNase-tr

The constructs of hgpASNase-tr and its variants possess a His-tag. Therefore, they could be purified using immobilized metal affinity chromatography (IMAC) with His-Trap column containing a resin charged with nickel-sepharose. Following cell disruption and centrifugation (Chapters 3.2.7 and 3.2.8), the supernatant was loaded onto the 5 mL column using wash buffer and washed afterwards. After a second washing step with 10 % elution buffer, the direction of the column flow was switched to upwards and 100 % elution buffer were applied for elution of bound proteins. Elution fractions containing the protein of interest were pooled and concentrated with a centrifugal concentrator (50K MWCO) to approximately 200µL and directly submitted to size exclusion chromatography (SEC).
Due to the smaller scale in which the variants and hgpASNase-tr were purified, an SEC column commonly applied in analytical gel filtration was used for preparative purpose (Superdex 200 10/300 GL). To remove aggregated proteins, the concentrated sample was centrifuged for 30 min at 15000 rpm and 4°C before loading it into a 200µL loop and injection. 0.5 mL samples were collected at a flow rate of 0.5 mL/min.

3.4.2 Purification of SUMO-protease bdSENP1

The purification of the highly specific SUMO-protease from the bacterium *Brachypodium distachyon* (bdSENP1) was carried out adapting the protocol described in the corresponding publication [Frey and Görlich, 2014]. After cell disruption and centrifugation (Chapters 3.2.7 and 3.2.8) the supernatant was loaded onto a 5 mL Ni Sepharose column for affinity chromatography equilibrated with lysis buffer and washed afterwards until a baseline was reached. The elution was initiated using 100 % elution buffer. To cleave of the purification tag, the peak fractions containing H14-TEV-bdSENP1 were pooled and digested by adding a 1/30 molar ratio of poly His-tagged TEV protease and incubating overnight at room temperature. Following digestion, the protein solution was concentrated to 1 mL (10 kDa MWCO).
The concentrated sample was subjected to gel filtration. The HiLoad 16/600 Superdex 200 pg column was equilibrated with gel filtration buffer and run with a flow rate of 1 mL/min.

To remove the His-tagged TEV protease and the cleaved of purification tag, a second affinity chromatography equivalent to the first one was carried out. This time, the protein of interest was collected in the flow through. For storage, the buffer of the purified bdSENP1 protease was exchanged to gel filtration buffer using a desalting column. After concentrating the protein solution, the concentration was adjusted to 100 µM in gel filtration buffer supplemented with 250 mM sucrose.

3.4.3 Purification of human asparaginase proteins and variants

Equivalent to the previously described purifications, the constructs of the human asparaginase proteins hASNase1-fl and hASNase1-tr and their variants possess a His-tag and could therefore be subjected to a Ni-affinity chromatography in the first step. The supernatant after centrifugation (Chapter 3.2.8) was loaded onto a 5 mL Ni Sepharose column equilibrated with lysis buffer. After reaching the baseline, a washing step over 100 mL with ATP-wash buffer was applied to remove chaperone proteins. The bound proteins were eluted using 100 % elution buffer. For buffer exchange to the gel filtration buffer without imidazole the pooled elution fractions were subjected to a desalting column. 100 nM of the previously purified SUMO protease bdSENP1 (Chapter 3.4.2) were added to the protein solution after desalt to cleave off the purification tag. The digestion was incubated for 1 hour at 6 °C while slowly shaking. Afterwards, the protein solution was again loaded onto the His-trap column, this time equilibrated with gel filtration buffer. The asparaginase enzyme is thereby separated from the cleaved off tag which binds to the column while the protein of interest remains in the flow-through.
Before the final purification step comprising gel filtration, the protein solution was concentrated to a volume of 1 mL.

3.5 Assays and crystallization

3.5.1 Activity assay

In order to assess the activity of the purified L-asparaginases and their variants a coupled activity assay could be used. The implemented assay depends on the formation of ammonia (NH_3) during the enzymatic hydrolysis of the substrate L-asparagine. NH_3 is subsequently exploited by the helping enzyme glutamate dehydrogenase (GDH) to convert α-ketoglutarate into glutamate (Figure 6). The simultaneous conversion of NADH into NAD^+ can be observed by a decrease in absorption at 340 nm over time.
To be close to physiological conditions, relevant for future application of potential L-asparaginases as therapeutics, the measurements were carried out at 37 °C and pH 7.5. Stock solutions for the substrates α-ketoglutarate (300 mM, pH 7.5), β-NADH (6 mM), L-asparagine (200 mM, pH 7.5) and the buffer Tris-HCl (100 mM, pH 7.5) were prepared. For each mea-

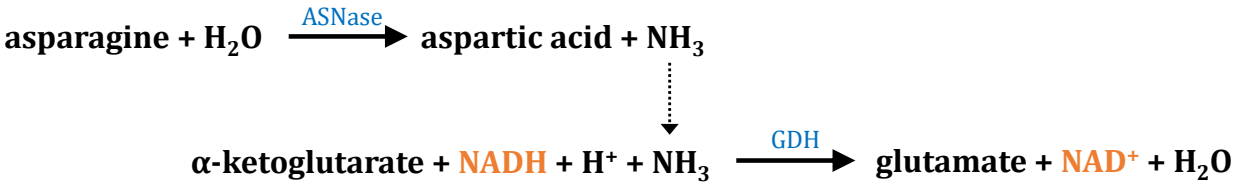

▲ **Figure 6: Schematic overview of the reactions during an NH_3-dependent activity assay.** Enzymes are written in blue: L-asparaginase (ASNase) and glutamate dehydrogenase (GDH). The absorption is measured at 340 nm to detect the oxidation of NADH to NAD^+ (orange).

surement of a data point the asparaginase enzyme was freshly diluted to an appropriate concentration, depending on the overall activity of the enzyme. A quartz cuvette with a width of 1 cm was used. The total reaction volume was adjusted to 1000 µL. The blank was done against air. After preparation of the sample without adding asparaginase (0.025-70 mM L-Asn, 15 mM α-KG, 0.3 mM NADH, 30 U/mL GDH, 50 mM Tris buffer), it was first incubated at room temperature (25 °C) for 10 min. Then, the sample was placed in the photometer (37 °C) and incubated for approximately 3 min while detecting the absorption at 340 nm until it was relatively stable (Figure A.1). Directly after addition of asparaginase, the absorption was measured over 600 seconds with a data pitch of 0.5 seconds.

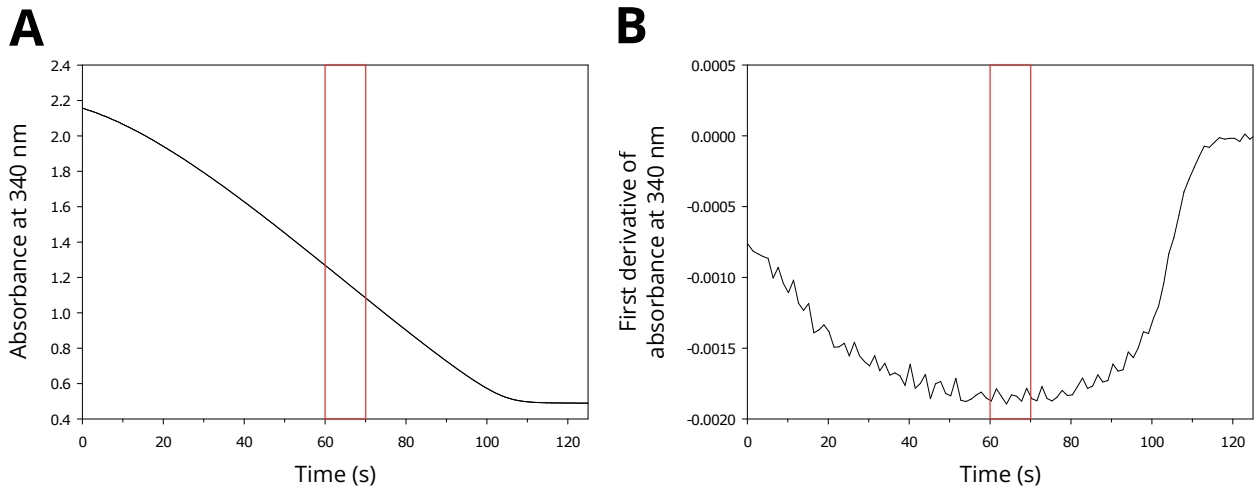

▲ **Figure 7: Example of raw data obtained from the coupled activity assay.** The absorbance measured at 340 nm is measured over time (**A**). With help of the first derivative of the absorbance (**B**) the interval with the steepest slope can be determined. It corresponds to the interval where the first derivative is minimal (marked in red). Here, the first derivative was calculated with *SigmaPlot* and the resulting data was smoothed using the provided smoothing algorithm *running average* with a sampling proportion of 0.005.

In this case, the raw data curves display a prominent lag phase in the beginning of the measurements. This results in an overall decrease in absorption which is not linear. Therefore, the curves were fitted in the interval with the steepest slope (Figure 7, A), selected with help of

the first derivative (Figure 7, B), to determine the change in absorption per minute.
From the obtained decrease in absorption per time (ΔAbs) the apparent reaction rate k^{app} (Equation 2) can be calculated:

$$k^{\mathrm{app}} = \Delta Abs \cdot \frac{\mathrm{MW_{ASNase}}}{\varepsilon_{\mathrm{NADH}} \cdot c_{\mathrm{ASNase}} \cdot d} \quad , \tag{2}$$

where MW is the molecular weight of the respective enzyme (g mol^{-1}), $\varepsilon_{\mathrm{NADH}}$ is the extinction coefficient of NADH (6220 M^{-1} cm^{-1}), c is the weight concentration of the enzyme (g L^{-1}) and d is the width of the cuvette (1 cm). The calculated apparent reaction rates were plotted against the corresponding asparagine concentration as scatter plot of the mean with error bars displaying the standard deviation (SigmaPlot Version 11.0) and fitted according to the Hill equation (Equation 3):

$$V = \frac{k_{\mathrm{cat}} \cdot [Asn]^{\mathrm{n}}}{(S_{0.5})^{\mathrm{n}} + [Asn]^{\mathrm{n}}} \quad , \tag{3}$$

where V is the reaction velocity, k_{cat} is the turnover number, $[Asn]$ is the concentration of the substrate L-asparagine, $\mathrm{S_{0.5}}$ is the substrate concentration at which the rate of the reaction is half-maximal and n is the Hill coefficient. Provided that an enzyme has no cooperativity among the ligand binding sites, the Hill coefficient n is close to 1 and the kinetic parameters can also be determined with the Michaelis-Menten function:

$$V = \frac{k_{\mathrm{cat}} \cdot [Asn]}{K_{\mathrm{M}} + [Asn]} \quad , \tag{4}$$

depending on the Michaelis constant K_{M}.

3.5.2 Screening for crystallization conditions

To find initial conditions for the crystallization of the human asparaginases, crystallization screening was performed at the crystallization facility of the Max Planck Institute for Multidisciplinary Sciences with the help of Elham Paknia from the department of Structural Dynamics. The applied screens are listed on Page 16 and screening was carried out at 20 °C with a protein concentration of 10 mg/mL.
After suitable starting crystallization conditions were determined, initial hits were reproduced manually. Both the hanging-drop and sitting-drop vapor diffusion approach were tested at 20 °C and 6 °C. Additionally, different concentrations of the precipitants and the enzyme were screened. To further improve the condition of the obtained crystals, an additive screen (Additive Screen HR2-428; Hampton Research, Aliso Viejo, CA, USA) was performed according to the manufacturer's manual.

3.5.3 Crystallization of hgpASNase-tr

For crystallization of hgpASNase-tr only freshly prepared protein stocks were used. After purification, the enzyme was stored on ice at 6 °C in gel filtration buffer with a high protein concentration (concentrated to a volume of approximately 200 µL). Directly before setting up the crystallization, the protein was centrifuged at 13000 rpm for 30 min at 4 °C to remove potential aggregates and dilution with concentrations of 4-7 mg/mL in gel filtration buffer were prepared.
Crystallization setups were prepared in a climate controlled room at 20 °C and crystallization was performed in sitting-drop crystallization plates. Each reservoir contained 350 µL reservoir solution made up of 0.1 M of the buffer 4-(2-hydroxyethyl)-1-piperazineethanesulfonic acid (HEPES) at pH 7.5 and 3.29 M of the precipitant sodium cloride (NaCl). Per 24-well plate the same precipitant concentration was applied six times (horizontally) and up to four different protein concentrations between 4-7 mg/mL (vertically) were tested. A drop of 0.5 µL reservoir solution was placed on the post of the well, mixed with 0.5 µL protein solution and 0.2 µL of the additive 2,5-hexanediol (40% v/v) were added. Two rows were prepared in this manner before they were sealed with Crystal Clear Sealing Tape (Hampton Research, Aliso Viejo, CA, USA). For crystal growth the plates were incubated for up to eight weeks at 20 °C. The first small crystals grew only after four weeks and reached an average final size of up to 100µm.
Upon reaching suitable sizes for measuring the crystals at the synchrotron, they were cryo protected by transferring them into a cryo-protection solution (0.1 M HEPES pH 7.5, 3.614 M NaCl, 17.7 % (w/v) 2,5-Hexanediol) using a crystal loop. To stabilize the crystals during this procedure, they were transferred to the final cryo-protection solution applying a linear approach with 5 steps. First, the crystals were transferred to a stabilization solution containing 0.1 M HEPES pH 7.5 and 3.614 M NaCl. This corresponds to the initial concentrations in the well with additional 10 % of NaCl. For the intermediate steps, the stabilization solution was mixed with the cryo-protection solution in ratios of 3:1, 1:1 and 1:3. From the final drop containing only cryo-protection solution, the crystals were fished using a crystal loop and plunged into liquid nitrogen.

3.5.4 Crystallization of hASNase-tr

For crystallization of hASNase1-tr only freshly prepared protein stocks not older than 5 days were used. After purification, the enzyme was stored on ice at 6 °C in gel filtration buffer with a high protein concentration (minimum 18 mg/mL). Directly before setting up the crystallization, the protein was centrifuged at 13000 rpm for 30 min at 4 °C to remove potential aggregates. If necessary, it was diluted to concentrations ranging from 18-24 mg/mL in gel filtration buffer.
Crystallization setups were prepared in a climate controlled room at 20 °C and crystallization was performed in hanging-drop crystallization plates. Each reservoir contained 350 µL reser-

voir solution made up of 0.1 M of the buffer 2-(*N*-morpholino)ethanesulfonic acid (MES) at pH 6.5 and 1.4-1.7 M of the precipitant magnesium sulfate ($MgSO_4$). Per 24-well plate up to six increasing precipitant concentrations (horizontally) and up to four different protein concentrations between 18-24 mg/mL (vertically) were tested. A drop of 2 µL reservoir solution was placed on a siliconized circular cover slide, mixed with 2 µL protein solution and 0.4 µL of one of the additives glycerol (GOL) or monoethylene glycol (MEG) (30% v/v) were added. One row of cover slides was prepared in this manner before placing them to cover the respective reservoir well. For crystal growth the plates were incubated for up to two weeks at 20 °C. The first small crystals grew after approximately five days and reached an average final size of up to 200µm.
For fishing, the crystals were transferred to a drop of the cryo-protection solution containing 15 µL of the respective reservoir solution supplemented with 5 µL of the corresponding additive GOL or MEG (100%) resulting in a final concentration of the cyroprotectant (GOL or MEG) of 25 %. Alternatively, the cryo-protection solution was composed of the reservoir solution saturated with sucrose. The crystals were fished using a crystal loop and plunged into liquid nitrogen.

3.5.5 In-house X-ray cryo-crystallography measurements

Testing the diffraction ability and the quality of crystals and cryo-protectants was performed in-house in the department of Molecular Structural Biology (CuKα radiation, wavelength 1.5418 Å).

3.5.6 Synchrotron X-ray diffraction data collection and processing

Complete datasets were measured under cryogenic conditions (100 K) at the Deutsches Elektronen-Synchrotron (DESY; Hamburg, Germany). The synchrotron data was collected at beamline P14 operated by the European Molecular Biology Laboratory (EMBL; Hamburg, Germany) at the PETRA III storage ring (DESY).
Data processing including indexing, integration and scaling of the resulting diffraction images was done with help of the *XDS* program-suite [Kabsch, 2010].

3.5.7 Phasing and initial structure determination

The molecular replacement method was used for initial phase determination of both hgpASNase-tr and hASNase1-tr. For the chimeric enzyme a search model was generated from the structure of the previously published catalytic subunit of guinea pig L-asparaginase 1 [Schalk et al., 2014] (PDB entry: 4R8K) [Berman et al., 2000] using *phenix.sculptor* [Bunkóczi and Read, 2011, Liebschner et al., 2019]. The molecular replacement was performed using *molrep*

[Vagin and Teplyakov, 1997] of the *CCP4* software suite [Winn et al., 2011].
For the subsequent structure determination of hASNase1-tr the determined final model of hgpASNase-tr was applied in molecular replacement.

3.5.8 Model building and refinement

Initial model building for hASNase1-tr was performed by *PHENIX AutoBuild* [Terwilliger et al., 2008, Liebschner et al., 2019]. With help of the software *Coot* [Emsley et al., 2010] the resulting structure models were completed manually.
Both structure models for were further improved applying *Coot* and *phenix.refine* crystallographic package [Afonine et al., 2012, Liebschner et al., 2019] in an iterative cycle. For structural representation *PyMOL Molecular Graphics System* [Schrödinger, 2015] was used.

4 Results

4.1 Chimeric L-asparaginase

4.1.1 Preliminary work

The primary goal of this PhD thesis as well as previous work on L-asparaginases in the department was to find an asparaginase with favorable kinetic properties for the treatment of acute lymphoblastic leukemia. As the current bacterial therapeutics cause various side effects including an immune response against the intended drug molecules, an asparaginase with human origin could be beneficial to reduce the risk of the aforementioned. However, the known human ASNases possess low affinity for the substrate L-asparagine and are therefore ineffective in the needed depletion of blood serum L-asparagine.
For this reason, the focus was laid on the development of an chimeric enzyme between the human asparaginase hASNase1 and the guinea pig asparaginase gpASNase1, since the latter, in contrast to the human enzyme, has suitable kinetic properties. The chimeric protein was obtained from the group of Manfred Konrad (Former department of Enzyme Biochemistry, former Max-Planck Institute for Biophysical Chemistry, Göttingen, Germany). It is composed of the first 246 amino acids of the N-terminus of hASNase1 and amino acids 247 to 362 of gpASNase1 (Figure 8). In contrast to the two mammalian enzymes the chimeric protein does not posses an ankyrin domain and is therefore called hgpASNase-truncated (hgpASNase-tr). It differs from the human asparaginase in only 31 amino acids and still has a high sequence identity to gpASNase1.

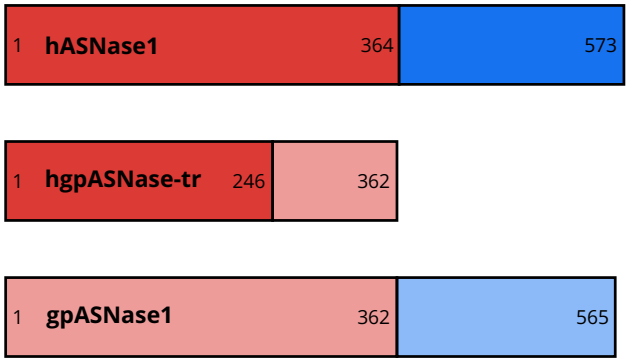

▲ Figure 8: Schematic organization of hgpASNase-tr in comparison to hASNase1 and gpASNase1. Depicted are the L-asparaginase domains of hASNase1 (red) and gpASNase1 (light red) as well as their respective ankyrin domains (blue and light blue). The first 246 amino acids of the N-terminus of the human enzyme were fused with amino acids 247-362 of gpASNase1. The chimeric enzyme hgpASNase-tr does not have an ankyrin domain.

Expression and purification of the chimeric protein were established in the group of Manfred Konrad and optimized during the Bachelor thesis of Marie Wensien [Wensien, 2017] as well

as during the work preceding this PhD thesis [Eulig, 2018]. In addition to that, the enzyme was kinetically characterized and protein crystallization was successful. Thereby, the crystal structure of hgpASNase-tr could be solved with a resolution of 3.1 Å using the in-house radiation source in the department of Molecular Structural Biology (Georg-August-University, Göttingen, Germany).
The overall quaternary structure of hgpASNase-tr was already analyzed [Eulig, 2018]. However, due to the low resolution it was only possible to model the structure as a polyalanine chain. Some regions could not be modeled at all, as no electron density was observed in the corresponding regions. In addition to that, the refinement parameters were of poor quality. The quaternary assembly closely resembled the published architecture of other L-asparaginases. Two monomers assemble into a tight dimer and the tetrameric structure is composed of two of these tight dimers.
A closer look into the structure was only possible after further improvement of the crystallization and cryoprotectant conditions as well as with data collection using synchrotron radiation.

4.1.2 Extended structural analysis of chimeric asparaginase hgpASNase1-tr

The structural analysis of the chimeric asparaginase hgpASNase-tr was expanded on during this PhD thesis. The crystallization and cryoprotectant conditions were further optimized to improve the diffraction of the crystals.

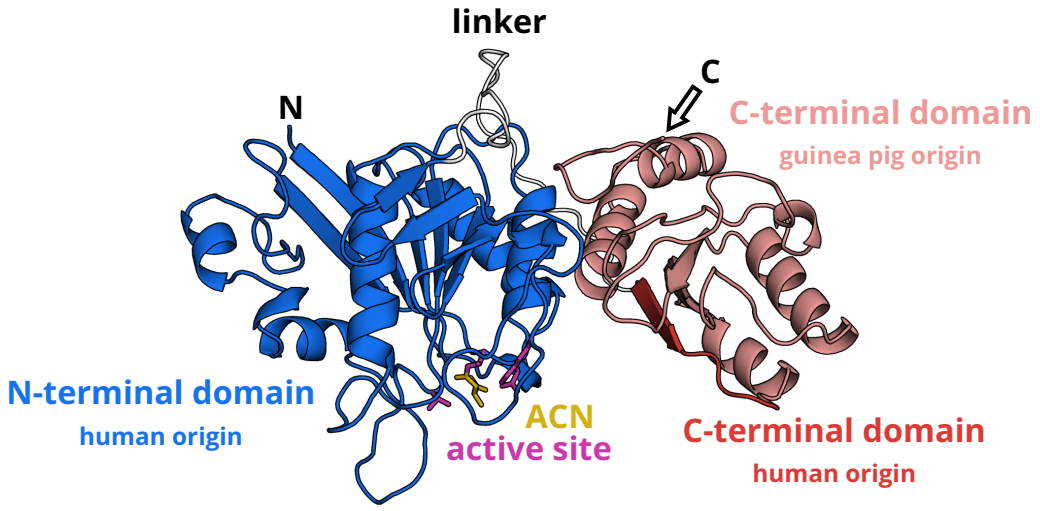

▲ **Figure 9: Protomer structure of hgpASNase-tr.** Cartoon representation of a hgpASNase-tr protomer showing the N-terminal domain colored in blue and the C-terminal domain in red. The light red section of the C-terminal domain originates from the guinea pig enzyme while the bright red segment is of human origin. Additionally, the N and C termini are indicated. The loop region acting as linker between the domains is depicted in white. Residues forming the active site are shown in stick representation and are colored in violet. Bound to the active site is an L-asparagine substrate molecule in form of a covalently attached acyl-intermediate (ACN, yellow).

Thereby, an improved data set with a resolution of 2.8 Å could be collected using synchrotron radiation source (beamline P14, DESY, Hamburg, Germany). Additional data collection and refinement statistics are given in Table 5.

▼ **Table 5: Data collection and refinement statistics for hgpASNase-tr in complex with a covalent acyl intermediate.** For data collection statistics the data for the highest-resolution shell are shown in parentheses.

Data collection	
Wavelength (Å)	1.00
Resolution range (Å)	119.0 - 2.8 (2.9 – 2.8)
Space group	$P6_422$
Cell dimensions	
α, β, γ (°)	90.0, 90.0, 120.0
a, b, c (Å)	137.36, 137.36, 93.45
Redundancy	8.1 (8.4)
Completeness (%)	99.8 (99.8)
Mean $I/\sigma I$	14.48 (1.08)
Wilson B-factor	87.80
R_{meas}	0.101 (1.876)
$CC_{1/2}$	0.999 (0.841)
Refinement	
Resolution (Å)	73.49 - 2.8
Reflections used in refinement	13172
Reflections used for R-free	663
R_{work}	27.01
R_{free}	32.07
No. of atoms	
Macromolecules	2709
Ligands	11
Waters	1
Protein residues	355
B factor (Å^2)	
Macromolecules	129.64
Ligands	103.87
Waters	80.57
rmsd	
Bond lengths (Å)	0.002
Bond angles (°)	0.488
Ramachandran plot	
Outliers (%)	1.98
Allowed (%)	5.10
Favored (%)	92.92

The asymmetric subunit contains one monomer of hgpASNase-tr. The structure of the protomer is depicted in Figure 9. It consists of a larger N-terminal domain which is covalently connected to the smaller C-terminal domain by a linker. The N-terminal domain, the linker and a small part of the C-terminal domain of the chimeric enzyme originate from the human asparaginase 1 while the majority of the C-terminal domain derives from the guinea pig asparaginase 1.
The asymmetric subunit contains only a single hgpASNase-tr monomer. However, by addition of symmetry mates the characteristic tetrameric quaternary structure model of L-asparaginases could be acquired (Figure 10). The tetramer consists of four identical monomers. The four active sites are located between adjacent monomers in a manner that two dimers form two complete active sites as indicated by the location of the bound substrate molecules.

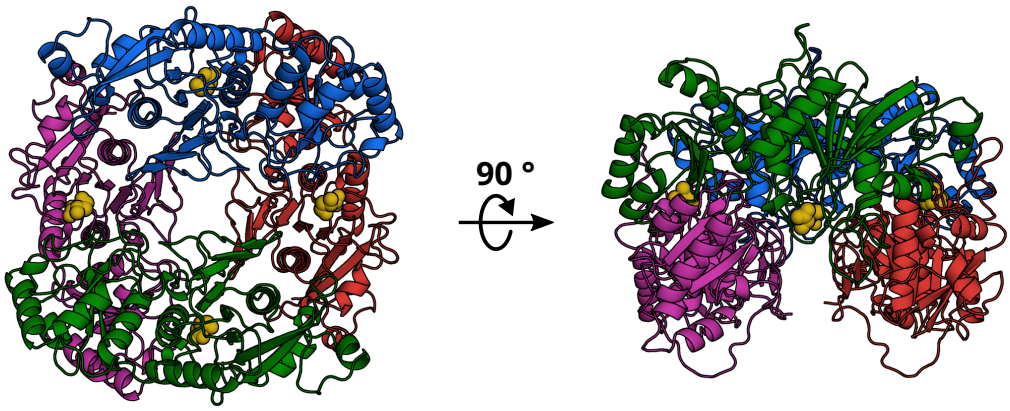

▲ **Figure 10: Tetrameric assembly of hgpASNase-tr.** The homotetramer is formed by a dimer of two close dimers. The four monomers are colored in red, blue, green and violet respectively. The L-asparagine substrate molecules bound to the active sites are represented in yellow spheres. The left image provides a top view of the enzyme, while the right image shows a side view.

The refined structure showed positive electron density in the active site indicating that a ligand or a crystallization component is bound to the enzyme. As the corresponding crystals were shortly soaked in L-asparagine before being plunged into liquid nitrogen, the substrate was modeled into the respective positive electron density. The electron density in the active site is near to and extended towards the residue Thr116. The density was interpreted as a covalent acyl intermediate as well as the product L-aspartic acid. However, the electron density best describes the acyl enzyme (Figure 11). The acyl intermediate is covalently bound to Thr116 and the active site residues Thr19, Asp117 and Lys188 are positioned in close proximity.

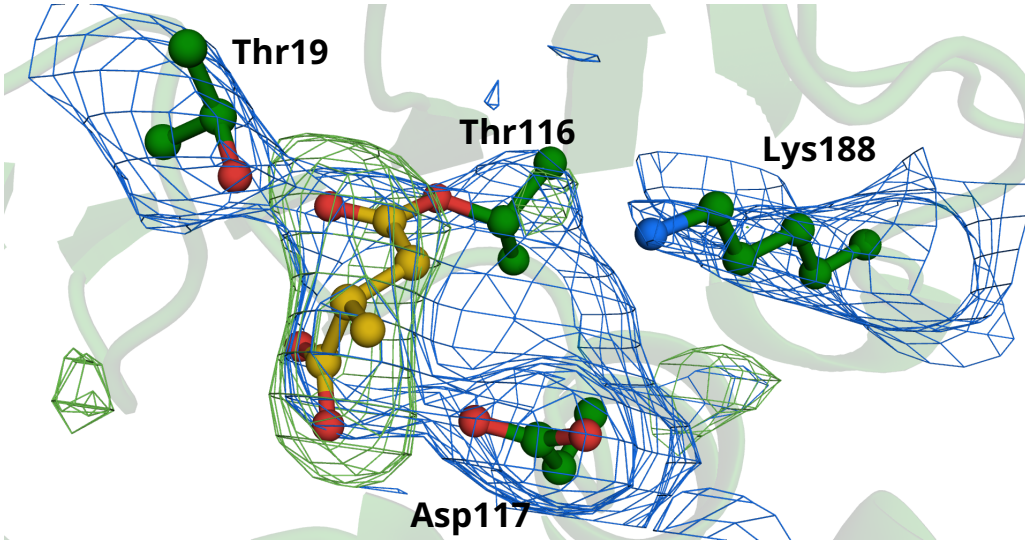

▲ **Figure 11: Active site of hgpASNase-tr.** L-asparagine (yellow) bound to Thr116 as covalent acyl intermediate. Additional conserved active site residues are colored green and are shown in ball-and-stick representation. 2Fo-Fc omit map (level 1.0 σ) is shown in blue. The Fo-Fc omit map (level 3.0 σ) shown in light green was obtained prior to ligand modeling.

4.1.3 Kinetic analysis of humanized mutants of hgpASNase-tr

To pursue the goal of developing a chimeric L-asparaginase based on the guinea pig enzyme gpASNase1 with therapeutically more suitable catalytic properties compared to its human homolog hASNase1, previous work on mutants of hgpASNase-tr was continued in order to further humanize the constructs.

▼ **Table 6: Humanized constructs of hgpASNase-tr.** The listed constructs were obtained during the preceding Master thesis by stepwise mutagenesis. Selected residues originating from the sequence of gpASNase1 were exchanged by the corresponding amino acid from hASNase1 to further humanize the constructs. The proteins were expressed and purified during the work on this PhD thesis.

Protein	Mutations
Mutant A	L338Q/E340G
Mutant B	L338Q/E340G/L321F/L360P/V318I/A351T/E344D
Mutant C	L338Q/E340G/L321F/L360P/V318I/A351T/E344D/R345V/Q347K

The constructs for three selected mutants listed in Table 6 were obtained during the preceding Master's thesis by stepwise mutagenesis and expressed and purified during the work on this PhD thesis as previously established for hgpASNase-tr. The three mutants as well as hgpASNase-tr for comparison were expressed and purified only in small scale for initial activity assessment. The constructs possess a hexa histidine-tag and the target proteins could therefore be isolated from the cell lysate using affinity chromatography in the first step. To remove remaining impurities and denatured or aggregated proteins, size exclusion chromatography was applied. In contrast to a large scale purification, the smaller SEC column commonly applied in analytical

gel filtration was used for preparative purpose (Chapter 3.4.1). The resulting proteins had sufficient purity, which was analyzed by SDS-PAGE, and their activity was assessed directly after the second purification step.

In order to test the activity of the three purified mutants and to compare it with the previously characterized chimeric enzyme hgpASNase-tr the macroscopic catalytic constants k_{cat} and K_M for the hydrolysis of the substrate L-asparagine were determined with help of a coupled activity assay. The conversion of L-asparagine to L-aspartic acid can be indirectly monitored as the second product of the reaction, NH_3, is used in the reaction of α-ketoglutarate to glutamic acid catalyzed by the auxiliary enzyme glutamate dehydrogenase (GDH). During the reaction NADH is oxidized to NAD^+ which can be detected by a decrease in absorption at 340 nm over time. Due to the fact that the raw data curves display a prominent lag phase and the overall decrease in absorption is not linear, the steepest interval of the curve correlating with the strongest decrease was selected with help of the first derivative. The slope for this interval was determined, the reaction velocity calculated and plotted against the corresponding substrate concentration (Chapter 3.5.1). The data points were fitted according to Michaelis and Menten (Eq. 4) analogous to hgpASNase-tr which did not show the sigmoidal behavior of the human L-asparaginase hASNase1.

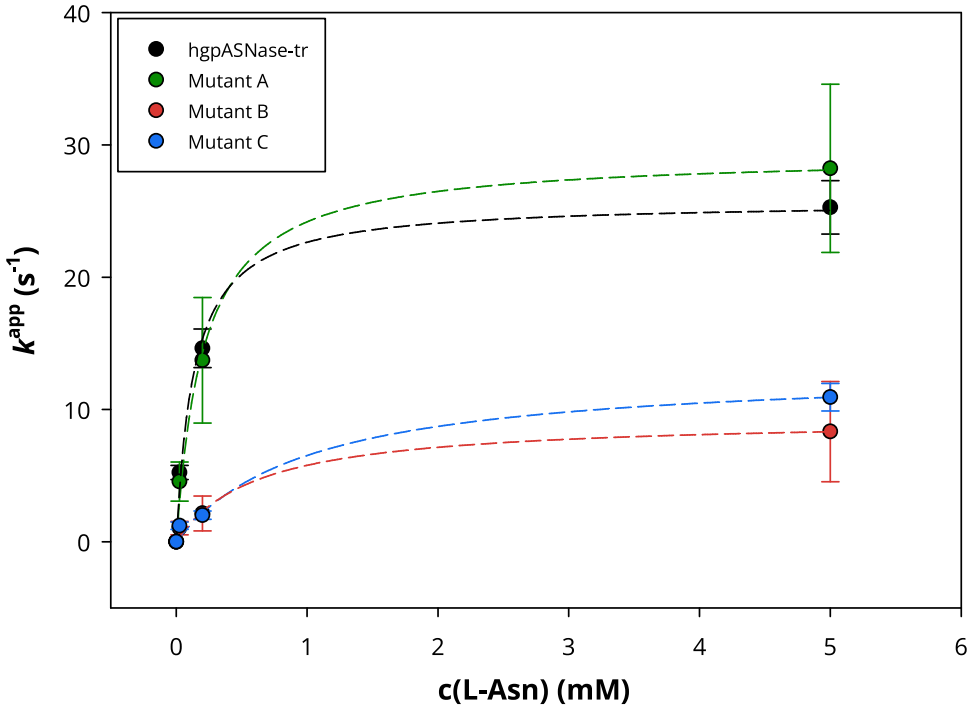

▲ **Figure 12: Activity measurements of hgpASNase-tr and three humanized mutants.** The calculated apparent reaction rate constant (k^{app} (s^{-1})) was plotted against the corresponding concentration of the substrate L-asparagine (0.025, 0.2 and 5 mM). The data points were fitted according to Michaelis and Menten (dashed lines) (Eq. 4).

Figure 12 shows the results of the activity assay measurements for hgpASNAse-tr and the three tested mutants. It is important to note that the proteins were purified in small amounts for initial testing only. Two proteins were purified in parallel and the activity measurements were carried out directly after the second purification step. Therefore, only three data points at different L-asparagine concentrations were collected as triplicates. Two low substrate concentrations (25 and 200 µM) were chosen for approximate determination of K_M values as well as a high substrate concentration (5 mM) where full saturation was expected and k_{cat} could be determined. The resulting values obtained from the respective fit parameters are compared in Table 7.

▼ **Table 7: Comparison of catalytic constants for hgpASNase-tr with mutants.** K_M and k_{cat} were obtained from the fit parameters of the Michaelis-Menten equation (Eq. 4).

Protein	$\boldsymbol{k_{cat}}$ **(s^{-1})**	$\boldsymbol{K_M}$ **(µM)**	$\boldsymbol{k_{cat}/K_M}$ **($\mu M^{-1}s^{-1}$)**
hgpASNase-tr	25.7 ± 0.9	135.8 ± 19.1	0.19
Mutant A	29.3 ± 2.4	210.1 ± 69.7	0.14
Mutant B	9.3 ± 1.6	618.9 ± 454.7	0.02
Mutant C	13.1 ± 0.9	1014.2 ± 287.6	0.01

In general the goal was to find a humanized variant of hgpASNase1-tr which possesses comparable or improved kinetic properties. However, only Mutant A with two amino acids exchanged for the residues from the human enzyme hASNase1 shows similar activity. The other two mutants exhibit considerably lower substrate affinities and turnover rates. Additionally, it can be observed that all mutants quickly loose activity over time (Figure A.2).
Considering that hgpASNase-tr still differs from hASNase1 in 31 amino acids exchanging only two of those amino acids without affecting the kinetic properties of the chimeric enzyme only slightly humanizes the construct. An approach of changing one amino acid after the other would not have been expedient. In addition to that it is likely that certain amino acids act in mutual dependence. Therefore all possible combinations of humanizing mutations would need to be tested to understand their impact on activity. The methods required for this kind of high-throughput screening were not available. Therefore, a new approach of finding a variant of hASNase1 which has promising kinetic properties for the application as a therapeutic in acute lymphoblastic leukemia treatment was chosen by developing new chimeric enzymes originating from the sequence of the human enzyme.

4.2 Human L-asparginases and variants

4.2.1 Wildtype enzymes

As a starting point for the development of asparaginase variants originating from the human enzyme the purification of the wildtype protein needed to be established and its activity verified. The production of hASNase1 has been challenging before as the commonly used bacterial host systems for expression tend to result in high amounts of insoluble protein leading to relatively low yields [Karamitros and Konrad, 2014, Schalk et al., 2014]. For further analysis including solving the still unknown structure of hASNase1 larger amounts of protein with high purity were required.

The expression and purification of the enzyme with help of the constructs provided by Manfred Konrad and the purification protocol established for the chimeric enzyme was not successful. Most of the expressed protein was insoluble and the SDS-PAGE gel after size exclusion chromatography showed several prominent impurities apart from a small amount of protein of interest.

Due to the fact that the original construct only contained a hexa histidine-tag, the aim was to increase the proteins solubility by generating a fusion protein with a Small Ubiquitin-like Modifier (SUMO) protein. The new construct was developed with the help of the department of Cellular Logistics of Dirk Görlich from the Max Planck Institute of Multidisciplinary Sciences. It contains a discontinuous N-terminal polyhistidine tag with 14 histidines in total as well as a following sequence for the cleavage tag of the highly specific SUMO-protease from the bacterium *Brachypodium distachyon* (bdSENP1) [Frey and Görlich, 2014]. The construct is referred to as H14-bdSUMO-hASNase1 in the following.

The fusion construct was expressed in *E.coli* NEBExpress, cells were harvested and lysed. SDS-PAGE samples from both the the supernatant and the pellet show broad bands slightly above 66 kDa (Figure 13, C) correlating with the calculated molecular weight of H14-bdSUMO-hASNase1 of 74.3 kDa indicating that only part of the target protein was expressed in a soluble form. The supernatant was applied to a Ni-affinity chromatography column which binds the polyhistidine tag of the construct. An additional washing step with ATP-wash buffer over 100 mL, indicated by a plateau in UV absorption (Figure 13, A), was carried out to remove chaperone proteins. The buffer of the eluted protein solution was exchanged by desalting and the protein was subjected to cleavage by addition of the specific protease bdSENP1. The construct without tag has a reduced size of 61.0 kDa (Figure 13, C) and can be separated from the cleaved off tag by a second Ni-affinity chromatography called Re-His (Figure 13, B). To remove remaining impurities and denatured or aggregated proteins, size exclusion chromatography was applied.

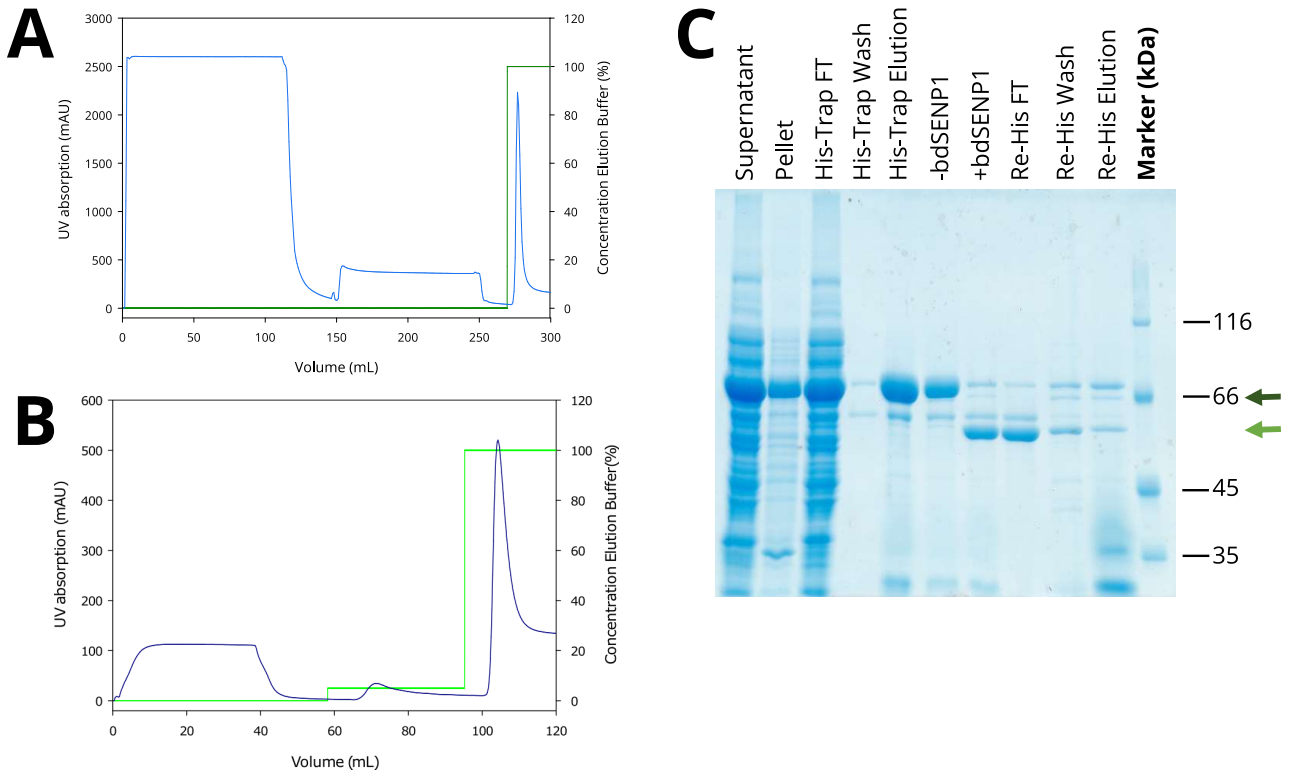

▲ **Figure 13: Chromatograms and SDS-PAGE gel of initial purification steps of hASNase1. A** and **B**: Ni-NTA affinity chromatography steps. The absorption at 280 nm in mAU (blue) was plotted against the elution volume (in mL). The green traces indicate the relative concentration of elution buffer. **C**: SDS-PAGE analysis of initial purification steps. The dark green arrow marks the bands for the fusion protein H14-bdSENP1 while the light green arrow indicates bands for the cleaved target protein hASNase1.

In the first overexpression attempts of H14-bdSUMO-hASNase1, the expression was induced by addition of IPTG to the growing cells. However, this only yielded a small amount of relatively pure protein after the final size exclusion chromatography. Most of the protein eluted in a high peak just after the void volume of the column at an elution volume of approximately 50 mL (Figure 14, A) indicating that the enzymes degraded and formed large aggregates. Additionally, the SDS-PAGE gel (Figure 14, B) shows prominent bands with a higher molecular weight than the protein of interest. A band at this height has previously been interpreted as the chaperone protein GroEL [Karamitros and Konrad, 2014]. The presence of chaperones indicates the formation of incorrectly folded or denatured proteins.

Especially for establishing the crystallization of proteins high amounts of pure protein are required. As most of the hASNase1 protein appeared to be insoluble or unstable, the expression method was adjusted. Lactose-driven autoinduction of recombinant protein expression is considered to result in a high cell density prior to induction. This in turn leads to higher yields of the target protein compared to IPTG induction. Additionally, the growth parameters were adapted to lower temperatures over several days. This gentler approach slows down growth and expression and allows more time for synthesis and folding of a stable target protein.

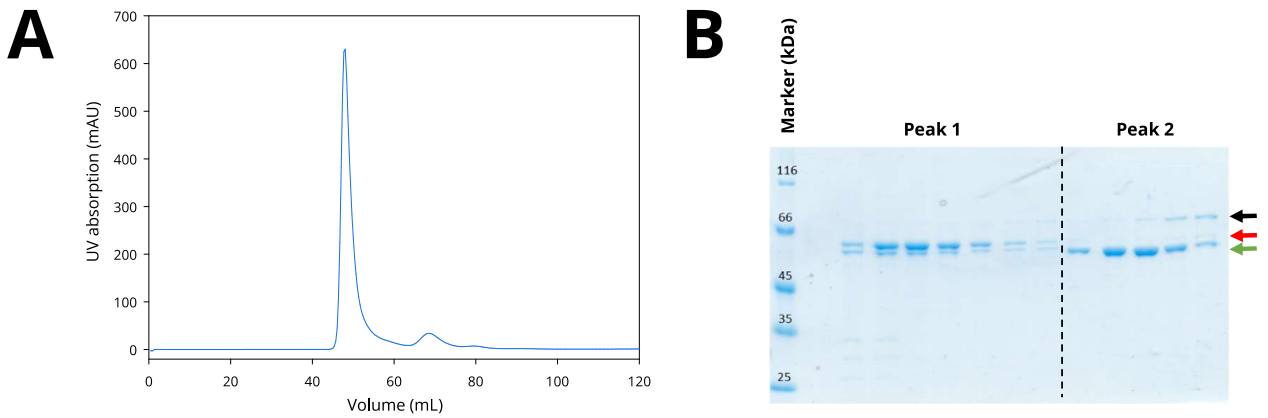

▲ **Figure 14: Chromatogram and SDS-PAGE gel of SEC during purification of hASNase1-fl after expression with IPTG induction.** **A**: The absorption at 280 nm in mAU (blue) was plotted against the elution volume (in mL). **B**: SDS-PAGE analysis of SEC samples. The green, red and black arrows indicate the bands for the target protein hASnase-fl, the chaperone GroEL and an unknown larger impurity, respectively.

Compared to the previous IPTG-induction the presence of target protein hASNase1 in the void volume peak of size exclusion chromatography significantly reduced after expression via autoinduction (Figure 15). In contrast to that the SDS-PAGE samples of the second elution peak show the presence of a protein with a molecular weight of about 60 kDa which corresponds to the calculated size of the target protein hASNase1-fl ($MW_{\text{hASNase1-fl}} = 60.8\,\text{kDa}$). Only a faint band at the height of the molecular weight of the slightly larger GroEL is visible, while most of the proposed chaperone elutes with the void volume in the first peak. Nevertheless, the fractions containing the target protein are still contaminated with an additional protein with a molecular weight of about 70 kDa. The identity of this protein remains unknown. However, it is presumably another protein chaperone.

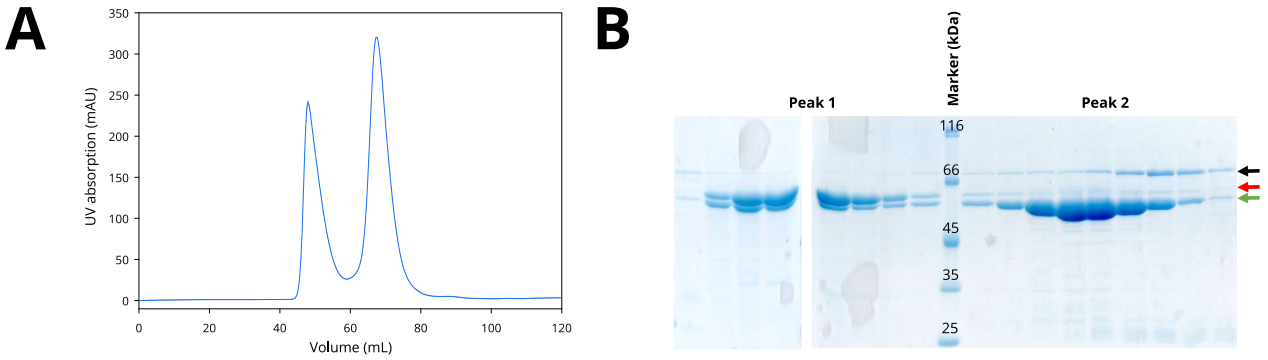

▲ **Figure 15: Chromatogram and SDS-PAGE gel of SEC during purification of hASNase1-fl after expression with auto induction.** **A**: The absorption at 280 nm in mAU (blue) was plotted against the elution volume (in mL). **B**: SDS-PAGE analysis of SEC samples. The green, red and black arrows indicate the bands for the target protein hASnase-fl, the chaperone GroEL and an unknown larger impurity, respectively.

In addition to the full-length human asparaginase (hASNase1-fl) containing the ankyrin domain, a truncated version was expressed and purified. The truncated hASNase1 enzyme (hASNase1-

tr) was cloned into the same vector system as the full-length enzyme and expressed and purified analogously. According to [Karamitros and Konrad, 2014] apart from the 364 amino acids of the N-terminal L-asparaginase domain five additional amino acids (VEERR) from the ankyrin domain are required for the production of the soluble and active human protein resulting in a total of 369 amino acids. Thereby, the truncated protein is approximately 20 kDa smaller than the full-length enzyme ($MW_{hASNase1\text{-}tr}$ = 39.9 kDa). This enables a better separation of the protein from remaining larger impurities with help of size exclusion chromatography (Figure 16).
The elution volume of both hASNase1-fl and hASNase1-tr corresponds to the tetrameric assembly of the enzymes with a total molecular weight of about 240 kDa and 160 kDa respectively.

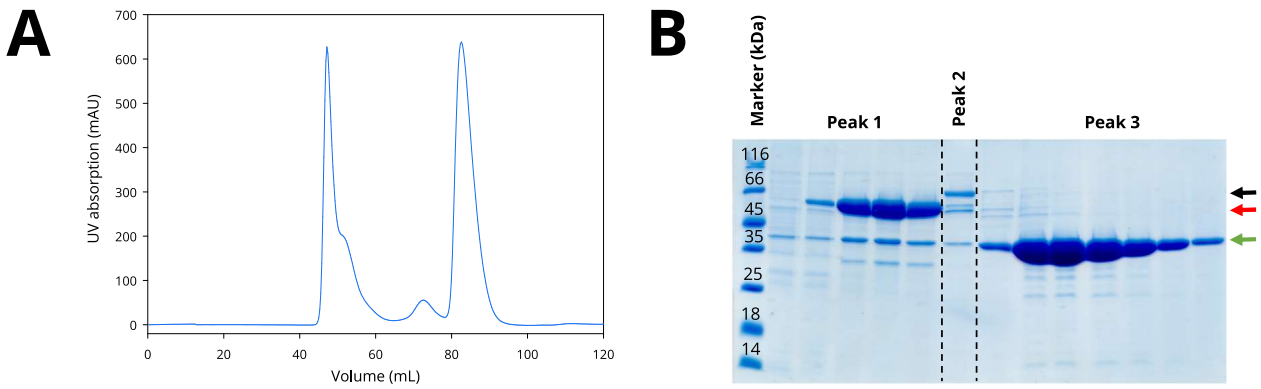

▲ **Figure 16: Chromatogram and SDS-PAGE gel of SEC during purification of hASNase1-tr after expression with auto induction.** **A**: The absorption at 280 nm in mAU (blue) was plotted against the elution volume (in mL). **B**: SDS-PAGE analysis of SEC samples. The green, red and black arrows indicate the bands for the target protein hASnase-fl, the chaperone GroEL and an unknown larger impurity, respectively.

In order to verify the activity of both purified proteins, the macroscopic catalytic constants k_{cat} and K_M for the hydrolysis of the substrate L-asparagine were determined with help of the coupled activity assay as established for the chimeric L-asparaginases (Chapter 4.1).
In contrast to the chimeric enzyme, hASNase1 is known to be regulated allosterically by its substrate resulting in a sigmoidal reaction curve [Karamitros and Konrad, 2014]. Therefore, the resulting data points were not fitted according to Michaelis and Menten (Eq. 4) but using the Hill equation (Eq. 3). For enzymes that do not follow Michaelis-Menten kinetics, $S_{0.5}$ is analogous to K_M. Figure 17 shows the results of the activity assay measurements for the full-length (Figure 17, A) and for the truncated (Figure 17, B) enzyme.
It is important to note that for the truncated enzyme the substrate saturation could not be reached. Higher values of substrate concentrations could not be determined due to the relatively low solubility of L-Asn with a maximum stock concentration at 200 mM. Additionally, the $S_{0.5}$ of hASNase1-tr is approximately ten times higher than that determined for the full-length enzyme.

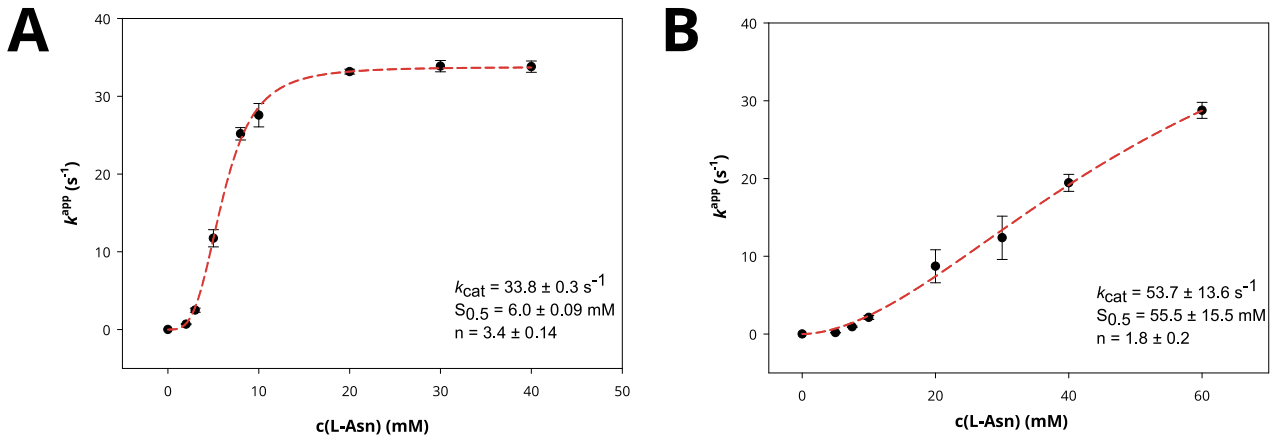

▲ **Figure 17: Activity of hASNase1-fl and hASNase1-tr.** The calculated apparent reaction rate constant (k^{app} (s^{-1})) was plotted against the corresponding concentration of the substrate L-asparagine (mM). The data points were fitted with the Hill equation (Eq. 3) (dashed lines). The catalytic constants k_{cat}, $S_{0.5}$ and the Hill coefficient n for hASNase1-fl (**A**) and hASNase1-tr (**B**) are obtained from the fit parameters.

4.2.2 Rosetta variants

In order to develop L-asparaginase variants originating from the sequence of the human enzyme hASNase1 with improved kinetic properties compared to the wild type enzyme, different methods can be applied. One approach of improving an enzyme's catalytic activity is by computational enzyme design. A popular tool for this task is the *Rosetta* software package. The general idea behind the algorithms is that the sequence of an enzyme defines its structure which in turn influences the enzymatic function. An example for a common approach is to stabilize the known structure of an enzyme by introducing stabilizing point mutations into the sequence. The Point mutant (pmut) scan application from *Rosetta* allows the calculation of single or double point mutations which increase the stability of a given protein structure [Kuhlman et al., 2003, Rosetta Commons, 2022b]. For this purpose the previously obtained structure of the chimeric enzyme hgpASNase-tr (Chapter 4.1) was humanized by exchanging the sequence for the amino acids of the catalytic subunit of hASNase1 and used as input for the pmut scan protocol. The scan for single point mutations resulted in a total of 187 variants for 62 amino acid positions. In case of the double mutant scan, which takes residue pairs into account which are close enough to interact, 1686 variants for 90 residue pairs were found. As the resulting list of mutants is far too long to test every variant, the choice of mutants to be tested had to be narrowed down significantly. The suggested variants were sorted into the six different groups shortly described in Table 8.

For the definition of suggested variants for the Hotspot group another computational tool for the design of mutations and smart libraries in protein engineering was used, *HotSpot Wizard* [Sumbalova et al., 2018]. With help of the web server *hot spots* were identified in the five

▼ **Table 8: Grouping of Rosetta hits.** The initial hits of the pmut scan for single and double point mutations were divided into six different groups. The Contact group is only applicable for double mutants.

Group	Description
Active Site	Residues 8 Å around active site
Allosteric Site	Residues of postulated allosteric site and 8 Å around it
Chimera	Residues in the chimeric region of hgpASNase-tr
Hotspot	Residues which were hits in a HotSpot Wizard scan of gpASNase structures
Contact	Double mutants with residues on different protomers
Other	Remaining residues

published structures of the highly active guinea pig asparaginase 1. Variants suggested by *Rosetta* were compared to the hits from the *HotSpot Wizard* scan and the intersecting amino acid positions were assigned to the Hotspot group. From each of the six groups a single and a double mutant were selected based on the initial *Rosetta* scoring (Table 9). Highly conserved amino acid residues were additionally identified with a *3DM* information system which is a third computational application in the field of protein engineering developed by the company Bio-Prodict (Nijmegen, Netherlands) [Kuipers et al., 2010]. Initially, the *3DM* system was also supposed to assist in the design of a functional human L-asparaginase. However, the compiled protein super-family platform did not provide any clear information on sequence-structure-function relations which could have helped to elucidate the function of individual amino acids or mutations. Therefore, this approach was discontinued.

▼ **Table 9: Selected single and double mutants from Rosetta output.** The mutants are the results of a *Rosetta* Point mutant (pmut) scan application. The initial hits were divided into six different groups. From each group a single and double mutant were selected based on the *Rosetta* scoring. The single mutant in close proximity to the active site was omitted due to high conservation of the residue and the Contact group is only applicable for double mutants.

Group	Single mutant	Double mutant
Active Site	-	F176A/Q177Y
Allosteric Site	C296V	E266L/H298Q
Chimera	A315G	F321G/T306Y
Hotspot	S124A	C79F/V14I
Contact	-	Q301R/R193H
Other	D237N	H50Y/R71I

The Rosetta Energy Units (REU) were calculated for the mutants listed in Table 9 and additionally for the best overall hit (E25G/V30G). The final score represents the average from ten calculated models of each variant. Table 10 lists the three mutants with the best scoring compared to the wildtype.

▼ **Table 10: Calculated Rosetta Energy Units for the best selected mutants.** The Rosetta Energy Units (REU) were calculated for the mutants listed in Table 9 as well as for the best overall hit (E25G/V30G). Here, the three mutatns with the best scoring compared to the wildtype are listed.

Mutation	Group	REU	ΔWT
E25G/V30G	Best hit	-3657 ± 4	81 ± 6
F176A/Q177Y	Active Site	-3626 ± 3	50 ± 5
F321G/T306Y	Chimera	-3617 ± 4	41 ± 6
Wild type	-	-3576 ± 4	-

These mutations were introduced into the H14-bdSUMO-hASNase1-fl construct by site-directed mutagenesis following the primer design for QuikChange PCR. The full-length construct of the human enzyme was chosen due to its significantly better affinity for the substrate L-asparagine compared to the truncated variant of the wild type.
Following this, the enzymes were expressed and purified as previously described for the wild type proteins (Chapter 4.2.1) and their activity assessed with the established coupled activity assay for L-asparaginases. Figure 18 shows the results of the activity measurements for the three mutants.

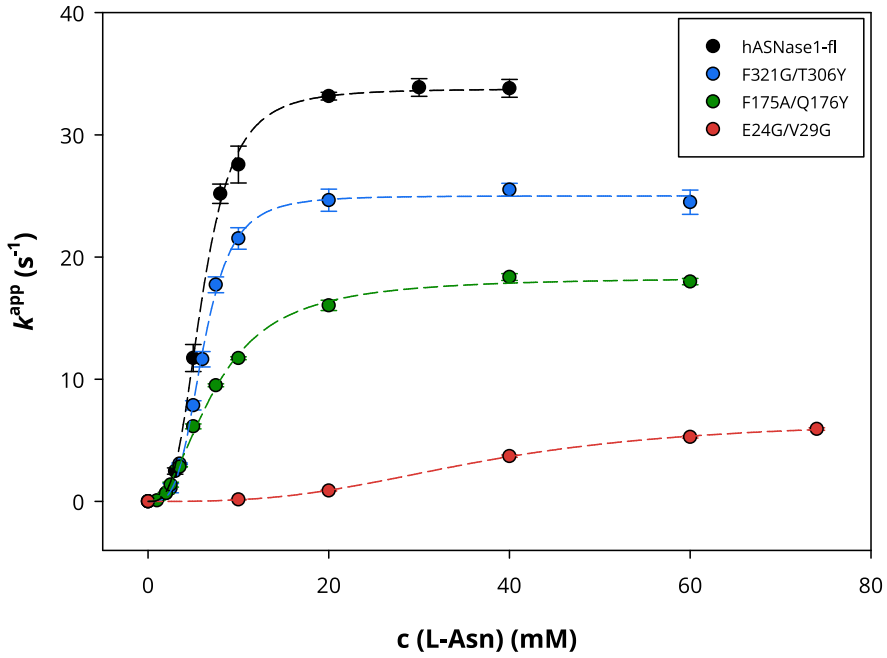

▲ **Figure 18: Activity of hASNase1-fl variants obtained with Rosetta approach.** The calculated apparent reaction rate constant (k^{app} (s^{-1})) was plotted against the corresponding concentration of the substrate L-asparagine (mM). The data points were fitted with the Hill equation (Eq. 3) (dashed lines).

All variants still display a sigmoidal course of the reaction curve meaning that these enzymes are allosterically regulated just like the wild type human asparaginase. The catalytic constants k_{cat}, $S_{0.5}$ and the Hill coefficient n were therefore obtained from the fit parameters of the Hill

equation (Eq. 3) and are compared in Table 11. The Hill coefficients of all three double mutants also depict the still existing cooperativity of the enzymes. The variant F321G/T306Y with mutations corresponding to residues in the chimeric region of the chimeric enzyme hgpASNase-tr only shows a slightly reduced k_{cat} value. In contrast to that the mutations in close proximity to the active site of the double mutant F175A/Q176Y appear to have an additional effect on the substrate affinity by increasing the $S_{0.5}$ value as well as further decreasing the turnover rate. The most prominent effect can be observed for the double mutant E24G/V29G which had the best overall *Rosetta* score. Not only does the k_{cat} value decrease by a factor of five, but also the $S_{0.5}$ value is six times higher compared to the wildtype enzyme.

▼ **Table 11: Comparison of catalytic constants for Rosetta variants.** The catalytic constants k_{cat}, $S_{0.5}$ and the Hill coefficient n were obtained from the fit parameters of a Hill equation (Eq. 3).

Protein	$\boldsymbol{k_{cat}}$ **(s^{-1})**	$\mathbf{S_{0.5}}$ **(mM)**	**Hill coefficient n**
hASNase-fl	33.8 ± 0.3	6.0 ± 0.09	3.4 ± 0.14
F321G/T306Y	25.0 ± 0.23	6.1 ± 0.07	3.8 ± 0.16
F175A/Q176Y	18.4 ± 0.22	7.4 ± 0.17	2.1 ± 0.09
E24G/V29G	6.67 ± 0.12	37.3 ± 0.69	2.9 ± 0.10

It was assumed that the structure of the chimeric asparaginase hgpASNase-tr represents the active folding state of a non allosterically regulated enzyme. *Rosetta* was expected to find mutations in the human amino acid sequence which stabilize this conformation resulting in a human variant without cooperativity. However, summing up the results of the design of variants with help of computational design none of the mutants showed the catalytic properties aimed for. Therefore, the following work focuses on solving the structure of human L-asparaginase 1 to further understand structure-function relations.

4.2.3 Structural analysis of human L-asparaginase

In order to obtain insight into the structure-function relations of human L-asparaginase 1 cryo-crystallography was applied to solve the protein structure.

Initial crystallization trials with the human full length enzyme hASNase1-fl failed to produce any crystals even in a large crystallization screen and formed solely precipitant or irregularly shaped aggregates. Therefore, crystallization attempts were continued with the truncated human enzyme hASNase1-tr. The motivation of this was that hASNase1-tr does not possess the additional ankyrin repeat domain only found in mammalian asparaginases. Ankyrin repeat domains are relatively flexible in conformation [Li et al., 2006]. This might hinder formation of protein crystals. In addition it is important to note, that in the crystallization setups for the homologous guinea pig asparaginase 1 the full-length enzyme was used. However, the solved structure only shows electron density for the L-asparaginase domain. The authors suggested

that proteolytic cleaving of the ankyrin domain is required for the formation of well ordered crystals [Schalk et al., 2014].
As for the full-length enzyme a variety of crystallization screens was applied to hASNase1-tr in order to find initial crystallization conditions. One promising hit is shown in Figure 19. Crystals obtained by crystallization screening were too small to use them for structure determination by X-ray crystallography. Therefore, the crystallization conditions had to be reproduced manually and adapted to a lager scale.

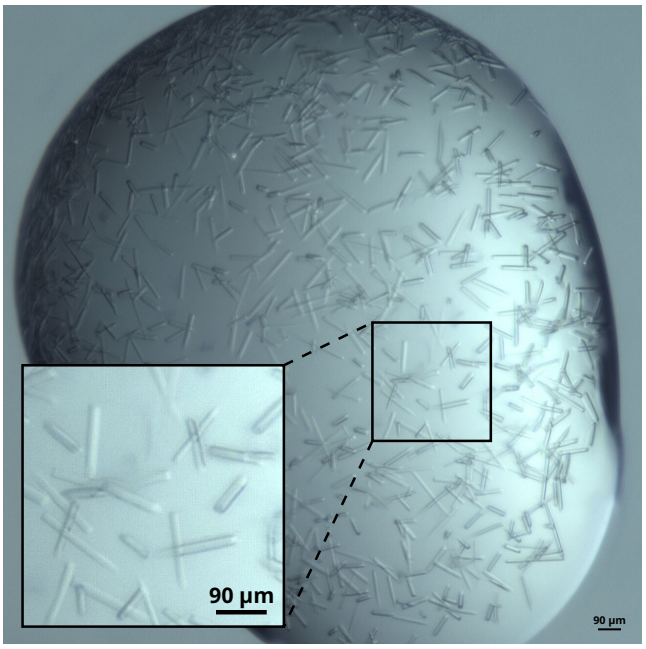

▲ **Figure 19: Initial hit obtained by crystallization screening.** The shown crystals grew in condition 86 of the ComPAS Suite (0.1 M MES pH 6.5, 1.6 M Magnesium sulfate). The enlarged image shows the marked area of the drop in detail. Initial crystals had a length of approximately 100 µm and had cylindrical shapes.

First, the crystal growth technique was adapted from sitting-drop to hanging-drop vapor diffusion for easier crystal handling. Additionally, different concentrations of the precipitant $MgSO_4$ and the enzyme as well as a pH range of the crystallization buffer MES and varying drop ratios were tested. To further improve the shape and size of the crystals an additive screen was performed. The best results were obtained from mixing 2 µL protein solution (24 mg/mL) with 2 µL well solution (1.5 M $MgSO_4$, 0.1 M MES pH 6.5) and adding 0.4 µL of the additive glycerol (30 % v/v) to the drop. Crystals grew at 20 °C after approximately seven days.
Figure 20 shows two images from X-ray diffraction data collection for hASNase1-tr carried out at beamline P14 at the DESY (Hamburg, Germany). The final crystals were approximately 400 µm large and had a long hexagonal shape. The diffraction pattern (Figure 20, B) extends to about 3 Å for the crystal shown in Figure 20A which corresponds to the final resolution obtained for the protein structure of hASNase1-tr.

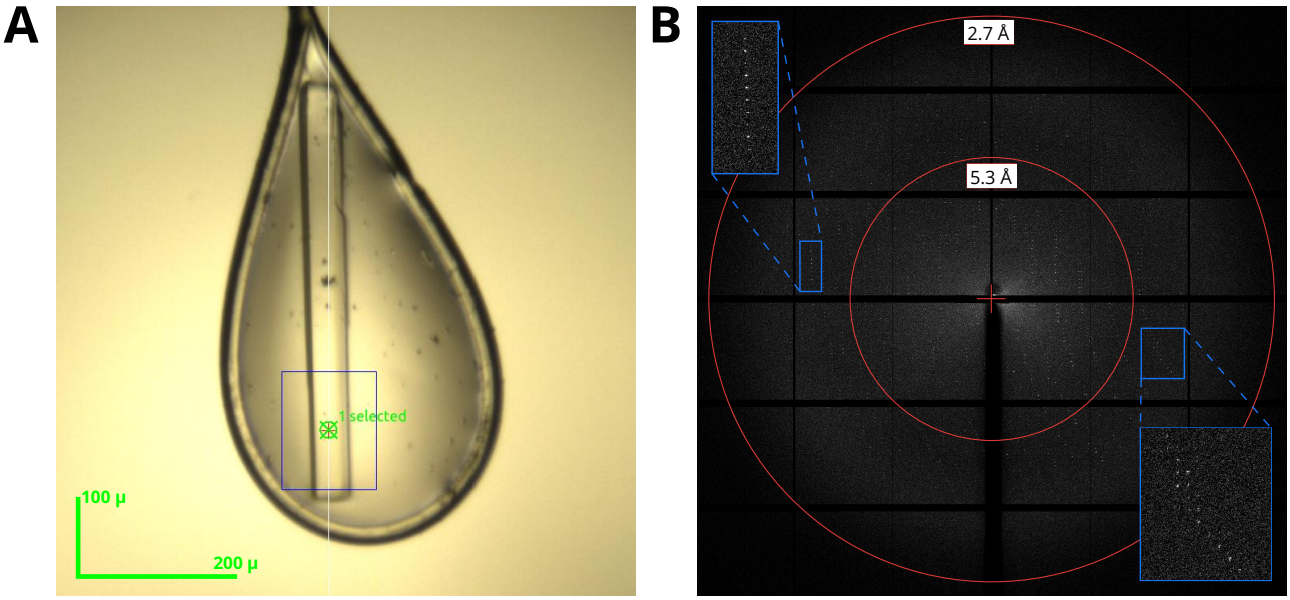

▲ **Figure 20: X-ray diffraction data collection for hASNase1-tr. (A)** The image shows a mounted crystal with a length of 400 µm which was fished in a nylon loop with 0.4 mm diameter. Marked in blue is the area of the X-ray beam. **(B)** The diffraction image shows a pattern with diffraction spots extending up to a resolution of approximately 3.0 Å obtained from the hASNase1-tr crystal shown in (A) using synchrotron radiation source (beamline P14, DESY, Hamburg, Germany). The enlarged images show the respective marked areas of the diffraction pattern in detail.

However, initial processing with unit cell constants a=131.110 Å, b=240.370 Å, c=92.600 Å, α=90.00 °, β=90.00 °, γ=90.00 ° in space group $C222_1$ failed due to translational noncrystallographic symmetry (tNCS). Therefore, the data set was reprocessed with a doubled c-axis, molecular replacement was performed and the atomic model was refined with R_{work}=29.8 % and R_{free}=38.5 % in space group $C222_1$ with six monomers in the asymmetric unit assembling into a tetramer and a dimer. Additional data collection and refinement statistics are given in Table 12.

▼ **Table 12: Data collection and refinement statistics for hASNase1.** The data for the highest-resolution shell are shown in parentheses.

Data collection	
Wavelength (Å)	0.689
Resolution range (Å)	61.83 - 3.0 (3.107 - 3.0)
Space group	$C222_1$
Cell dimensions	
α, β, γ (°)	90.0, 90.0, 90.0
a, b, c (Å)	131.17, 240.43, 185.38
No. total reflections	799051 (82046)
No. unique reflections	57851 (5111)
Redundancy	13.8 (14.2)
Completeness (%)	97.86 (87.73)
Mean $I/\sigma I$	11.53 (1.66)
Wilson B-factor	63.31
R_{merge}	0.2188 (2.009)
R_{meas}	0.2273 (2.083)
$CC_{1/2}$	0.997 (0.601)
Refinement	
Reflections used in refinement	57618 (5111)
Reflections used for R-free	2740 (248)
R_{work}	0.2977 (0.4022)
R_{free}	0.3845 (0.4135)
No. of atoms	
Macromolecules	14523
Ligands	0
Waters	0
Protein residues	1900
B factor (Å^2)	
Macromolecules	57.7
rmsd	
Bond lengths (Å)	0.003
Bond angles (°)	0.83
Ramachandran plot	
Outliers (%)	6.83
Allowed (%)	16.83
Favored (%)	76.34

The biological assembly of a hASNase1-tr tetramer is shown in Figure 21. The tetramer consists of four identical monomers of hASNase-tr and can also be described as a dimer of dimers. Thereby, the overall quaternary structure is identical to the structure of the previously discussed chimeric enzyme hgpASNase as well as published structure models of other asparaginases [Lubkowski and Wlodawer, 2021]. The monomers assemble as a dimer orienting the C-terminal domains of two adjacent monomers close to each other. The tetramer assembles by locating the N-terminal domains from the neighboring monomers next to each other. The resulting stacked arrangement of the monomers can be seen best in the side view of the tetrameric enzyme (Figure 21, right side).

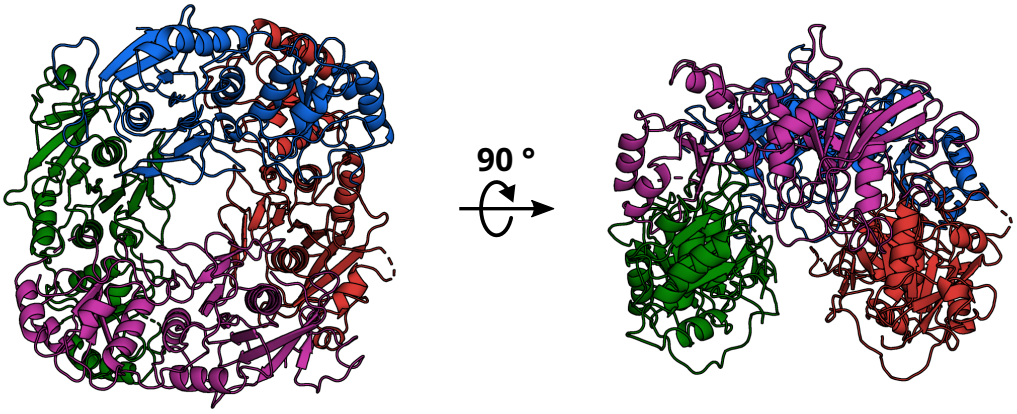

▲ **Figure 21: Tetrameric assembly of hASNase1-tr.** The homotetramer is formed by a dimer of two close dimers. The four monomers are colored in red, blue, green and violet respectively. The first image gives a top view of the enzyme and the second image shows a side view.

A closer look at one protomer of hASNase1-tr (Figure 22, A) gives insight into the tertiary structure of the enzyme's subunits which is also highly conserved (Chapter 1.1.3). Each protomer consists of two domains. The N-terminal domain is connected by an amino acid linker to the C-terminal domain. The main active site residues are located in the N-terminal domain of the enzyme. Close to this lies the potential allosteric site, which is formed primarily by the C-terminal domain. The residues participating in the additional binding of a substrate molecule have been first shown for the homologous *E. coli* asparaginase 1 [Yun et al., 2007] and are conserved in the human enzyme. An additional allosteric binding site for L-asparagine in hASNase1-tr would explain the observed allosteric behavior in enzymatic assays (Chapter 4.2.1).

The overall topology (Figure 22, B) of both domains is also very similar to previously published structure models [Swain et al., 1993]. The N-terminal domain is composed of an eight-stranded mixed β-sheet (Nβ1-Nβ6 and Nβ9-Nβ10) as well as two α-helices (Nα3 and Nα4) located between the two domains and three α-helices (Nα1-Nα2 and Nα5) facing the solvent. The second α-helix lies on an additional loop also previously described for the homologous mammalian asparaginase 1 from guinea pig [Schalk et al., 2014]. Furthermore, two antiparallel β-strands

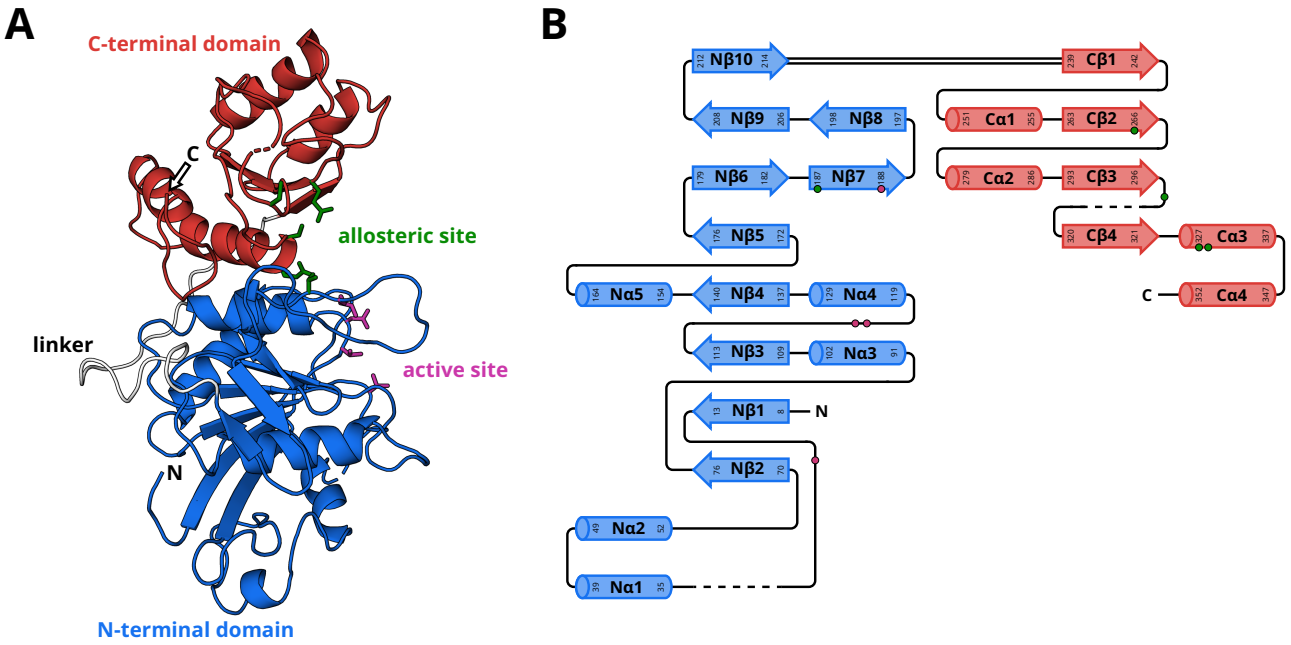

▲ **Figure 22: Protomer structure of hASNase1-tr. (A)** Cartoon representation of a hASNase1-tr protomer showing the N-terminal domain colored in blue and the C-terminal domain in red. Additionally, the N and C termini are indicated. The loop region acting as linker between the domains is depicted in white. Residues forming the active site are shown in stick representation and are colored in violet and residues of the allosteric site equivalent to the residues proposed for the homologous *E. coli* asparaginase 1 are colored in green. **(B)** Schematic representation of the protein topology for a protomer. The coloring is equivalent to (**A**). Beta strands are depicted as arrows while alpha helices are shown as cylinders. They are labeled referring to their domain and numbered consecutively. Secondary structure elements lying on the interdomain side of the two prominent beta sheets are located between the domains while secondary structure elements positioned on the solvent-exposed side of the beta sheets are located on the left and right edge. Colored dots mark the approximate location of the catalytic and allosteric residues. Dashed lines indicate loop regions which are not entirely resolved. Secondary structure assignment was performed using the *DSSP* program [Kabsch and Sander, 1983, Joosten et al., 2011].

(Nβ7-Nβ8) form a beta hairpin positioned toward the interior of the quaternary tetramer. On the other hand, the smaller C-terminal domain is only formed by a four-stranded parallel β-sheet (Cβ1-Cβ4) and two α-helices on either side (Cα1-Cα2 and Cα3-Cα4).

Figure 23 provides a closer look at the arrangement of the active site residues which have been shown to be crucial for catalysis and are invariant in most asparaginases: Thr19, Thr116, Asp117 and Lys188. It is important to note that the active site is missing the fifth main catalytic residue Tyr308' which is contributed by the adjacent monomer (annotated with an apostrophe ') and located in the C-terminal domain in mammalian asparaginases. However, as already shown in the view of the protomer and the topology plot (Figure 22) the loop containing the tyrosine is not entirely resolved and could therefore not be modeled completely.

As briefly described before, the potential allosteric site (Figure 24) is primarily formed by the C-terminal domain of the enzyme. The amino acids involved in the allosteric regulation are analogous to the residues in *E. coli* ASNase 1: Thr187, Glu266, Csy299, Ser327 and Glu328.

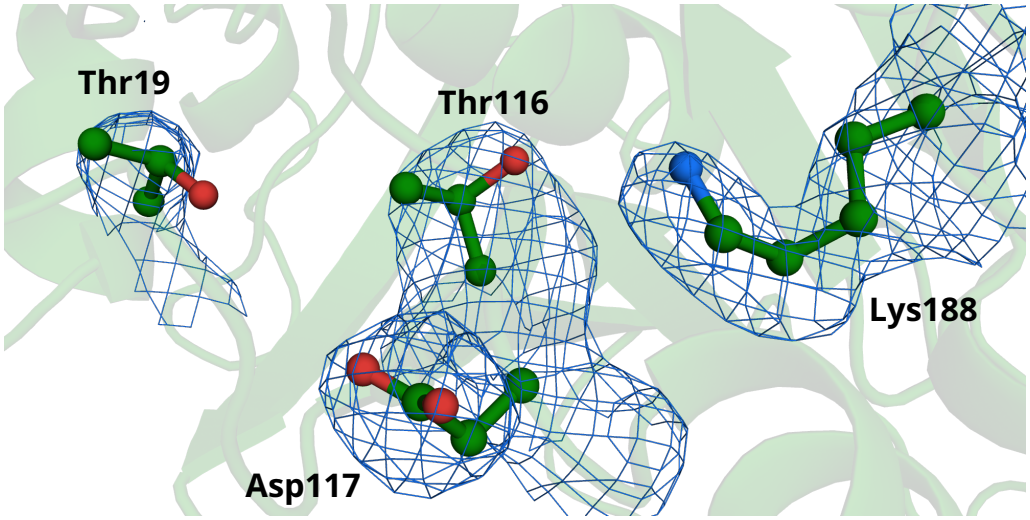

▲ **Figure 23: Active site of hASNase1-tr.** Active site residues are colored in green and shown in ball-and-stick representation. 2Fo-Fc omit map (level 1.0 σ) is shown in blue.

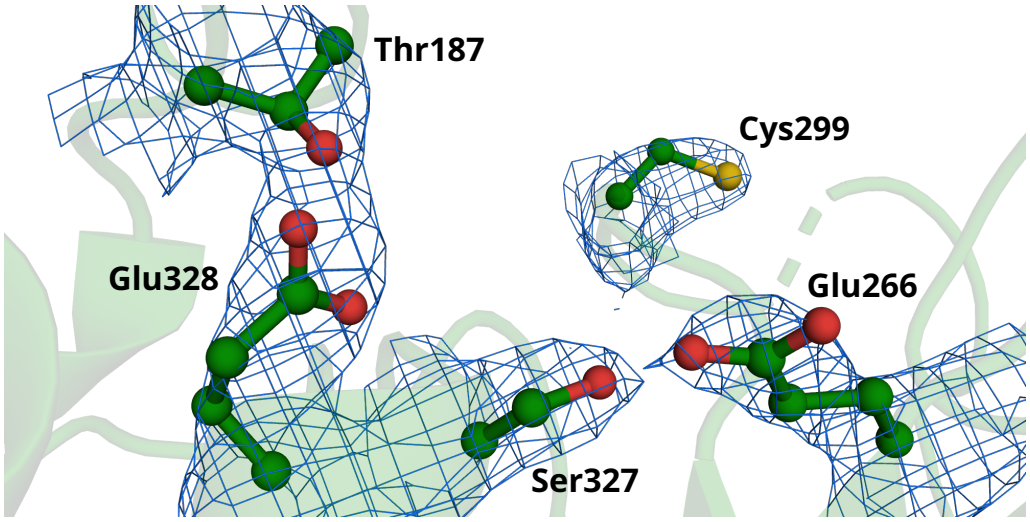

▲ **Figure 24: Location of proposed allosteric site in hASNase1-tr.** Residues of the allosteric site equivalent to the residues proposed for the homologous *E. coli* asparaginase 1 are colored in green and shown in ball-and-stick representation. 2Fo-Fc omit map (level 1.5 σ) is shown in blue.

Nonetheless, the structure for hASNase1-tr was only solved in the absence of the substrate L-asparagine as neither co-crystallization of the protein with substrate or the product L-aspartic acid nor soaking experiments with grown resting-state crystals were successful. Therefore, the identity of an allosteric site which is indicated by the allosteric behavior of hASNase wildtype enzymes in enzymatic assays could not be verified.

The obtained structure model for the human L-asparaginase 1 enzyme was compared with the previously determined protein structure of the chimeric protein hgpASNase-tr. An overlay of the protomers (Figure 25) shows two distinct regions which differ prominently between the two structures. The loop located in the N-terminal region is commonly referred to as the N-terminal

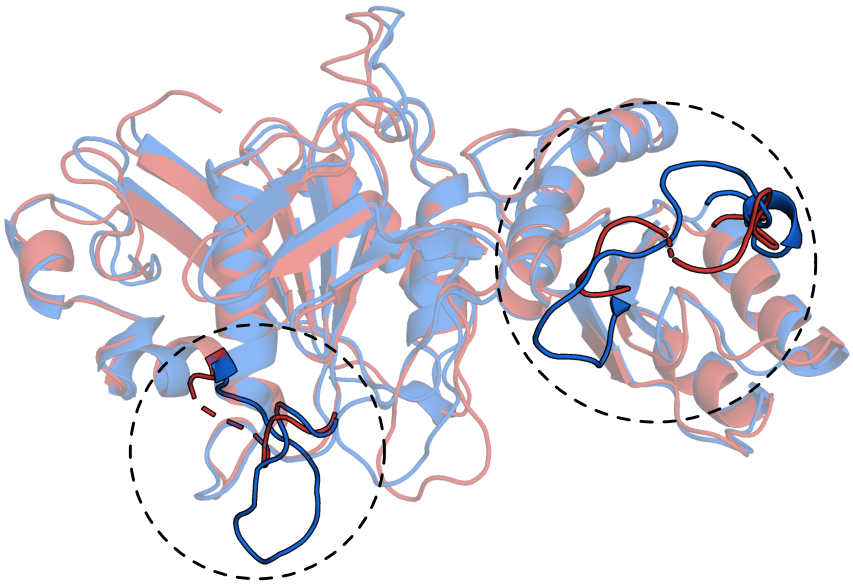

▲ **Figure 25: Structural comparison of hASNase1-tr with the chimeric hgpASNase-tr.** Overlay of a hASNase1-tr protomer (red) with a hgpASNase-tr protomer (blue). The most prominent differences are depicted in non-transparent colors and circled in black. In the N-terminal region (left) a flexible loop located close to the active site is not entirely resolved. A second loop located in the C-terminal domain is also missing seven amino acids. Both loops appear to be more flexible compared to the chimeric enzyme.

flexible loop [Nguyen et al., 2016]. It is usually disordered when the active site does not contain a ligand which is the case for the structure of the human asparaginase and could therefore not be resolved completely. A second loop in the C-terminal domain of the hASNase1-tr protomer is also not entirely resolved. As mentioned before it contains the catalytically important residue Tyr308' which is contributed to the active site of the neighboring protomer. The corresponding loop in hgpASNase-tr appears to be more rigid. This part of the chimeric enzyme originates from the sequence of the guinea pig enzyme gpASNase1. Both the chimeric and the guinea pig enzymes are not allosterically regulated and the C-terminal flexible loop is located close to the proposed allosteric site and even contains one of its residues (Cys299). This indicates that a less flexible conformation of the C-terminal loop as present in the chimeric and the guinea pig asparaginase could suppress the allosteric regulation.

4.2.4 Rational design of structure based variants

Based on the structural model obtained for the truncated human L-asparaginase 1 variants could be rationally designed. The focus lay on the aforementioned C-terminal flexible loop whose conformation differs significantly between the structures of hASNase1-tr and the chimeric enzyme hgpASNase-tr. A sequence alignment of the region of interest performed for three designed variants against hASNase1 and gpASNase1 is depicted in Figure 26. The first variant, called gp297-298, is a double mutant in which the first two amino acids of the diverging loop were exchanged by the respective residues from gpASNase1 (T297S/H298Q). A second interesting difference between the two enzymes immediately apparent from the sequence alignment is an insertion of two amino acids in hASNase1: Gly311 and Met312. As the two additional amino acids closely follow the catalytically active Tyr308 in sequence it was previously suggested that the insertion influences the dynamic properties of the C-terminal flexible loop [Schalk et al., 2014]. For this reason the gap was removed in the second variant gp310-312. In the third variant gp297-316, the complete loop from hASNase1 was exchanged by the corresponding sequence from gpASNase1 resulting in an exchange of ten amino acids and the removal of the two additional amino acids from hASNase1.

▲ **Figure 26: Multiple sequence alignment of C-terminal loop region.** The multiple sequence alignment was performed for hASNase1, the three rationally designed variants and gpASNase1. Marked in red are the amino acids residues which differ from the sequence of the human enzyme. A blue frame indicates the respective region in the variants which was exchanged for the amino acid residues from gpASNase1. The alignment was carried out using MAFFT [Katoh et al., 2019] with BLOSUM62 [Henikoff and Henikoff, 1992] as substitution matrix and visualized with Biotite [Kunzmann and Hamacher, 2018].

The three rationally designed variants were generated by introducing the mutations into the construct H14-bdSUMO-hASNase1-tr with help of Site-Directed Mutagenesis PCR using primers designed with the *NEBaseChanger* tool. In this case the truncated construct of the human enzyme was chosen as template because the structure of the full-length enzyme including the ankyrin domain could not be obtained. Rational design of the variants was therefore based on the comparison of the truncated human asparaginase with the previously obtained chimeric

protein structure which also does not possess an ankyrin domain.
Sufficient amounts with high purity of the three variants could be obtained by applying the established protocols for expression and purification. Afterwards, their activity was evaluated again using the coupled activity assay.

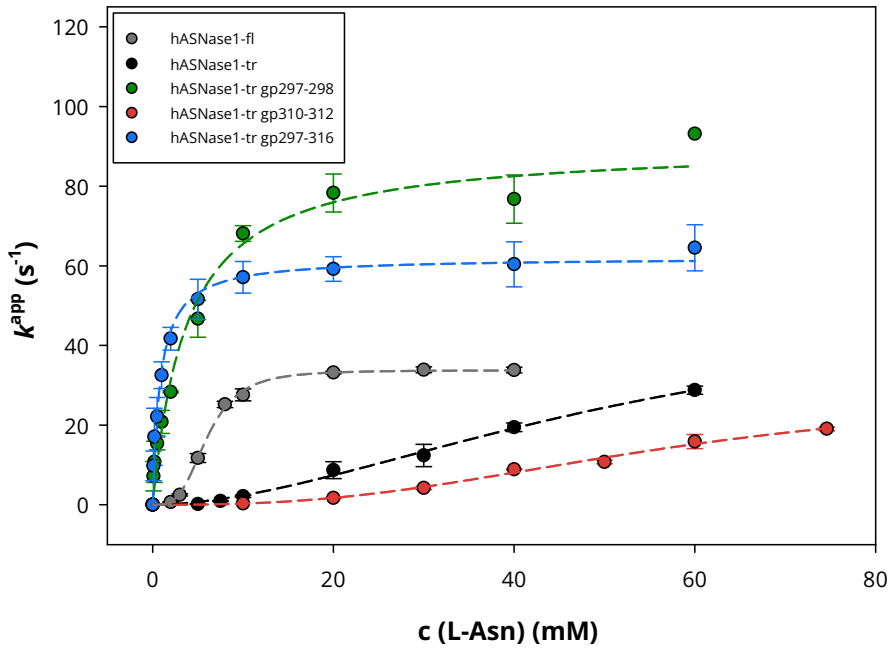

▲ **Figure 27: Activity of structure based variants of hASNase1-tr.** The calculated apparent reaction rate constant (k^{app} (s^{-1})) was plotted against the corresponding concentration of the substrate L-asparagine (mM). The data points were either fitted with a Michaelis-Menten (Eq. 4) or in case of a sigmoidal course of the reaction curve with the Hill equation (Eq. 3) (dashed lines).

The results were compared with the activity of the wild type enzyme hASNase1-tr (Figure 27). Whereas the variant gp310-312, where the two additional amino acids of the human enzyme compared to the guinea pig enzyme were removed, still shows cooperativity evidenced in a Hill coefficient greater than 1 and an even lower turnover rate, the other two rationally designed variants differ significantly from these catalytic properties. Both the double mutant gp297-298 and the variant gp297-316 where the complete loop was exchanged for the corresponding one from gpASNase1 no longer show a sigmoidal reaction curve. If fitted with the Hill equation (Eq. 3), the Hill coefficient n is close to 1. Therefore, the data points were again fitted with a Michaelis-Menten equation (Eq. 4) (Figure 27). From the fit, the parameters k_{cat} and K_M were obtained (Table 13). In contrast to the wild type enzyme the k_{cat} values are even higher while the substrate affinity is significantly improved depicted in considerably lower K_M values. For the double mutant the K_M value decreases by a factor of 14 and for the loop hASNase1-tr-loop variant the K_M value is 66 times lower than $S_{0.5}$ for the wild type protein.

▼ **Table 13: Comparison of catalytic constants for structure based variants.** The wildtype enzymes hASNase1-fl and hASNase1-tr as well as the variant gp310-312 are allosterically regulated resulting in the catalytic constants k_{cat}, $S_{0.5}$ and the Hill coefficient. In contrast to that the other two mutants, gp297-298 and gp297-316, follow Michaelis-Menten kinetics. Therefore, k_{cat} and K_M were obtained from the fit parameters of the Michaelis-Menten equation (Eq. 4). To compare the catalytic efficiency of the enzymes, k_{cat}/K_M was calculated.

Protein	k_{cat} (s^{-1})	K_M (mM)	**Hill coefficient n**	k_{cat}/K_M ($mM^{-1}s^{-1}$)
hASNase-fl	33.8 ± 0.3	6.0 ± 0.09 [a]	3.4 ± 0.14	5.6 [b]
hASNase-tr	53.7 ± 13.6	55.5 ± 15.5 [a]	1.8 ± 0.2	0.97 [b]
hASNase-tr gp310-312	29.0 ± 5.3	57.7 ± 8.8 [a]	2.6 ± 0.4	0.50 [b]
hASNase-tr gp297-298	90.4 ± 3.6	3.8 ± 0.6	N.A.	23.8
hASNase-tr gp297-316	62.1 ± 1.3	0.84 ± 0.09	N.A.	73.9

[a] Enzyme does not follow the Michaelis-Menten kinetics. The marked term is called $S_{0.5}$.
[b] Calculated from $S_{0.5}$ for comparison.

Hence, the rational design of structure based variants was successful. Already the double mutant T297S/H298Q shows a significant improvement in the catalytic properties and the loop variant possesses an even better activity than the wild type enzyme.

5 Discussion

5.1 Humanization of the chimeric asparaginase

The first approach to establish an asparaginase with favorable kinetic properties for the treatment of acute lymphoblastic leukemia was to further humanize the chimeric asparaginase hgpASNase-tr. In order to keep the side effects at a minimum the chimeric asparaginase was initially developed to have predominantly residues of human origin. Most of the C-terminal domain of the enzyme was exchanged with the sequence of gpASNase1. However, as the human and guinea pig enzyme already share a sequence identity of about 70 % the chimeric enzyme only differs in 31 amino acid positions from the human protein.

To achieve the goal of humanization without affecting the kinetic properties of the chimeric enzyme, amino acids in hgpASNase originating from gpASNase1 were mutated to the corresponding amino acids from hASNase1 consecutively. Thus, the three variants described in Chapter 4.1 were obtained. Only residues which are supposedly not critical were exchanged, meaning that they are located close to the surface of the enyzme and far enough from the active and the putative allosteric site of hASNase1 to neither influence activity nor lead to an allosteric regulation. In addition to that, the residues are not involved in interactions with the adjacent protomer (Figure 28).

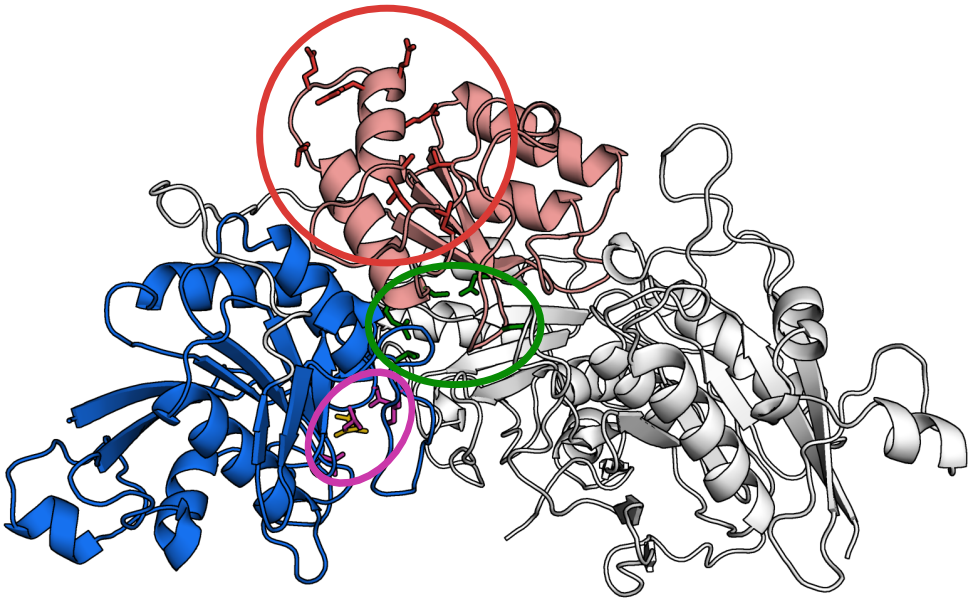

▲ **Figure 28: Location of mutated residues in hgpASNase-tr variants.** The N-terminal domain of one protomer of hgpASNase-tr is colored in blue while its C-terminal domain is depicted in light red. The second protomer of the intimate dimer is shown in white. Shown as sticks are the active site residues (violet), the residues of the putative allosteric site of cooperative asparaginases (green) and the mutated residues in hgpASNase-tr variants (red). The groups are encircled in the respective color to highlight them further.

The three tested variants of hgpASNase-tr showed no improvement in regard to kinetic properties but rather a significant decrease in the turnover rate for at least two of the tested variants and an even more critical decrease in affinity for the substrate. This results in a catalytic efficiency reduced by about 95 % for Mutant B and Mutant C compared to the chimeric enzyme. Even though the double-mutant (Mutant A) showed similar efficiency (74 %), exchanging merely two of the amino acids to the human equivalent only slightly humanizes the enzyme. In addition to that, the K_M of neither hgpASNase-tr nor its double-mutant is sufficient for the treatment of ALL.
It is important to note, that only nine positions in which hgpASNase-tr differs from hASNase1 were targeted at all and just three variants were tested. Considering that it is likely that certain amino acids act in mutual dependence all possible combinations of humanizing mutations would need to be tested to evaluate their impact on enzyme activity.

5.2 Modeling asparaginase variants with improved stability

Another approach to engineer a human asparaginase with improved kinetic properties was done applying computational enzyme design with help of the *Rosetta* software suite. Specifically, increasing the stability of an enzyme is a common goal in protein engineering. By assuming that the obtained structure for the chimeric asparaginase hgpASNase-tr represents the active folding state of a non-allosteric enzyme, a humanized structure model could be used as input for the pmut scan application of *Rosetta*. The goal was to find stabilizing single or double point mutations which result in a human variant without cooperativity. However, none of the three tested variants calculated by *Rosetta* showed the desired kinetic properties.
As for the previously discussed variants of the chimeric enzyme hgpASNase-tr (Chapter 5.1) the challenge of a computational approach is that the initial numerous hits have to be narrowed down significantly. Therefore, only a small subset of suggested variants was selected and even fewer mutants were tested. This leaves many more possibilities. The correct variant which stabilizes the enzyme and thereby prevents an allosteric regulation might simply not have been tested.
Additionally, the *Rosetta* pmut scan protocol has its limitations. On the one hand not all predicted mutations are stabilizing, on the other hand stabilizing mutations can be missed. One reason for this is, that the energy function of *Rosetta* is “imperfect” [Rosetta Commons, 2022b]. It does not accurately take all intra- and intermolecular interactions into account which can lead to wrong predictions regarding the stabilizing effect of mutants. Furthermore, the protocol does not allow backbone flexibility. This can have a negative influence on predication accuracy especially if the input model does not ideally represent the modeling target. Even though the chimeric enzyme hgpASNase-tr and the truncated human asparaginase hASNase1-tr share a high sequence identity, the C-terminal domain in which the putative allosteric site is located in

hASNase1 is of guinea pig origin. This could further affect the effectiveness of the modeling. Another explanation is that the structural input model of hgpASNAse-tr did not have a high resolution. While the *Rosetta* protocol recommends a resolution better than 2 Å, the input model only had a resolution of 2.8 Å. The *Rosetta* tutorial states that starting from poorer quality structures results in "less efficient and effective" modeling [Rosetta Commons, 2022a]. In addition to that the exact location and orientation of the mutated residues in the obtained structure of hASNase1 is not possible. Three of the residues are located in unresolved segments of the protein structure. Both E24G and V30G are close to the catalytically active Thr19 and lie on the same loop which is not completely resolved in the structure of the human enzyme. The same applies to T306Y being located in close proximity to Tyr308 which is contributed to the active site of the adjacent protomer. Both residues are also located on a flexible loop for which the electron density is not defined. Mutations in these parts of the enzyme and close to catalytically important residues could have an influence on structural organization and thereby the activity of the enzyme variants.

5.3 Structural conservation of active site

The active site residues are highly conserved in sequence among many asparaginases from all families and subgroups even though the enzymes posses varying catalytic properties. For example, the active site residues are conserved among the mammalian asparaginases gpASNase1 and hASNase1 as well as the bacterial enzymes from *Escherichia coli* and *Erwinia chrysanthemi* (EwASNase) (Figure 2). A difference lies in the catalytic tyrosine residue of mammalian asparaginases which is contributed by the C-terminal domain of the adjacent monomer while it is located in the N-terminal domain in the bacterial enzymes.
The newly solved crystal structures of hASNase1-tr and the chimeric enzyme hgpASNase-tr reveal that the active sites of both enzymes also share close structural similarity with the previously published structure of the guinea pig asparaginase gpASNase1 (Figure 29).

▼ **Table 14: RMSD between active site residues of hgpASNase-tr and hASNase1-tr to gpASNase1 residues.** The structures of the three enzymes were superimposed with Pymol and the RMSD between the active site residue atoms (excluding backbone atoms) of gpASNase1 and hgpASNase-tr or hASNase1-tr was calculated with *Biotite* [Kunzmann and Hamacher, 2018].

	RMSD (Å) to gpASNase1 residue					
	Thr19	Thr116	Asp117	Lys188	Tyr308'	ligand
hgpASNase-tr	0.92	1.50	1.33	0.54	17.14	1.23
hASNase1-tr	1.54	1.82	1.62	2.72	N.A.	N.A.

Especially the catalytic residues Thr19, Asp117 and Lys188 are close to each other in location and orientation (Table 14). However, the latter is organized in a more compact conformation in the human enzyme in comparison to the extended structure in hgpASNase-tr and gpASNase1

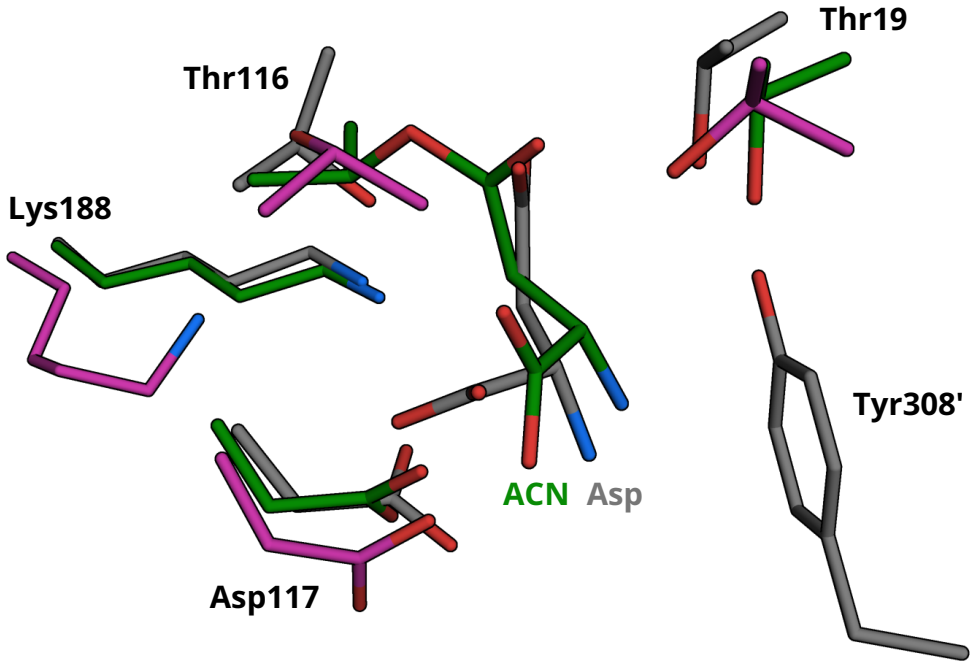

▲ **Figure 29: Overlay of active sites of hASNase1-tr and hgpASNase-tr and guinea pig asparaginase 1 in complex with aspartic acid.** The acrive site residues of hASNase1-tr are represented by violet sticks. Depicted in green are the active site residues of the chimeric asparaginase hgpASNase-tr with the covalently bound acyl intermediate (ACN). The active site residues of guinea pig asparaginase 1 (PDB ID: 4R8L) are shown and labeled in grey with a bound aspartic acid (Asp). An apostrophe (') marks the tyrosine residue contributed to the active site by the neighboring protomer of the intimate dimer.

resulting in a higher RMSD (2.72 Å) . Another apparent difference between the three structures is the localization of the catalytic tyrosine residue. In the human enzyme structure the amino acid could not be modeled because part of the C-terminal loop where it is located is not resolved. It was shown before for the homologous gpASNase1 that the C-terminal loop containing the catalytic tyrosine is quite flexible in the apo-structure of the enzyme. Upon binding of the substrate the loop becomes more ordered and Tyr308' occupies an orientation pointing towards the active site [Schalk et al., 2014]. This would also be expected for the structure of the chimeric asparaginase hgpASNase-tr in complex with a covalently bound acyl-intermediate. However, in the obtained structure the catalytic tyrosine is not located in close proximity to the active site. The RMSD between the active site residue Tyr308' of gpASNase1 and of hgpASNase-tr is remarkably high with 17.14 Å. This shows, that the C-terminal loop did not become ordered upon binding of the substrate in the chimeric enzyme structure. The B-factor diagram (Figure 30, B) also depicts high B-factor values for the respective C-terminal loop underpinning that this region of the enzyme is strikingly flexible. However, as the lattice of protein crystals often only allows very small motions, conclusions on protein dynamics have to be considered carefully and protein structures determined with X-ray crystallography do not necessarily depict the conformation of proteins in solution.

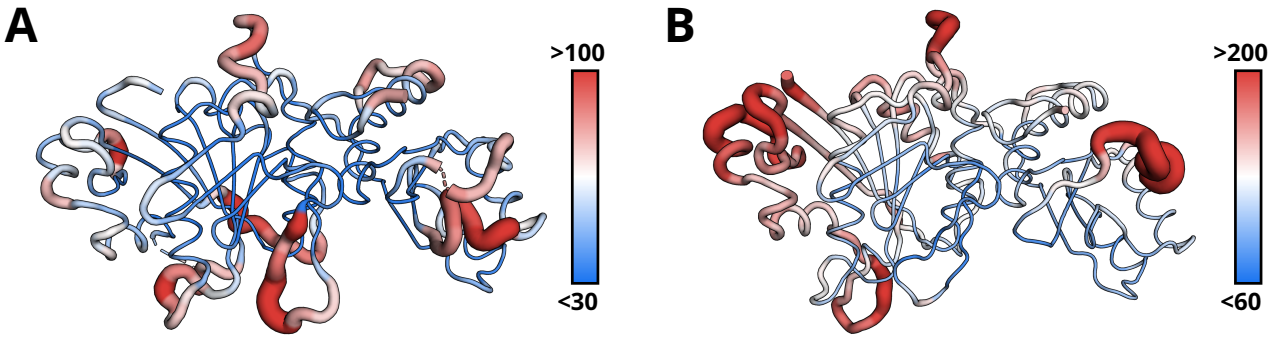

▲ **Figure 30: B-factor diagram of protomeric hASNase1-tr (A) and hgpASNase-tr (B).** The B-factors values are illustrated by color, ranging from low (blue) to high (red), and by wideness of the tubes.

As mentioned before, the structure of hgpASNase-tr was modeled in complex with an acyl-intermediate of the substrate which is covalently bound to the threonine residue at position 116. In contrast to that the published structure of gpASNase1 contains a non-covalently bound aspartate molecule. Both ligands share a similar location inside the active site, however, they are rotated against each other, resulting in a RMSD of 1.23 Å. In addition to that, the position of Thr116 which supposedly acts as primary nucleophile in the chimeric enzyme forming the covalent bond to the substrate slightly differs in gpASNase1 and hgpASNase-tr. In the human enzyme the residue is additionally flipped facing away from a potential ligand.

5.4 Covalent intermediate in the active site

In 1996 the first crystal structure of an L-asparaginase in complex with aspartic acid bound as a covalent acyl-enzyme intermediate (AEI) was published [Palm et al., 1996]. This finding supported the proposal that the hydrolysis of asparagine by L-asparaginases follows a double-displacement mechanism. However, subsequent to the work no further analysis of the reaction mechanism was done. In addition to that, several other reports put the previous results into question as their research findings either supported the single-displacement mechanism [Gesto et al., 2013] or were not able to reproduce crystal structures with bound covalent intermediates for several catalytically deficient L-asparaginase enzymes [Schalk et al., 2016].
Recently, an extensive study again strengthened the proposition of a double-displacement mechanism [Lubkowski et al., 2020]. Various of the published structures of *E. coli* asparaginase 2 variants which catalyze hydrolysis of asparagine at a low rate contained covalently bound acyl intermediates.
The newly solved structure of the chimeric asparaginase hgpASNase-tr was also modeled with a covalent intermediate in the active site. However, contradictory to the previously published structures of *Ec*ASNase2 the covalent bond is not formed between the C^{γ} of the substrate

and O^{γ} of Thr12 corresponding to Thr19 in hgpASNase. Instead, the covalent bond is formed between the substrate and Thr116 which corresponds to Thr89 in *Ec*ASNase2 (Figure 31). Yet, it is important to note that the resolution of the structure of hgpASNase-tr with 2.8 Å is relatively low and no water molecules were modeled into the electron density. Therefore, it is not possible to observe mechanistic details. Furthermore, the electron density map was interpreted to contain a covalent acyl intermediate on basis of the observed positive electron density in the Fo-Fc omit map (Figure 11). Even though the distance between Thr116 and the ligand is shorter than that between Thr19 and the ligand, the electron density extends towards both residues. Additionally, as mentioned before in Chapter 5.3 the fifth catalytically active residue Tyr308', contributed to the active site by the neighboring protomer of the intimate dimer, is not located in close proximity to the active site as would be expected in the substrate-bound conformation of the enzyme. Hence, the interpretation of the positive electron density in the active site is not without doubt and does not serve as proof that type 1 asparaginases as hASNase1 and gpASNase1 or asparaginases in general catalyze the hydrolysis of asparagine in a double-displacement mechanism.

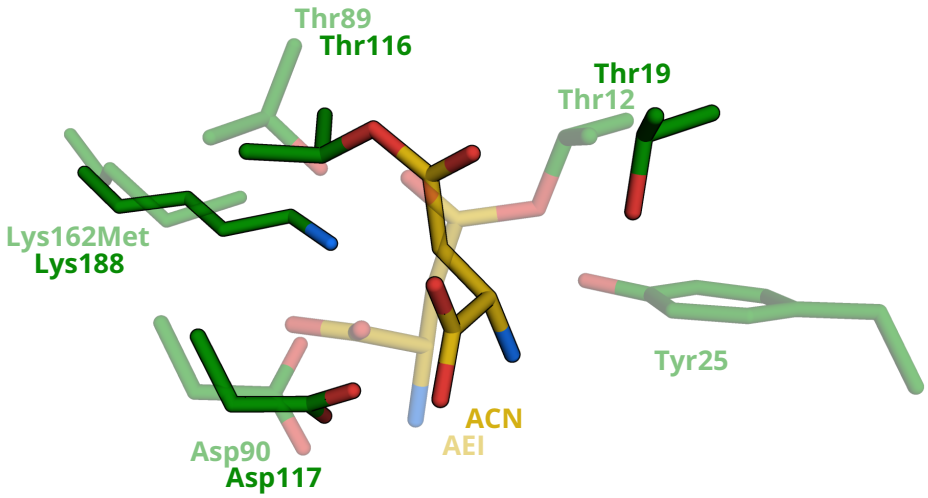

▲ **Figure 31: Overlay of active sites of hgpASNase-tr and *E. coli* asparaginase 2.** Depicted in green are the active site residues of the chimeric asparaginase hgpASNase-tr with the covalently bound acyl intermediate (ACN, yellow). The active site residues of the *Ec*ASNase2 mutant K162M (PDB ID: 6V25) are shown and labeled in light green in complex with a covalent acyl-enzyme intermediate (AEI, light yellow).

5.5 Insights into allosteric regulation

Another characteristic of some asparaginases which is still under debate is the additional allosteric regulation of the enzyme by its substrate asparagine. This has been observed for the high K_M asparaginase from *E. coli* [Yun et al., 2007], *Ec*ASNase 1, as well as the type 1 enzyme from *Saccharomyces cerevisiae* [Costa et al., 2016] and a thermostable asparaginase from *Anoxybacillus flavithermus* [Maqsood et al., 2020]. However, the allosteric regulation is not a property shared by all asparaginases of type 1. For instance, neither the *Pyrococcus furiosus* L-asparaginase *Pf*ASNase1 [Bansal et al., 2012] nor the mammalian guinea pig asparaginase 1 (gpASNase1) seem to be allosterically regulated [Schalk et al., 2014].

Until recently, the only determined structure of an allosteric asparaginase was obtained for *Ec*ASNase 1. The crystal structure of *Ec*ASNase 1 (PDB ID: 2P2N) did not only accommodate asparagine as substrate in the active sites but also in another region of the protein with residues predominantly located in the C-terminal domain of the protomer but close to the interface of an intimate dimer [Yun et al., 2007].

During the work on this thesis, it was shown again in enzymatic assays that the human asparaginase 1 (hASNase) does not follow Michaelis-Menten kinetics, suggesting an allosteric regulation. More importantly, the crystal structure of hASNAse1 could be solved albeit at the relatively low resolution of 3.0 Å. However, the structure was only obtained in the enzyme's *apo* state.

Nevertheless, the overlay of the allosteric site residues from *Ec*ASNase 1 with the corresponding amino acid residues from hASNAse1 suggests how the putative allosteric site for the human enzyme in complex with the allosteric regulator asparagine could be formed (Figure 32).

Thr187 and Glu328 are both conserved in sequence and share close structural conservation in the overlay with *Ec*ASNase1. Even though a serine (Ser327) residue is found instead of a valine (Val302), the residues have the same orientation and the backbone amino group could form a hydrogen bond to the substrate. Another key difference in the putative allosteric site of the human enzyme is Glu266 in contrast to Arg240 in the *E. coli* asparaginase. One of the O^{ϵ} atoms of Glu266 is positioned in the same location as N^{ϵ} in Arg240 which makes an interaction with the bound substrate. Assuming that the glutamate residue is deprotonated and the O^{ϵ} is negatively charged under physiological conditions, this would hinder the formation of a hydrogen bond to asparagine due to electrostatic repulsion.

The two remaining residues, Thr297 and Cys299, are also conserved in sequence. However, they are located on a loop which is quite flexible in the human enzyme. The distances from the backbone oxygen atoms of threonine and serine to the N atom of the substrate are 5.8 Å and 9.0 Å respectively. Therefore, they are not positioned in close proximity to the ligand and could not stabilize the asparagine substrate in this structural conformation.

Nevertheless, even though a cooperativity was observed in enzymatic assays for hASNase1

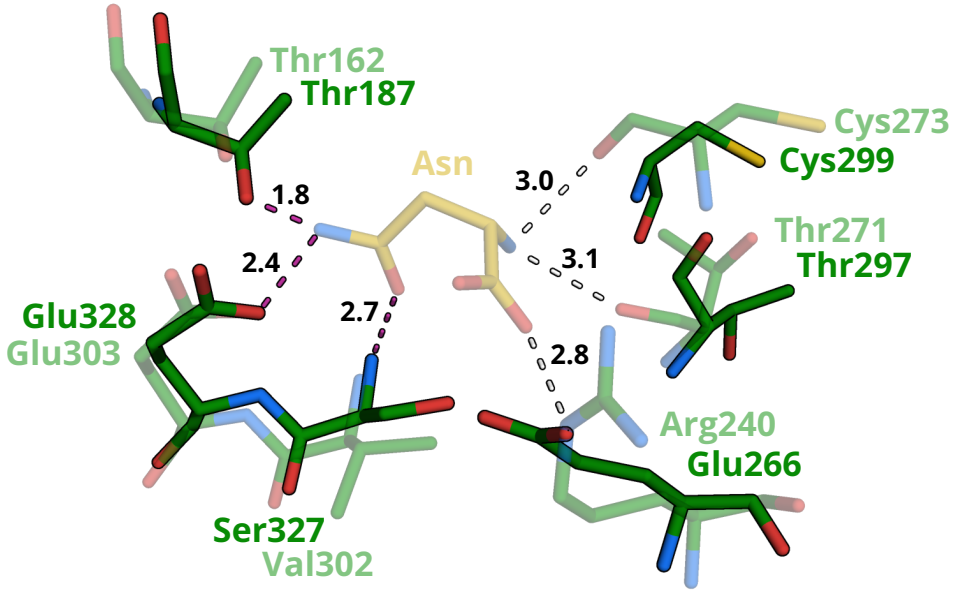

▲ Figure 32: Overlay of allosteric site of *E.coli* ASNase 1 and putative allosteric site in hASNase1. The residues of the allosteric asparagine binding pocket of *E. coli* asparaginase 1 (PDB ID: 2P2N) are shown and labeled in light green, while the bound asparagine ligand (Asn) is shown in light yellow. The corresponding amino acid residues in hASNase1 are depicted in green. Dashed white lines indicate the hydrogen bonding interactions between the ligand and residues von *E. coli*, whereas dashed violet lines indicate the interactions which could also be made between Asn and residues from hASNase1. The distances are labeled in Å.

which strongly indicates an allosteric regulation, the obtained structure does not serve as clear evidence for the identity of the allosteric site as only a structure of the apo enzyme was solved. A second aspect to look at regarding the allosteric regulation of asparaginases is the observed change in shape of the quaternary structure assembly of the allosteric *Ec*ASNase1 upon binding of a ligand. As observed by Yun et al. [Yun et al., 2007] the monomers of the *E. coli* asparaginase are located closer together when aspartic acid is bound to the enzyme. Thereby, the overall shape transfers from an open, doughnut shaped structure into a much more compact conformation (Figure 33, A). Arguably, *Ec*ASNase1 is the only asparaginase enzyme so far for which such a change in the tetrameric arrangement was observed. The low-K_M-asparaginase *Ec*ASNase2 retains a compact packing of the monomers regardless of the absence or presence of a ligand, while the mammalian asparaginase gpASNase1 which also has a high affinity for asparagine keeps a doughnut shaped conformation upon binding of a ligand (Figure 33, B).
For both hASNase1 as well as the chimeric enzyme hgpASNase in complex with asparagine the crystal structures revealed an open conformation (Figure 33, C and D) resembling the doughnut-shape of gpASNase1 and *Ec*ASNase1 in absence of a ligand. However, neither a structure of hASNase1 with a ligand bound to the putative allosteric site nor an apo structure of hgpASNase could be obtained. Therefore, it is not possible to determine, whether either of the enzymes is subject to a change in conformation upon binding of a ligand. Furthermore,

assumptions about protein dynamics based on crystallographic data always have to be made with extreme caution. Certain conformations could only be owed to the crystal packing rather than depicting the actual protein folding in solution. A notable example for this are the crystal structures of *Ec*ASNase1. The crystals for the determination of the *apo* structure (PDB 2P2D) and the protein structure in complex with aspartic acid (PDB 2P2N) were grown under quite different crystallization conditions and the structures possess completely different unit cells [Yun et al., 2007]. Therefore, it is uncertain if the conformational change was just observed due to a crystallization artifact. Such findings on protein dynamics would need to be verified by obtaining data from protein solutions applying for example fluorescence resonance energy transfer (FRET).

Nevertheless, if a change in the quaternary structure upon binding of a ligand should prove to be characteristic for allosteric L-asparaginases, it would be expected for hASNase1 but not for the chimeric enzyme and could serve as an identifier of additional asparaginase enzymes which are allosterically regulated.

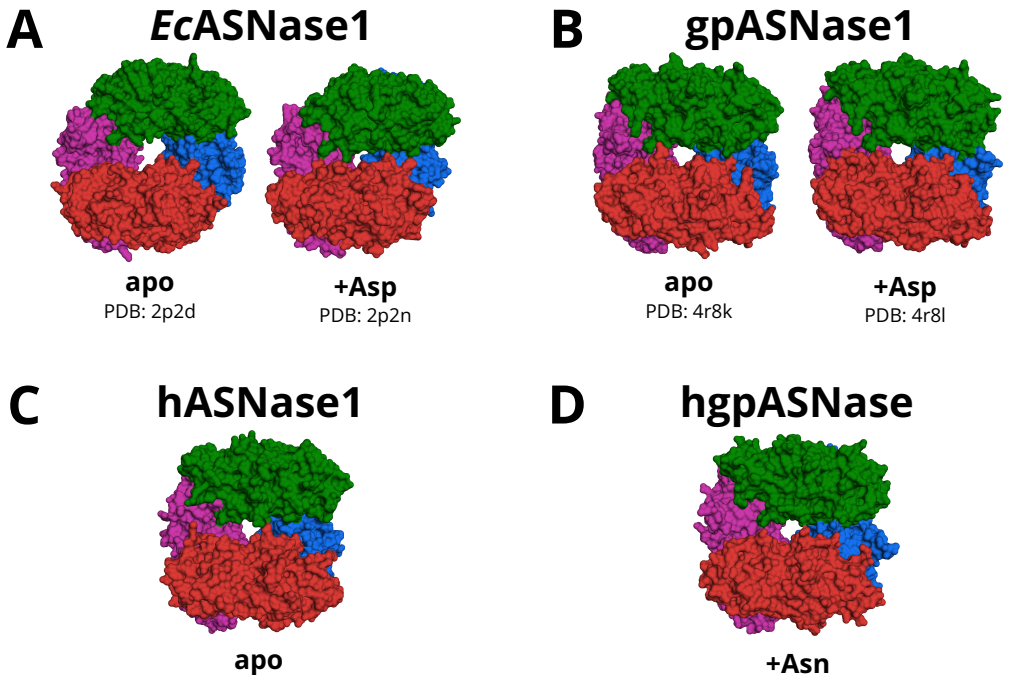

▲ **Figure 33: Quaternary structure assembly of L-asparaginases in comparison.** Each protomer of the tetrameric enzymes is colored differently (red, blue, green, violet). The structures were aligned in Pymol and are shown in the same orientation. While the *E. coli* enzyme 1 adopts a more compact form upon binding of a ligand (**A**), the asparaginase from guinea pig keeps an open, doughnut shaped conformation in the presence of a ligand (**B**). hASNase1 displays the same open conformation in the absence of a ligand (**C**) as does the chimeric enzyme hgpASNase in complex with asparagine (**D**).

5.6 Improvement of hASNase1 activity

Based on the assumption that certain loops of the asparaginase structure play a role in the regulation of the active site, exchanges to the amino acids from gpASNase1 were introduced into a C-terminal loop region which is partly not resolved in the crystal structure of hASNase1 (Figure 34, A). In addition to the missing electron density definition for seven amino acids, the relatively high B-factors in this region compared to the overall structure (Figure 30, A) indicate a higher flexibility than for the guinea pig enzyme gpASNase1. As the loop does not only include the catalytically active Tyr308, but also two of the residues of the putative allosteric site of the human enzyme it could both influence the activity of the asparaginase as well as contribute to allosteric regulation.

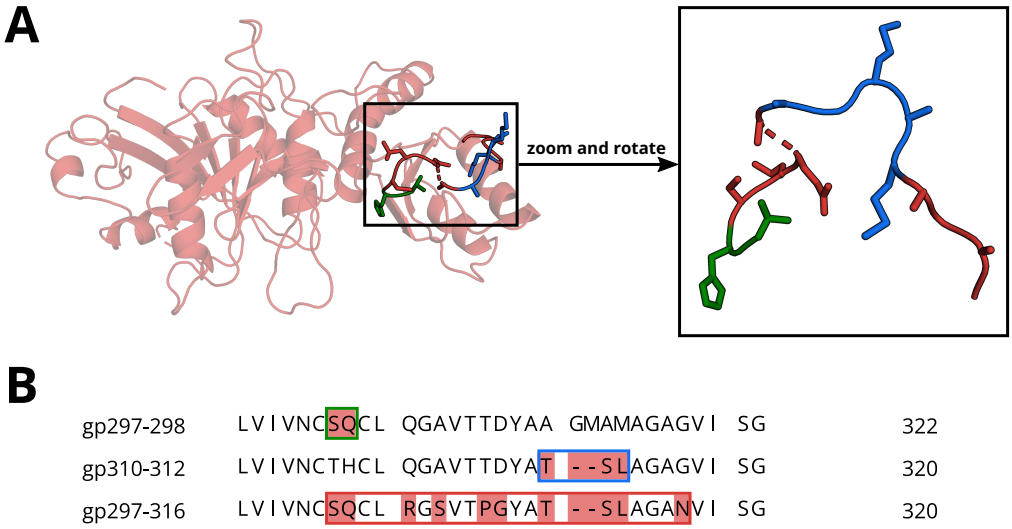

▲ **Figure 34: Location of modified C-terminal loop region in an hASNAse1-tr protomer and introduced variants. A** gives an overview of an hASNAse1-tr protomer with the location of the C-terminal loop which was modified, as well as a zoomed in figure of the loop. The coloring was done according to **B** which shows the sequences of the loop region for the three rationally designed variants of hASNase1-tr. Marked in light red are the residues which were exchanged by the corresponding amino acids from gpASNase1.

Furthermore, the loop in hASNase1 contains one of the major sequence differences compared to gpASNase1 as the human enzyme has a two-residue insertion with glycine at position 311 and methonine at position 312. As suggested by Schalk et al. the additional amino acids might modify the dynamic properties of this region which is also important for catalysis as mentioned before [Schalk et al., 2014].

Therefore, the variant gp310-312 (Figure 34, B) was designed in a way to remove the two additional amino acids and exchange the adjacent amino acids for the corresponding residues from gpASNase1. However, the resulting variant showed a significant decrease of the turnover rate compared to the truncated wild type enzyme from 53.7 s^{-1} to 29.0 s^{-1}. Meanwhile, the K_M for the substrate did not change measurably and the allosteric behavior of the human enzyme is

still present. The kinetic properties of gp310-312 indicate that the insertion in hASNase1 does not result in a lower affinity for the substrate and does not alone cause the cooperativity but might influence the overall activity of the enzyme.

In addition to the previously discussed removal of the insertion in hASNase1, a variant which exchanges the first two amino acids of the loop to the corresponding residues from gpASNase1 was constructed. The variant called gp297-298 (Figure 34, B) no longer displays an allosteric regulation in the activity assays. More importantly, it possesses significantly better affinity for the substrate and additionally an increased k_{cat} value, resulting in a 24 times higher catalytic efficiency.

Interestingly, the cooperativity of the human enzyme is already removed with this double point mutation. An explanation for this might be, that one of the exchanged residues T297 belongs to the putative allosteric site of hASNase1. However, as the alternative serine residue is highly similar to threonine and the hydrogen bond is theoretically formed by the backbone oxygen atom as shown for the *E. coli* asparaginase 1 a serine should still be able to form a hydrogen bond to an asparagine in the allosteric site. Additionally, the following histidine is exchanged by a glutamine. The effect of this is not clear as structural information on a possible rearrangement of the allosteric site in the variant is not available. Furthermore, it is important to note that both the allosteric *Ec*ASNase1 and the non-allosteric gpASNase1 contain a glutamine residue at this position (Figure 2, Glu298 in gpASNase1 and Glu263 in *Ec*ASNase1). This suggests that the exchange of histidine to glutamine in the hASNase1 double variant does not influence the allosteric behavior.

In the third rationally designed variant gp297-316 (Figure 34, B) the complete loop was exchanged by the sequence from gpASNase1 resulting in an exchange of ten amino acids and the removal of the previously discussed two-residue insertion in the human enzyme. This mutant is also not allosterically regulated and the affinity for the substrate is even higher than for the double mutant. Even though the turnover rate is only slightly better than for the truncated wildtype enzyme hASNase1-tr this results in a catalytic efficiency 75 times higher than for hASNase1-tr. At the concentration of L-asparagine in the human blood of 50 µM the reaction velocity of the variant gp297-316 is increased by a factor of almost 20,000 compared to the truncated wildtype enzyme. This context again demonstrates the importance of engineering a non-allosteric regulated hASNase asparaginase in the first place.

However, comparing the catalytic efficiency with the one of the therapeutic enzymes from *Escherichia coli* (*Ec*ASNase2) and *Erwinia chrysanthemi* (EwASNase) reveals that the catalytic properties of the variant gp297-316 are still far from optimal. The therapeutic enzymes have a catalytic efficiency which is 47 times higher for *Ec*ASNase2 and even 62 times higher for EwASNase. Especially the K_{M} needs to be further improved.

It is important to note, that the mutations were only introduced into the truncated hASNase1

enzyme. As the full-length enzyme with ankyrin domain showed considerably better catalytic properties (Table 15) than hASNase1-tr, the double point mutation from gp297-298 as well as the complete loop exchange (variant gp297-316) should be introduced into the full-length construct hASNase1-fl to evaluate the effect of the mutations. This might provide an even more active human L-asparaginase variant for therapeutic use.

▼ **Table 15: Comparison of kinetic constants of different L-asparaginases.** Given are the turnover rate k_{cat}, the Michaelis constant K_M, the Hill coefficient n and for non-allosterically regulated enzymes the catalytic efficiency k_{cat}/K_M. For better comparison between allosteric and non-allosteric L-asparaginases, $V_{50\mu M}$ gives the calculated reaction velocity at a substrate concentration of 50 µM which corresponds to the L-asparagine level in the human blood.

Enzyme	k_{cat} (s^{-1})	K_M (µM)	**Hill coefficient** n	k_{cat}/K_M ($\mu M^{-1}s^{-1}$)	$V_{50\mu M}$ (s^{-1})
*Ec*ASNase2 [a]	48.9 ± 0.6	14.9 ± 1.3	N.A.	3.28	37.7
EwASNase [a]	207.5 ± 3.6	47.5 ± 3.5	N.A.	4.37	106.4
gpASNase1[a]	38.6 ± 1.4	57.7 ± 6.4	N.A.	0.67	17.9
hgpASNase-tr[c]	25.7 ± 0.9	135.8 ± 19.1	N.A.	0.19	6.9
hASNase1-fl [c]	33.8 ± 0.3	6000 ± 90 [b]	3.4 ± 0.1	N.A.	$2.9 \cdot 10^{-6}$
hASNase1-tr [c]	53.7 ± 13.6	55500 ± 15500 [b]	1.8 ± 0.2	N.A.	$177.1 \cdot 10^{-6}$
gp297-316 [c]	62.1 ± 1.3	840 ± 90	N.A.	0.07	3.5

[a] Data taken from [Schalk et al., 2014]

[b] Enzyme does not follow the Michaelis-Menten kinetics. The marked term is called $S_{0.5}$.

[c] Data obtained during this Ph.D. thesis

N.A.: not applicable

In summary, these findings indicate that the C-terminal loop which shows a different structural organization in the obtained structure of hASNase1 plays a role in the allosteric regulation of the human enzyme and also attributes to the low affinity for the substrate asparagine. The impact of the insertion in hASNase1 on the catalytic properties of the enzyme remains unclear. While the removal of the additional amino acids alone resulted in a less efficient enzyme, the exchange of the complete loop including the insertion showed significantly improved catalytic properties. This indicates an interaction or dependence between exchanged amino acid residues which is not yet understood.

Furthermore, as none of the variants could be crystallized to date an estimation of the dynamic properties of the respective modified loops cannot be made for now.

6 Conclusion and outlook

In the present work a novel crystal structure for the previously not structurally characterized human L-asparaginase hASNase1 was solved. It was shown that not only the sequence is highly conserved among different L-asparaginases but also that the entire structure and especially the active site architecture shares close similarity to previously published L-asparaginase structures. As the structure was obtained for the truncated enzyme lacking the ankyrin domain, the question remains which role this additional domain unique for mammalian asparaginases has.
The second structural model for the human-guinea pig chimera provided in this work indicates the involvement of a covalently bound substrate molecule in the catalyzed reaction. This would support the double-displacement mechanism suggested for L-asparaginases.
The comparison of the two obtained structures showed that the C-terminal loop region is critical for allosteric regulation. These findings enabled the rational design of structure-based variants of the human asparaginase which possess improved catalytic properties compared to the wild-type enzyme. Most importantly, two of the variants no longer show an allosteric regulation in the performed activity assays.
It remains unclear which of the specific single mutations are relevant for the changed behavior. To identify the important residues, the kinetic properties of the successful variants should be tested separately especially for the double point mutant. Additionally, introducing the mutations into the full-length enzyme hASNase1-fl could provide an even more active human L-asparaginase. Furthermore, crystallization and subsequent structure determination of the variants would help to elucidate the dynamics involved in catalysis.
Interestingly, the variant of hASNAse1-tr E266L/H298Q calculated by the *Rosetta* software suite overlaps with the promising rationally designed double point mutant T297S/H298Q. As the suggested Rosetta variant was not tested, it would be worthwhile to investigate whether it shares the improved catalytic properties including removed allosteric regulation.
It is important to note, that even though the engineered structural variants of hASNase1-tr surpass the wildtype enzyme, their catalytic properties are still far from attaining the kinetic constants of the pharmaceutical bacterial asparaginases. Further optimization of the sequence is necessary to primarily improve the affinity for the substrate. At the same time, it is crucial to limit the deviation from the human sequence to a minimum in order to keep the immunogenicity of potential therapeutic enzymes low. Moreover, preventing a severe immune response during treatment of acute lymphoblastic leukemia might allow the administration of higher or more frequent doses compared to drugs with bacterial origin. This could compensate for a substrate affinity which is lower than that of currently established asparaginase medications. To assess the therapeutic potential of developed variants of hASNase1, the extent to which an immune response is triggered needs to be evaluated in model cell lines.
It is still debated whether the additional glutaminase activity observed for some L-asparaginases

is therapeutically necessary or conversely dispensable and even harmful by causing various other side effects. Nevertheless, it is still relevant to also test potential future drug candidates for additional glutaminase activity and to assess the extent in comparison to asparagine depletion. Summarizing the results covered in the present work, important steps towards the development of a therapeutically suitable human L-asparaginase for the treatment of acute lymphoblastic leukemia were made.

References

[Afonine et al., 2012] Afonine, P. V., Grosse-Kunstleve, R. W., Echols, N., Headd, J. J., Moriarty, N. W., Mustyakimov, M., Terwilliger, T. C., Urzhumtsev, A., Zwart, P. H., and Adams, P. D. (2012). Towards automated crystallographic structure refinement with *phenix.refine*. *Acta Crystallographica Section D: Biological Crystallography*, 68(Pt 4):352–367.

[Avramis, 2014] Avramis, V. I. (2014). Is glutamine depletion needed in all disease? *Blood*, 123(23):3532–3533.

[Bansal et al., 2012] Bansal, S., Srivastava, A., Mukherjee, G., Pandey, R., Verma, A. K., Mishra, P., and Kundu, B. (2012). Hyperthermophilic asparaginase mutants with enhanced substrate affinity and antineoplastic activity: structural insights on their mechanism of action. *The FASEB Journal*, 26(3):1161–1171.

[Beckett and Gervais, 2019] Beckett, A. and Gervais, D. (2019). What makes a good new therapeutic l-asparaginase? *World Journal of Microbiology and Biotechnology*, 35(10):152.

[Berman et al., 2000] Berman, H. M., Westbrook, J., Feng, Z., Gilliland, G., Bhat, T. N., Weissig, H., Shindyalov, I. N., and Bourne, P. E. (2000). The Protein Data Bank. *Nucleic acids research*, 28(1):235–242.

[Borek and Jaskólski, 2001] Borek, D. and Jaskólski, M. (2001). Sequence analysis of enzymes with asparaginase activity. *Acta biochimica Polonica*, 48(4):893–902.

[Broome, 1961] Broome, J. D. (1961). Evidence that the L-Asparaginase Activity of Guinea Pig Serum is responsible for its Antilymphoma Effects. *Nature*, 191(4793):1114–1115.

[Bunkóczi and Read, 2011] Bunkóczi, G. and Read, R. J. (2011). Improvement of molecular-replacement models with *Sculptor*. *Acta Crystallographica Section D: Biological Crystallography*, 67(Pt 4):303–312.

[Campbell et al., 1967] Campbell, H. A., Mashburn, L. T., Boyse, E. A., and Old, L. J. (1967). Two L-asparaginases from *Escherichia coli* B. Their Separation, Purification, and Antitumor Activity. *Biochemistry*, 6(3):721–730.

[Cancer Research UK, 2021a] Cancer Research UK (2021a). Symptoms of acute lymphoblastic leukaemia (ALL). Retrieved from `https://www.cancerresearchuk.org/about-cancer/acute-lymphoblastic-leukaemia-all/symptoms`. Last checked on Feb 13, 2022.

[Cancer Research UK, 2021b] Cancer Research UK (2021b). What is acute lymphoblastic leukaemia (ALL)? Retrieved from `https://www.cancerresearchuk.org/about-cancer/acute-lymphoblastic-leukaemia-all/about`. Last checked on Feb 13, 2022.

[Cantor et al., 2012] Cantor, J. R., Panayiotou, V., Agnello, G., Georgiou, G., and Stone, E. M. (2012). Engineering reduced-immunogenicity enzymes for amino acid depletion therapy in cancer. In Wittrup, K. D. and Verdine, G. L., editors, *Protein engineering for therapeutics*, volume 502 of *Methods in enzymology, 0076-6879*, pages 291–319. Elsevier, Amsterdam.

[Carter and Wells, 1988] Carter, P. and Wells, J. A. (1988). Dissecting the catalytic triad of a serine protease. *Nature*, 332(6164):564–568.

[Chan et al., 2019] Chan, W.-K., Horvath, T. D., Tan, L., Link, T., Harutyunyan, K. G., Pontikos, M. A., Anishkin, A., Di Du, Martin, L. A., Yin, E., Rempe, S. B., Sukharev, S., Konopleva, M., Weinstein, J. N., and Lorenzi, P. L. (2019). Glutaminase activity of l-asparaginase contributes to durable preclinical activity against acute lymphoblastic leukemia. *Molecular cancer therapeutics*, 18(9):1587–1592.

[Chan et al., 2014] Chan, W. K., Lorenzi, P. L., Anishkin, A., Purwaha, P., Rogers, D. M., Sukharev, S., Rempe, S. B., and Weinstein, J. N. (2014). The glutaminase activity of l-asparaginase is not required for anticancer activity against asns-negative cells. *Blood*, 123(23):3596–3606.

[Clementi, 1922] Clementi, A. (1922). La désamidation enzymatique de l'asparagine chez les différentes espèces animales et la signification physio logique de sa présence dans l'organisme. *Archives Internationales de Physiologie*, 19(4):369–398.

[Cooney et al., 1970] Cooney, D. A., Capizzi, R. L., and Handschumacher, R. E. (1970). Evaluation of L-asparagine Metabolism in Animals and Man. *Cancer Research*, 30(4):929–935.

[Costa et al., 2016] Costa, I. M., Schultz, L., de Araujo Bianchi Pedra, B., Leite, M. S. M., Farsky, S. H. P., de Oliveira, M. A., Pessoa, A., and Monteiro, G. (2016). Recombinant L-asparaginase 1 from *Saccharomyces cerevisiae*: an allosteric enzyme with antineoplastic activity. *Scientific Reports*, 6(1):36239.

[Covini et al., 2012] Covini, D., Tardito, S., Bussolati, O., Chiarelli, L. R., Pasquetto, M. V., Digilio, R., Valentini, G., and Scotti, C. (2012). Expanding Targets for a Metabolic Therapy of Cancer: L-asparaginase. *Recent Patents on Anti-Cancer Drug Discovery*, 7(1):4–13.

[Dinndorf et al., 2007] Dinndorf, P. A., Gootenberg, J., Cohen, M. H., Keegan, P., and Pazdur, R. (2007). Fda drug approval summary: pegaspargase (oncaspar) for the first-line treatment of children with acute lymphoblastic leukemia (all). *The Oncologist*, 12(8):991–998.

[Emsley et al., 2010] Emsley, P., Lohkamp, B., Scott, W. G., and Cowtan, K. (2010). Features and development of *Coot*. *Acta Crystallographica Section D: Biological Crystallography*, 66(Pt 4):486–501.

[Endicott et al., 2021] Endicott, M., Jones, M., and Hull, J. (2021). Amino acid metabolism as a therapeutic target in cancer: a review. *Amino Acids*, 53(8):1169–1179.

[Eulig, 2018] Eulig, N. (2018). *Further humanization and structural analysis of a human-guinea pig chimeric L-asparaginase*. Unpublished master thesis, Department of Molecular Enzymology, Georg-August-University Göttingen, Germany.

[Fonseca et al., 2021] Fonseca, M. H. G., Da Fiúza, T. S., de Morais, S. B., de Souza, T. A. C. B., and Trevizani, R. (2021). Circumventing the side effects of l-asparaginase. *Biomedicine & pharmacotherapy = Biomedecine & pharmacotherapie*, 139:111616.

[Frey and Görlich, 2014] Frey, S. and Görlich, D. (2014). A new set of highly efficient, tag-cleaving proteases for purifying recombinant proteins. *Journal of chromatography. A*, 1337:95–105.

[Fürth and Friedmann, 1910] Fürth, O. and Friedmann, M. (1910). Über die Verbreitung asparaginspaltender Organfermente. *Biochem Z*, 26:435–440.

[Gasteiger et al., 2005] Gasteiger, E., Hoogland, C., Gattiker, A., Duvaud, S., Wilkins, M. R., Appel, R. D., and Bairoch, A. (2005). Protein Identification and Analysis Tools on the ExPASy Server. In Walker, J. M., editor, *Proteomics protocols handbook*, pages 571–607. Humana Press, Totowa, N.J.

[Gesto et al., 2013] Gesto, D. S., Cerqueira, N. M. F. S. A., Fernandes, P. A., and Ramos, M. J. (2013). Unraveling the Enigmatic Mechanism of L-asparaginase II with QM/QM Calculations. *Journal of the American Chemical Society*, 135(19):7146–7158.

[Gonnermann, 1902] Gonnermann, M. (1902). Ueber die Verseifbarkeit einiger Säure-Amide und Säure-Anilide durch Fermente. *Archiv für die gesamte Physiologie des Menschen und der Tiere*, 89(9-10):493–516.

[Henikoff and Henikoff, 1992] Henikoff, S. and Henikoff, J. G. (1992). Amino acid substitution matrices from protein blocks. *Proceedings of the National Academy of Sciences*, 89(22):10915–10919.

[Ho et al., 1970] Ho, D. H., Whitecar, J. P., Luce, J. K., and Frei, E. (1970). L-asparagine Requirement and the Effect of L-asparaginase on the Normal and Leukemic Human Bone Marrow. *Cancer Research*, 30(2):466–472.

[Ho et al., 1989] Ho, S. N., Hunt, H. D., Horton, R. M., Pullen, J. K., and Pease, L. R. (1989). Site-directed mutagenesis by overlap extension using the polymerase chain reaction. *Gene*, 77(1):51–59.

[Howlader et al., 2021] Howlader, N., Noone, A. M., Krapcho, M., Miller, D., Brest, A., Yu, M., Ruhl, J., Tatalovich, Z., Mariotto, A., Lewis, D. R., Chen, H. S., Feuer, E. J., and Cronin, K. A. (2021). SEER Cancer Statistics Review, 1975-2018, National Cancer Institute. Bethesda, MD. Available at `https://seer.cancer.gov/csr/1975_2018/`. Based on November 2020 SEER data submission, posted to the SEER web site, April 2021.

[Inoue et al., 1990] Inoue, H., Nojima, H., and Okayama, H. (1990). High efficiency transformation of *Escherichia coli* with plasmids. *Gene*, 96(1):23–28.

[Jiang et al., 2021] Jiang, J., Batra, S., and Zhang, J. (2021). Asparagine: A Metabolite to Be Targeted in Cancers. *Metabolites*, 11(6).

[Joosten et al., 2011] Joosten, R. P., te Beek, T. A. H., Krieger, E., Hekkelman, M. L., Hooft, R. W. W., Schneider, R., Sander, C., and Vriend, G. (2011). A series of PDB related databases for everyday needs. *Nucleic acids research*, 39(Database issue):D411–9.

[Kabsch, 2010] Kabsch, W. (2010). Integration, scaling, space-group assignment and post-refinement. *Acta Crystallographica Section D Biological Crystallography*, 66(Pt 2):133–144.

[Kabsch and Sander, 1983] Kabsch, W. and Sander, C. (1983). Dictionary of Protein Secondary Structure: Pattern Recognition of Hydrogen-Bonded and Geometrical Features. *Biopolymers*, 22(12):2577–2637.

[Karamitros and Konrad, 2014] Karamitros, C. S. and Konrad, M. (2014). Human 60-kDa Lysophospholipase Contains an N-terminal L-asparaginase Domain That Is Allosterically Regulated by L-asparagine. *The Journal of biological chemistry*, 289(19):12962–12975.

[Karamitros and Konrad, 2016] Karamitros, C. S. and Konrad, M. (2016). Fluorescence-Activated Cell Sorting of Human L-asparaginase Mutant Libraries for Detecting Enzyme Variants with Enhanced Activity. *ACS Chemical Biology*, 11(9):2596–2607.

[Katoh et al., 2019] Katoh, K., Rozewicki, J., and Yamada, K. D. (2019). MAFFT online service: multiple sequence alignment, interactive sequence choice and visualization. *Briefings in Bioinformatics*, 20(4):1160–1166.

[Kidd, 1953] Kidd, J. G. (1953). Regression of transplanted lymphomas induced in vivo by means of normal guinea pig serum. II. studies on the nature of the active serum constituent: histological mechanism of the regression: tests for effects of guinea pig serum on lymphoma cells in vitro: discussion. *Journal of Experimental Medicine*, 98(6):583–606.

[Knott et al., 2018] Knott, S. R. V., Wagenblast, E., Khan, S., Kim, S. Y., Soto, M., Wagner, M., Turgeon, M.-O., Fish, L., Erard, N., Gable, A. L., Maceli, A. R., Dickopf, S.,

Papachristou, E. K., D'Santos, C. S., Carey, L. A., Wilkinson, J. E., Harrell, J. C., Perou, C. M., Goodarzi, H., Poulogiannis, G., and Hannon, G. J. (2018). Asparagine bioavailability governs metastasis in a model of breast cancer. *Nature*, 554(7692):378–381.

[Kuhlman et al., 2003] Kuhlman, B., Dantas, G., Ireton, G. C., Varani, G., Stoddard, B. L., and Baker, D. (2003). Design of a novel globular protein fold with atomic-level accuracy. *Science (New York, N.Y.)*, 302(5649):1364–1368.

[Kuipers et al., 2010] Kuipers, R. K., Joosten, H.-J., van Berkel, W. J. H., Leferink, N. G. H., Rooijen, E., Ittmann, E., van Zimmeren, F., Jochens, H., Bornscheuer, U., Vriend, G., dos Santos, V. A. P. M., and Schaap, P. J. (2010). 3DM: systematic analysis of heterogeneous superfamily data to discover protein functionalities. *Proteins*, 78(9):2101–2113.

[Kunzmann and Hamacher, 2018] Kunzmann, P. and Hamacher, K. (2018). Biotite: a unifying open source computational biology framework in Python. *BMC Bioinformatics*, 19(1):346.

[Lang and Uber, 1904] Lang, S. and Uber (1904). Desamidierung im Tierkörper. *Beitraege zur Chemischen Physiologie und Pathologie*, 190:5321–5345.

[Li et al., 2006] Li, J., Mahajan, A., and Tsai, M.-D. (2006). Ankyrin Repeat: a Unique Motif Mediating Protein-Protein Interactions. *Biochemistry*, 45(51):15168–15178.

[Liebschner et al., 2019] Liebschner, D., Afonine, P. V., Baker, M. L., Bunkóczi, G., Chen, V. B., Croll, T. I., Hintze, B., Hung, L. W., Jain, S., McCoy, A. J., Moriarty, N. W., Oeffner, R. D., Poon, B. K., Prisant, M. G., Read, R. J., Richardson, J. S., Richardson, D. C., Sammito, M. D., Sobolev, O. V., Stockwell, D. H., Terwilliger, T. C., Urzhumtsev, A. G., Videau, L. L., Williams, C. J., and Adams, P. D. (2019). Macromolecular structure determination using X-rays, neutrons and electrons: recent developments in *Phenix*. *Acta crystallographica. Section D, Structural biology*, 75(Pt 10):861–877.

[Linares et al., 2017] Linares, J. F., Cordes, T., Duran, A., Reina-Campos, M., Valencia, T., Ahn, C. S., Castilla, E. A., Moscat, J., Metallo, C. M., and Diaz-Meco, M. T. (2017). ATF4-Induced Metabolic Reprograming Is a Synthetic Vulnerability of the p62-Deficient Tumor Stroma. *Cell Metabolism*, 26(6):817–829.e6.

[Loch and Jaskolski, 2021] Loch, J. I. and Jaskolski, M. (2021). Structural and biophysical aspects of l-asparaginases: a growing family with amazing diversity. *IUCrJ*, 8(Pt 4):514–531.

[Lubkowski et al., 2003] Lubkowski, J., Dauter, M., Aghaiypour, K., Wlodawer, A., and Dauter, Z. (2003). Atomic resolution structure of *Erwinia chrysanthemi* L-asparaginase. *Acta Crystallographica Section D Biological Crystallography*, 59(Pt 1):84–92.

[Lubkowski et al., 2020] Lubkowski, J., Vanegas, J., Chan, W.-K., Lorenzi, P. L., Weinstein, J. N., Sukharev, S., Fushman, D., Rempe, S., Anishkin, A., and Wlodawer, A. (2020). Mechanism of Catalysis by L-Asparaginase. *Biochemistry*, 59(20):1927–1945.

[Lubkowski and Wlodawer, 2021] Lubkowski, J. and Wlodawer, A. (2021). Structural and biochemical properties of L-asparaginase. *The FEBS Journal*, 288(14):4183–4209.

[Maqsood et al., 2020] Maqsood, B., Basit, A., Khurshid, M., and Bashir, Q. (2020). Characterization of a thermostable, allosteric L-asparaginase from *Anoxybacillus flavithermus*. *International Journal of Biological Macromolecules*, 152:584–592.

[Mashburn and Wriston, 1964] Mashburn, L. T. and Wriston, J. C. (1964). Tumor Inhibitory Effect of L-asparaginase from *Escherichia coli*. *Arch Biochem Biophys*, 105:450–452.

[Michalska and Jaskolski, 2006] Michalska, K. and Jaskolski, M. (2006). Structural aspects of L-asparaginases, their friends and relations. *Acta biochimica Polonica*, 53(4):627–640.

[Narta et al., 2007] Narta, U. K., Kanwar, S. S., and Azmi, W. (2007). Pharmacological and clinical evaluation of L-asparaginase in the treatment of leukemia. *Critical Reviews in Oncology/Hematology*, 61(3):208–221.

[National Cancer Institute, 2021] National Cancer Institute (2021). What Is Cancer? Retrieved from `https://www.cancer.gov/about-cancer/understanding/what-is-cancer`. Last checked on Feb 15, 2022.

[Nguyen et al., 2016] Nguyen, H. A., Su, Y., and Lavie, A. (2016). Design and Characterization of *Erwinia Chrysanthemi* L-Asparaginase Variants with Diminished L-Glutaminase Activity. *The Journal of biological chemistry*, 291(34):17664–17676.

[Palm et al., 1996] Palm, G. J., Lubkowski, J., Derst, C., Schleper, S., Röhm, K.-H., and Wlodawer, A. (1996). A covalently bound catalytic intermediate in *Escherichia coli* asparaginase : Crystal structure of a Thr-89-Val mutant. *FEBS Letters*, 390(2):211–216.

[Pavlova et al., 2018] Pavlova, N. N., Hui, S., Ghergurovich, J. M., Fan, J., Intlekofer, A. M., White, R. M., Rabinowitz, J. D., Thompson, C. B., and Zhang, J. (2018). As Extracellular Glutamine Levels Decline, Asparagine Becomes an Essential Amino Acid. *Cell Metabolism*, 27(2):428–438.e5.

[Pavlova and Thompson, 2016] Pavlova, N. N. and Thompson, C. B. (2016). The emerging hallmarks of cancer metabolism. *Cell Metabolism*, 23(1):27–47.

[Perel et al., 2002] Perel, Y., Auvrignon, A., Leblanc, T., Vannier, J.-P., Michel, G., Nelken, B., Gandemer, V., Schmitt, C., Lamagnere, J.-P., de Lumley, L., Bader-Meunier, B., Couillaud,

G., Schaison, G., Landman-Parker, J., Thuret, I., Dalle, J.-H., Baruchel, A., and Leverger, G. (2002). Impact of addition of maintenance therapy to intensive induction and consolidation chemotherapy for childhood acute myeloblastic leukemia: results of a prospective randomized trial, LAME 89/91. Leucámie Aiqüe Myéloïde Enfant. *Journal of Clinical Oncology*, 20(12):2774–2782.

[Radadiya et al., 2020] Radadiya, A., Zhu, W., Coricello, A., Alcaro, S., and Richards, N. G. J. (2020). Improving the treatment of acute lymphoblastic leukemia. *Biochemistry*, 59(35):3193–3200.

[Rigouin et al., 2017] Rigouin, C., Nguyen, H. A., Schalk, A. M., and Lavie, A. (2017). Discovery of human-like L-asparaginases with potential clinical use by directed evolution. *Scientific Reports*, 7(1):10224.

[Rosetta Commons, 2022a] Rosetta Commons (2022a). Getting started. Retrieved from `https://www.rosettacommons.org/docs/latest/getting_started/Getting-Started`. Last checked on Jan 19, 2022.

[Rosetta Commons, 2022b] Rosetta Commons (2022b). Point mutant ("pmut") scan application, pmut_scan_parallel. Retrieved from `https://www.rosettacommons.org/docs/latest/application_documentation/design/pmut-scan-parallel`. Last checked on Jan 19, 2022.

[Samson et al., 2005] Samson, R., Legendre, J. B., Christen, R., Saux, M. F.-L., Achouak, W., and Gardan, L. (2005). Transfer of *Pectobacterium chrysanthemi* (Burkholder et al. 1953) Brenner et al. 1973 and *Brenneria paradisiaca* to the genus *Dickeya* gen. nov. as *Dickeya chrysanthemi* comb. nov. and *Dickeya paradisiaca* comb. nov. and delineation of four novel species, *Dickeya dadantii* sp. nov., *Dickeya dianthicola* sp. nov., *Dickeya dieffenbachiae* sp. nov. and *Dickeya zeae* sp. nov. *International Journal of Systematic and Evolutionary Microbiology*, 55(Pt 4):1415–1427.

[Schalk et al., 2016] Schalk, A. M., Antansijevic, A., Caffrey, M., and Lavie, A. (2016). Experimental Data in Support of a Direct Displacement Mechanism for Type I/II L-Asparaginases. *The Journal of biological chemistry*, 291(10):5088–5100.

[Schalk et al., 2014] Schalk, A. M., Nguyen, H.-A., Rigouin, C., and Lavie, A. (2014). Identification and Structural Analysis of an L-asparaginase Enzyme from Guinea Pig with Putative Tumor Cell Killing Properties. *The Journal of biological chemistry*, 289(48):33175–33186.

[Schrödinger, 2015] Schrödinger (2015). The PyMOL Molecular Graphics System, Version 2.0 Schrödinger, LLC.

[Seemüller et al., 1996] Seemüller, E., Lupas, A., and Baumeister, W. (1996). Autocatalytic processing of the 20S proteasome. *Nature*, 382(6590):468–471.

[Sircar et al., 2012] Sircar, K., Huang, H., Hu, L., Cogdell, D., Dhillon, J., Tzelepi, V., Efstathiou, E., Koumakpayi, I. H., Saad, F., Luo, D., Bismar, T. A., Aparicio, A., Troncoso, P., Navone, N., and Zhang, W. (2012). Integrative Molecular Profiling Reveals Asparagine Synthetase Is a Target in Castration-Resistant Prostate Cancer. *The American Journal of Pathology*, 180(3):895–903.

[SnapGene software (from Insightful Science), 2022] SnapGene software (from Insightful Science) (2022). Available at `https://www.snapgene.com`.

[Stams et al., 2005] Stams, W. A. G., den Boer, M. L., Holleman, A., Appel, I. M., Beverloo, H. B., van Wering, E. R., Janka-Schaub, G. E., Evans, W. E., and Pieters, R. (2005). Asparagine synthetase expression is linked with L-asparaginase resistance in *TEL-AML1*-negative but not *TEL-AML1*-positive pediatric acute lymphoblastic leukemia. *Blood*, 105(11):4223–4225.

[Studier, 2005] Studier, F. W. (2005). Protein production by auto-induction in high density shaking cultures. *Protein expression and purification*, 41(1):207–234.

[Sumbalova et al., 2018] Sumbalova, L., Stourac, J., Martinek, T., Bednar, D., and Damborsky, J. (2018). HotSpot Wizard 3.0: web server for automated design of mutations and smart libraries based on sequence input information. *Nucleic acids research*, 46(W1):W356–W362.

[Swain et al., 1993] Swain, A. L., Jaskólski, M., Housset, D., Rao, J. K., and Wlodawer, A. (1993). Crystal structure of *Escherichia coli* L-asparaginase, an enzyme used in cancer therapy. *Proceedings of the National Academy of Sciences*, 90(4):1474–1478.

[Terwilliger et al., 2008] Terwilliger, T. C., Grosse-Kunstleve, R. W., Afonine, P. V., Moriarty, N. W., Zwart, P. H., Hung, L. W., Read, R. J., and Adams, P. D. (2008). Iterative model building, structure refinement and density modification with the *PHENIX AutoBuild* wizard. *Acta Crystallographica Section D Biological Crystallography*, 64(Pt 1):61–69.

[Vagin and Teplyakov, 1997] Vagin, A. and Teplyakov, A. (1997). *MOLREP*: an Automated Program for Molecular Replacement. *Journal of Applied Crystallography*, 30(6):1022–1025.

[Voronin and Kiseleva, 2008] Voronin, D. A. and Kiseleva, E. V. (2008). Functional Role of Proteins Containing Ankyrin Repeats. *Cell and Tissue Biology*, 2(1):1–12.

[Wensien, 2017] Wensien, M. (2017). *Expression, Aufreinigung und Bestimmung der Aktivität von Varianten der humanen L-Asparaginase*. Unpublished bachelor thesis, Department of Molecular Enzymology, Georg-August-University Göttingen, Germany.

[Winn et al., 2011] Winn, M. D., Ballard, C. C., Cowtan, K. D., Dodson, E. J., Emsley, P., Evans, P. R., Keegan, R. M., Krissinel, E. B., Leslie, A. G. W., McCoy, A., McNicholas, S. J., Murshudov, G. N., Pannu, N. S., Potterton, E. A., Powell, H. R., Read, R. J., Vagin, A., and Wilson, K. S. (2011). Overview of the *CCP4* suite and current developments. *Acta Crystallographica Section D Biological Crystallography*, 67(Pt 4):235–242.

[Yun et al., 2007] Yun, M.-K., Nourse, A., White, S. W., Rock, C. O., and Heath, R. J. (2007). Crystal Structure and Allosteric Regulation of the Cytoplasmic *Escherichia coli* L-asparaginase I. *Journal of Molecular Biology*, 369(3):794–811.

A Appendix

Activity measurements

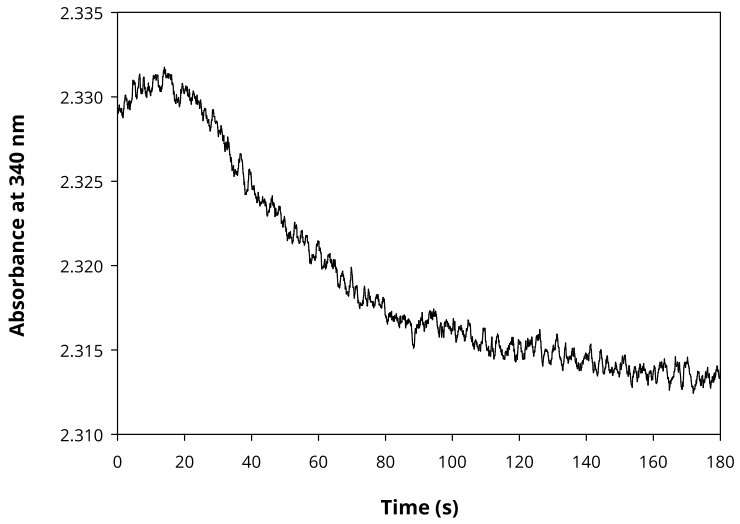

▲ **Figure A.1: Incubation of samples before activity measurements.** Before addition of asparaginase enzyme to the reaction mixture, the sample was placed in the photometer and incubated for approximately 3 min while detecting the absorption at 340 nm until it was relatively stable. The plot shows an exemplary measurement of the incubation.

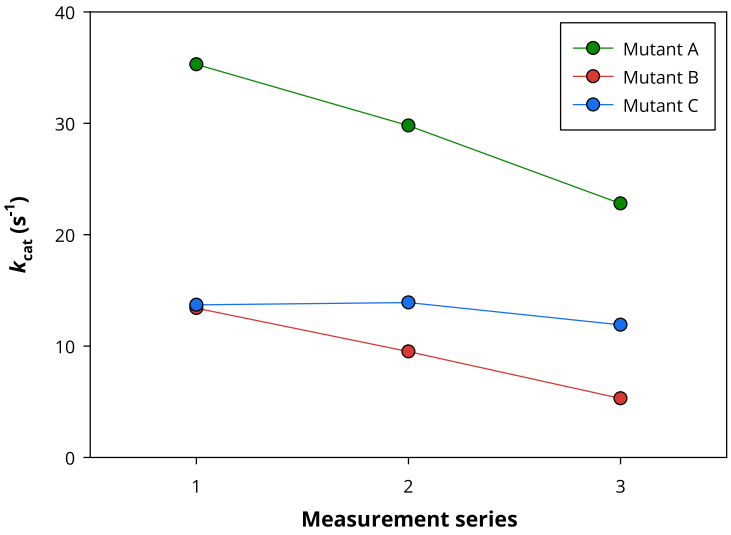

▲ **Figure A.2: Change of protein activity for hgpASNase-tr mutants over time.** The plot displays the turnover rates (k_{cat}) for the three hgpASNase-tr mutants obtained from fitting the data points from each measurement series separately according to Michaelis and Menten (Eq. 4). The measurement series were carried out in chronological order.

Plasmids

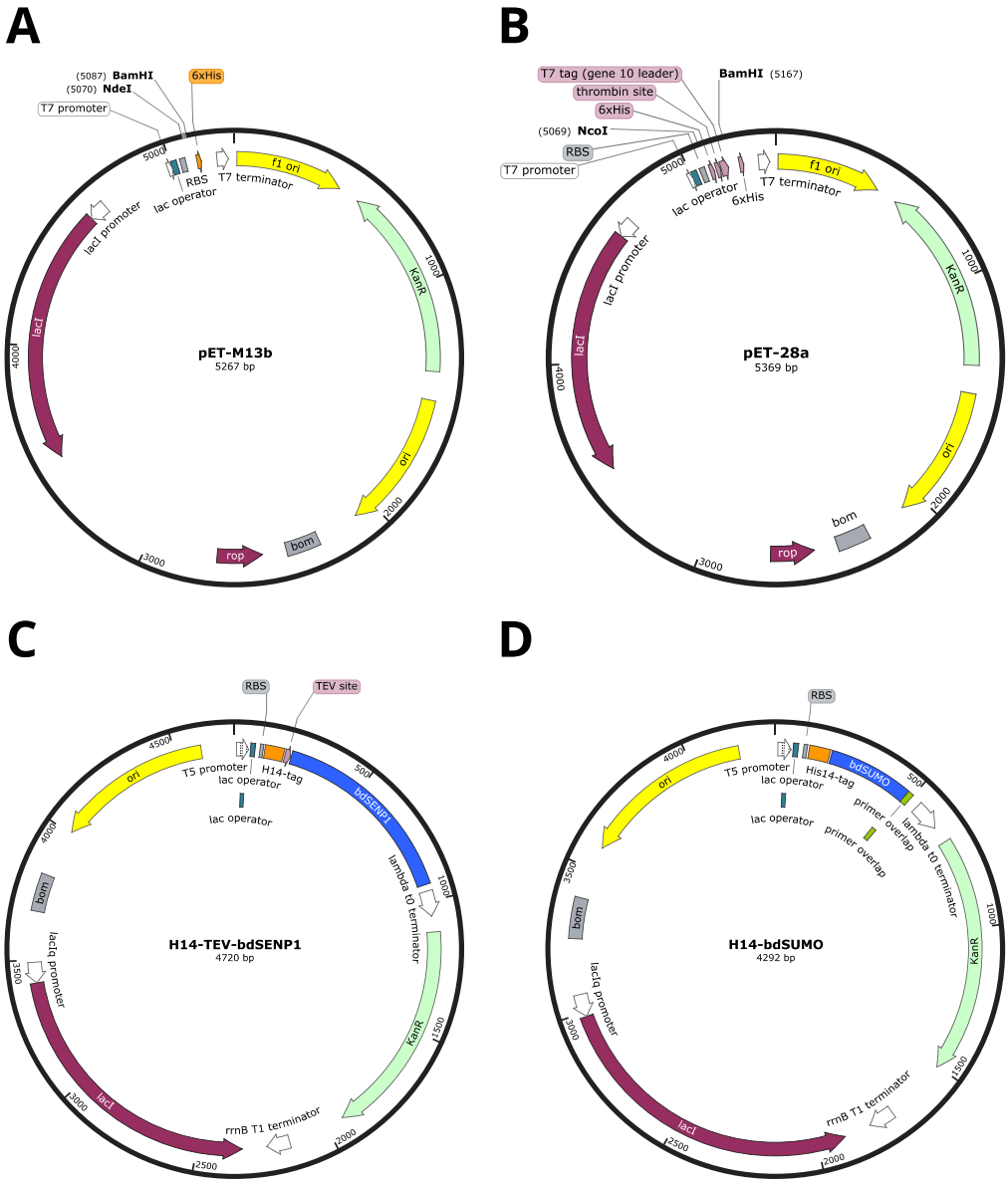

▲ **Figure A.3: Plasmids used during the work of this thesis.** **A** pET-M13b is a modified pET-M13 vector. The restriction site *NcoI* was exchanged by *NdeI* and the sequence between the restriction sites *SacI* and *XhoI* was removed. **B** pET-28a with inserted sequence of hASNase1-fl was ordered from *GeneArt Gene Synthesis* (Thermo Fisher Scientific). **C** The expression plasmid pSF1389 encoding His14-TEV-bdSENP1 was a gift from Dirk Görlich (Addgene plasmid #104962 ; `http://n2t.net/addgene:104962`; RRID:Addgene_104962). **D** The H14-bdSUMO plasmid containing the sequence for hASNase1-fl was obtained from Renate Rees from the department of Cellular Logistics of Dirk Görlich from the Max Planck Institute of Multidisciplinary Sciences. The plasmid maps were created with SnapGene Viewer [SnapGene software (from Insightful Science), 2022].

Sequences

hgpASNase-tr nucleotide sequence

plasmid: pET-M13b

5' restriction site: NdeI (CATATG)

3' restriction site: BamHI (GGATCC)

CATATGGCACGTGCAGTTGGTCCGGAACGTCGTCTGCTGGCAGTTTATACCGGTGGCACCATTGGTATGCGTAGCGAACTGGGTGTTCTGG
TTCCGGGTACAGGTCTGGCAGCAATTCTGCGTACCCTGCCGATGTTTCATGATGAAGAACATGCCCGTGCACGTGGTCTGAGCGAAGATAC
CCTGGTTCTGCCTCCGGCAAGCCGTAATCAGCGTATTCTGTATACCGTTCTGGAATGTCAGCCGCTGTTTGATAGCAGCGATATGACCATT
GCAGAATGGGTTTGTCTGGCACAGACCATTAAACGTCATTATGAACAGTATCATGGCTTCGTTGTTATTCATGGCACCGATACCATGGCAT
TTGCAGCAAGCATGCTGAGCTTTATGCTGGAAAATCTGCAGAAAACCGTTATTCTGACCGGTGCACAGGTTCCGATTCATGCACTGTGGTC
AGATGGTCGTGAAAACCTGCTGGGTGCACTGCTGATGGCAGGTCAGTATGTTATTCCGGAAGTTTGTCTGTTTTTTCAGAATCAGCTGTTT
CGTGGTAATCGTGCAACCAAAGTTGATGCACGTCGTTTTGCAGCATTTTGTAGCCCGAATCTGCTGCCGCTGGCAACCGTTGGTGCAGATA
TTACCATTAATCGTGAACTGGTTCGTAAAGTGGATGGTAAAGCAGGTCTGGTTGTTCATAGCAGCATGGAACAGGATGTTGGTCTGCTGCG
TCTGTATCCGGGTATTCCGGCATCACTGGTTCGTGCCTTTCTGCAGCCTCCGCTGAAAGGTGTTGTGCTGGAAACCTTTGGTAGCGGTAAT
GGTCCGAGCAAACCGGATCTGCTGCAAGAACTGCGTGCAGCAGCACAGCGTGGTCTGATTATGGTTAATTGTAGCCAGTGTCTGCGTGGTA
GCGTTACACCGGGTTATGCGACCAGCCTGGCAGGCGCAAATATTGTTAGCGGTCTGGATATGACCTCAGAAGCAGCACTGGCAAAACTGAG
CTATGTTCTGGGCCTGCCGGAACTGAGCCTGGAACGTCGTCAAGAGCTGCTGGCAAAAGATCTGCGTGGCGAAATGACACTGCCGACATTA
GGATCCGAATTCGAGCTCCTCGAGCACCACCACCACCACCACTGA

hgpASNase-tr peptide sequence

plasmid: pET-M13b

MARAVGPERRLLAVYTGGTIGMRSELGVLVPGTGLAAILRTLPMFHDEEHARARGLSEDTLVLPPASRNQRILYTVLECQPLFDSSDMTIA
EWVCLAQTIKRHYEQYHGFVVIHGTDTMAFAASMLSFMLENLQKTVILTGAQVPIHALWSDGRENLLGALLMAGQYVIPEVCLFFQNQLFR
GNRATKVDARRFAAFCSPNLLPLATVGADITINRELVRKVDGKAGLVVHSSMEQDVGLLRLYPGIPASLVRAFLQPPLKGVVLETFGSGNG
PSKPDLLQELRAAAQRGLIMVNCSQCLRGSVTPGYATSLAGANIVSGLDMTSEAALAKLSYVLGLPELSLERRQELLAKDLRGEMTLPTLG
SEFELLEHHHHHH*

ASNase sequence Linker His-tag * Stop codon

hASNase1-fl nucleotide sequence

plasmid: pET-28a

5' restriction site: NcoI (CCATGG)

3' restriction site: BamHI (AAGCTT)

CCATGGCGAGAGCAGTTGGTCCGGAACGTCGTCTGCTGGCAGTTTATACCGGTGGCACCATTGGTATGCGTAGCGAACTGGGTGTTCTGGT
TCCTGGCACCGGTCTGGCAGCAATTCTGCGTACCCTGCCGATGTTTCATGATGAAGAACATGCACGTGCCCGTGGTCTGAGCGAAGATACC
CTGGTTCTGCCTCCGGCAAGCCGTAATCAGCGTATTCTGTATACCGTTCTGGAATGTCAGCCGCTGTTTGATAGCAGCGATATGACCATTG
CAGAATGGGTTTGTCTGGCACAGACCATTAAACGTCATTATGAACAGTATCATGGCTTCGTTGTTATTCATGGCACCGATACAATGGCATT
TGCAGCAAGCATGCTGAGCTTTATGCTGGAAAATCTGCAGAAAACCGTTATTCTGACAGGTGCACAGGTTCCGATTCATGCACTGTGGTCA
GATGGTCGTGAAAACCTGCTGGGTGCACTGCTGATGGCAGGTCAGTATGTTATTCCGGAAGTTTGTCTGTTTTTTCAGAATCAGCTGTTTC
GTGGTAATCGTGCAACCAAAGTTGATGCACGTCGTTTTGCAGCATTTTGTAGCCCGAATCTGCTGCCGCTGGCAACCGTTGGTGCAGATAT
TACCATTAATCGTGAACTGGTTCGTAAAGTGGATGGTAAAGCAGGTCTGGTTGTTCATAGCAGCATGGAACAGGATGTTGGTCTGCTGCGT
CTGTATCCGGGTATTCCGGCAGCGCTGGTTCGTGCATTTCTGCAGCCTCCGCTGAAAGGTGTTGTTATGGAAACCTTTGGTAGCGGTAATG
GTCCGACCAAACCGGATCTGCTGCAAGAACTGCGTGTTGCAACCGAACGTGGTCTGGTTATTGTTAATTGTACCCATTGTCTGCAGGGTGC
AGTTACCACCGATTATGCAGCAGGTATGGCAATGGCTGGTGCCGGTGTTATTAGCGGTTTTGATATGACCTCAGAAGCAGCACTGGCAAAA
CTGAGCTATGTTCTGGGTCAGCCAGGTCTGAGCCTGGATGTGCGTAAAGAACTGCTGACCAAAGATCTGCGTGGTGAAATGACCCCTCCGA
GCGTTGAAGAACGCCGTCCGAGCCTGCAGGGTAATACCTTAGGTGGTGGTGTTAGCTGGCTGCTGAGCCTGAGCGGTAGCCAAGAGGCAGA
TGCACTGCGTAATGCCCTGGTGCCGAGCCTGGCCTGTGCAGCAGCACATGCCGGTGATGTTGAAGCACTGCAGGCACTGGTTGAACTGGGT
AGCGATTTAGGTCTGGTGGATTTTAATGGCCAGACACCGCTGCATGCCGCAGCACGTGGTGGTCATACCGAAGCCGTTACCATGCTGTTAC
AGCGTGGTGTTGATGTTAATACACGTGATACCGATGGTTTTAGTCCGCTGCTGCTGGCCGTTCGTGGTCGTCATCCGGGTGTTATTGGCCT
GCTGCGCGAAGCCGGTGCAAGCCTGAGCACCCAAGAACTGGAAGAGGCAGGCACCGAACTGTGTCGTCTGGCATATCGTGCAGATCTGGAA
GGTCTGCAGGTTTGGTGGCAGGCAGGCGCTGATCTGGGCCAGCCTGGTTATGATGGTCATAGCGCACTGCATGTTGCAGAAGCCGCAGGTA
ATCTGGCAGTTGTTGCCTTTCTGCAGTCACTGGAAGGTGCAGTTGGTGCCCAGGCACCGTGTCCGGAAGTGCTGCCTGGTGTTAAGCTTGC
GGCCGCACTCGAGCACCACCACCACCACCACTGA

hASNase1-fl peptide sequence

plasmid: pET-28a

MARAVGPERRLLAVYTGGTIGMRSELGVLVPGTGLAAILRTLPMFHDEEHARARGLSEDTLVLPPASRNQRILYTVLECQPLFDSSDMTIA
EWVCLAQTIKRHYEQYHGFVVIHGTDTMAFAASMLSFMLENLQKTVILTGAQVPIHALWSDGRENLLGALLMAGQYVIPEVCLFFQNQLFR
GNRATKVDARRFAAFCSPNLLPLATVGADITINRELVRKVDGKAGLVVHSSMEQDVGLLRLYPGIPAALVRAFLQPPLKGVVMETFGSGNG
PTKPDLLQELRVATERGLVIVNCTHCLQGAVTTDYAAGMAMAGAGVISGFDMTSEAALAKLSYVLGQPGLSLDVRKELLTKDLRGEMTPPS
VEERRPSLQGNTLGGGVSWLLSLSGSQEADALRNALVPSLACAAAHAGDVEALQALVELGSDLGLVDFNGQTPLHAAARGGHTEAVTMLLQ
RGVDVNTRDTDGFSPLLLAVRGRHPGVIGLLREAGASLSTQELEEAGTELCRLAYRADLEGLQVWWQAGADLGQPGYDGHSALHVAEAAGN
LAVVAFLQSLEGAVGAQAPCPEVLPGVKLAAALEHHHHHH*

ASNase sequence Linker His-tag * Stop codon

H14-TEV-bdSENP1 nucleotide sequence

ATGAGCAAGCATCACCATCATTCAGGCCATCACCATACCGGACACCACCATCATTCAGGCAGTCATCACCATACCGGCGAGAACCTGTATT
TTCAGGGTACCAAGGAAGAAGTGCCGGAACCGTTTGTGCCGTTGACCGACGAAGACGAAGATAACGTTCGTCACGCACTGGGTGGCCGCAA
ACGTTCGGAAACCCTGTCCGTGCACGAAGCGTCAAATATTGTGATCACGCGCGAGATCCTGCAGTGTCTGAACGACAAAGAATGGCTGAAT
GATGAGGTTATCAACCTGTACCTGGAACTGCTGAAAGAGCGTGAACTGCGTGAACCGAACAAATTTCTGAAATGTCATTTCTTCAATACGT
TTTTCTACAAAAAGCTGATTAACGGCGGCTATGATTACAAAAGCGTTCGTCGCTGGACTACGAAACGCAAACTGGGTTACAACCTGATTGA
TTGCGACAAAATCTTCGTGCCGATTCACAAAGATGTTCATTGGTGCCTGGCTGTAATTAACATCAAAGAAAAGAAATTCCAGTATCTCGAT
AGCCTGGGCTATATGGATATGAAAGCGCTGCGCATTCTGGCTAAATATCTCGTGGACGAAGTAAAAGACAAATCCGGTAAGCAGATCGACG
TTCACGCGTGGAAACAGGAGGGTGTTCAGAACCTGCCGCTGCAGGAAAACGGTTGGGATTGCGGTATGTTCATGCTGAAGTATATCGATTT
CTATTCTCGTGACATGGAACTGGTCTTTGGCCAGAAACACATGTCGTACTTTCGTCGTCGTACCGCTAAAGAAATCCTGGATCTGAAGGCC
GGTTAG

H14-TEV-bdSENP1 peptide sequence

MSKHHHHSGHHHTGHHHHSGSHHHTGENLYFQGTKEEVPEPFVPLTDEDEDNVRHALGGRKRSETLSVHEASNIVITREILQCLNDKEWLN
DEVINLYLELLKERELREPNKFLKCHFFNTFFYKKLINGGYDYKSVRRWTTKRKLGYNLIDCDKIFVPIHKDVHWCLAVINIKEKKFQYLD
SLGYMDMKALRILAKYLVDEVKDKSGKQIDVHAWKQEGVQNLPLQENGWDCGMFMLKYIDFYSRDMELVFGQKHMSYFRRRTAKEILDLKA
G*

His-tag TEV sequence Spacer bdSENP1 sequence * Stop codon

H14-bdSUMO-hASNase1-fl nucleotide sequence

ATGAGCAAGCATCACCATCATTCAGGCCATCACCATACCGGACACCACCATCATTCAGGCAGTCATCACCATTCCGGATCTGCTGCGGGTG
GCGAAGAAGATAAGAAACCGGCAGGTGGCGAAGGTGGCGGTGCCCATATCAACCTGAAAGTGAAAGGTCAAGACGGCAACGAAGTCTTTTT
CCGCATCAAACGTTCTACCCAGCTGAAAAAGCTGATGAACGCATACTGTGACCGTCAGTCTGTAGACATGACCGCAATTGCTTTCCTGTTT
GATGGTCGTCGCCTGCGTGCGGAACAGACCCCGGATGAACTGGAGATGGAAGATGGCGACGAAATCGACGCAATGCTTCATCAGACTGGTG
GCAGCGGGGGGGCGAGAGCAGTTGGTCCGGAACGTCGTCTGCTGGCAGTTTATACCGGTGGCACCATTGGTATGCGTAGCGAACTGGGTGT
TCTGGTTCCTGGCACCGGTCTGGCAGCAATTCTGCGTACCCTGCCGATGTTTCATGATGAAGAACATGCACGTGCCCGTGGTCTGAGCGAA
GATACCCTGGTTCTGCCTCCGGCAAGCCGTAATCAGCGTATTCTGTATACCGTTCTGGAATGTCAGCCGCTGTTTGATAGCAGCGATATGA
CCATTGCAGAATGGGTTTGTCTGGCACAGACCATTAAACGTCATTATGAACAGTATCATGGCTTCGTTGTTATTCATGGCACCGATACAAT
GGCATTTGCAGCAAGCATGCTGAGCTTTATGCTGGAAAATCTGCAGAAAACCGTTATTCTGACAGGTGCACAGGTTCCGATTCATGCACTG
TGGTCAGATGGTCGTGAAAACCTGCTGGGTGCACTGCTGATGGCAGGTCAGTATGTTATTCCGGAAGTTTGTCTGTTTTTTCAGAATCAGC
TGTTTCGTGGTAATCGTGCAACCAAAGTTGATGCACGTCGTTTTGCAGCATTTTGTAGCCCGAATCTGCTGCCGCTGGCAACCGTTGGTGC
AGATATTACCATTAATCGTGAACTGGTTCGTAAAGTGGATGGTAAAGCAGGTCTGGTTGTTCATAGCAGCATGGAACAGGATGTTGGTCTG
CTGCGTCTGTATCCGGGTATTCCGGCAGCGCTGGTTCGTGCATTTCTGCAGCCTCCGCTGAAAGGTGTTGTTATGGAAACCTTTGGTAGCG
GTAATGGTCCGACCAAACCGGATCTGCTGCAAGAACTGCGTGTTGCAACCGAACGTGGTCTGGTTATTGTTAATTGTACCCATTGTCTGCA
GGGTGCAGTTACCACCGATTATGCAGCAGGTATGGCAATGGCTGGTGCCGGTGTTATTAGCGGTTTTGATATGACCTCAGAAGCAGCACTG
GCAAAACTGAGCTATGTTCTGGGTCAGCCAGGTCTGAGCCTGGATGTGCGTAAAGAACTGCTGACCAAAGATCTGCGTGGTGAAATGACCC
CTCCGAGCGTTGAAGAACGCCGTCCGAGCCTGCAGGGTAATACCTTAGGTGGTGGTGTTAGCTGGCTGCTGAGCCTGAGCGGTAGCCAAGA
GGCAGATGCACTGCGTAATGCCCTGGTGCCGAGCCTGGCCTGTGCAGCAGCACATGCCGGTGATGTTGAAGCACTGCAGGCACTGGTTGAA
CTGGGTAGCGATTTAGGTCTGGTGGATTTTAATGGCCAGACACCGCTGCATGCCGCAGCACGTGGTGGTCATACCGAAGCCGTTACCATGC
TGTTACAGCGTGGTGTTGATGTTAATACACGTGATACCGATGGTTTTAGTCCGCTGCTGCTGGCCGTTCGTGGTCGTCATCCGGGTGTTAT
TGGCCTGCTGCGCGAAGCCGGTGCAAGCCTGAGCACCCAAGAACTGGAAGAGGCAGGCACCGAACTGTGTCGTCTGGCATATCGTGCAGAT
CTGGAAGGTCTGCAGGTTTGGTGGCAGGCAGGCGCTGATCTGGGCCAGCCTGGTTATGATGGTCATAGCGCACTGCATGTTGCAGAAGCCG
CAGGTAATCTGGCAGTTGTTGCCTTTCTGCAGTCACTGGAAGGTGCAGTTGGTGCCCAGGCACCGTGTCCGGAAGTGCTGCCTGGTGTTTA
A

H14-bdSUMO-hASNase1-fl peptide sequence

MSKHHHHSGHHHTGHHHHSGSHHHSGSAAGGEEDKKPAGGEGGGAHINLKVKGQDGNEVFFRIKRSTQLKKLMNAYCDRQSVDMTAIAFLF
DGRRLRAEQTPDELEMEDGDEIDAMLHQTGGSGGARAVGPERRLLAVYTGGTIGMRSELGVLVPGTGLAAILRTLPMFHDEEHARARGLSE
DTLVLPPASRNQRILYTVLECQPLFDSSDMTIAEWVCLAQTIKRHYEQYHGFVVIHGTDTMAFAASMLSFMLENLQKTVILTGAQVPIHAL
WSDGRENLLGALLMAGQYVIPEVCLFFQNQLFRGNRATKVDARRFAAFCSPNLLPLATVGADITINRELVRKVDGKAGLVVHSSMEQDVGL
LRLYPGIPAALVRAFLQPPLKGVVMETFGSGNGPTKPDLLQELRVATERGLVIVNCTHCLQGAVTTDYAAGMAMAGAGVISGFDMTSEAAL
AKLSYVLGQPGLSLDVRKELLTKDLRGEMTPPSVEERRPSLQGNTLGGGVSWLLSLSGSQEADALRNALVPSLACAAAHAGDVEALQALVE
LGSDLGLVDFNGQTPLHAAARGGHTEAVTMLLQRGVDVNTRDTDGFSPLLLAVRGRHPGVIGLLREAGASLSTQELEEAGTELCRLAYRAD
LEGLQVWWQAGADLGQPGYDGHSALHVAEAAGNLAVVAFLQSLEGAVGAQAPCPEVLPGV*

His-tag bdSUMO sequence Spacer ASNase sequence * Stop codon

H14-bdSUMO-hASNase1-tr nucleotide sequence

ATGAGCAAGCATCACCATCATTCAGGCCATCACCATACCGGACACCACCATCATTCAGGCAGTCATCACCATTCCGGATCTGCTGCGGGTG
GCGAAGAAGATAAGAAACCGGCAGGTGGCGAAGGTGGCGGTGCCCATATCAACCTGAAAGTGAAAGGTCAAGACGGCAACGAAGTCTTTTT
CCGCATCAAACGTTCTACCCAGCTGAAAAAGCTGATGAACGCATACTGTGACCGTCAGTCTGTAGACATGACCGCAATTGCTTTCCTGTTT
GATGGTCGTCGCCTGCGTGCGGAACAGACCCCGGATGAACTGGAGATGGAAGATGGCGACGAAATCGACGCAATGCTTCATCAGACTGGTG
GCAGCGGGGGGGCGAGAGCAGTTGGTCCGGAACGTCGTCTGCTGGCAGTTTATACCGGTGGCACCATTGGTATGCGTAGCGAACTGGGTGT
TCTGGTTCCTGGCACCGGTCTGGCAGCAATTCTGCGTACCCTGCCGATGTTTCATGATGAAGAACATGCACGTGCCCGTGGTCTGAGCGAA
GATACCCTGGTTCTGCCTCCGGCAAGCCGTAATCAGCGTATTCTGTATACCGTTCTGGAATGTCAGCCGCTGTTTGATAGCAGCGATATGA
CCATTGCAGAATGGGTTTGTCTGGCACAGACCATTAAACGTCATTATGAACAGTATCATGGCTTCGTTGTTATTCATGGCACCGATACAAT
GGCATTTGCAGCAAGCATGCTGAGCTTTATGCTGGAAAATCTGCAGAAAACCGTTATTCTGACAGGTGCACAGGTTCCGATTCATGCACTG
TGGTCAGATGGTCGTGAAAACCTGCTGGGTGCACTGCTGATGGCAGGTCAGTATGTTATTCCGGAAGTTTGTCTGTTTTTTCAGAATCAGC
TGTTTCGTGGTAATCGTGCAACCAAAGTTGATGCACGTCGTTTTGCAGCATTTTGTAGCCCGAATCTGCTGCCGCTGGCAACCGTTGGTGC
AGATATTACCATTAATCGTGAACTGGTTCGTAAAGTGGATGGTAAAGCAGGTCTGGTTGTTCATAGCAGCATGGAACAGGATGTTGGTCTG
CTGCGTCTGTATCCGGGTATTCCGGCAGCGCTGGTTCGTGCATTTCTGCAGCCTCCGCTGAAAGGTGTTGTTATGGAAACCTTTGGTAGCG
GTAATGGTCCGACCAAACCGGATCTGCTGCAAGAACTGCGTGTTGCAACCGAACGTGGTCTGGTTATTGTTAATTGTACCCATTGTCTGCA
GGGTGCAGTTACCACCGATTATGCAGCAGGTATGGCAATGGCTGGTGCCGGTGTTATTAGCGGTTTTGATATGACCTCAGAAGCAGCACTG
GCAAAACTGAGCTATGTTCTGGGTCAGCCAGGTCTGAGCCTGGATGTGCGTAAAGAACTGCTGACCAAAGATCTGCGTGGTGAAATGACCC
CTCCGAGCGTTGAAGAACGCCGTTAA

H14-bdSUMO-hASNase1-tr peptide sequence

MSKHHHHSGHHHTGHHHHSGSHHHSGSAAGGEEDKKPAGGEGGGAHINLKVKGQDGNEVFFRIKRSTQLKKLMNAYCDRQSVDMTAIAFLF
DGRRLRAEQTPDELEMEDGDEIDAMLHQTGGSGGARAVGPERRLLAVYTGGTIGMRSELGVLVPGTGLAAILRTLPMFHDEEHARARGLSE
DTLVLPPASRNQRILYTVLECQPLFDSSDMTIAEWVCLAQTIKRHYEQYHGFVVIHGTDTMAFAASMLSFMLENLQKTVILTGAQVPIHAL
WSDGRENLLGALLMAGQYVIPEVCLFFQNQLFRGNRATKVDARRFAAFCSPNLLPLATVGADITINRELVRKVDGKAGLVVHSSMEQDVGL
LRLYPGIPAALVRAFLQPPLKGVVMETFGSGNGPTKPDLLQELRVATERGLVIVNCTHCLQGAVTTDYAAGMAMAGAGVISGFDMTSEAAL
AKLSYVLGQPGLSLDVRKELLTKDLRGEMTPPSVEERR*

His-tag bdSUMO sequence Spacer ASNase sequence * Stop codon